

TOPICS IN ONE-DIMENSIONAL MAGNETISM

By

BRUCE DOUGLAS GAULIN, B.Sc.

A Thesis .

Submitted to the School of Graduate Studies

in Partial Fulfilment of the Requirements

for the Degree

Doctor of Philosophy

McMaster University

April 1986



Library
COPY

TOPICS IN ONE-DIMENSIONAL MAGNETISM

[Handwritten signature]

DOCTOR OF PHILOSOPHY (1986)
(Physics)

McMASTER UNIVERSITY
Hamilton, Ontario

TITLE: Topics in One-Dimensional Magnetism

AUTHOR: Bruce Douglas Gaulin, B.Sc. (McGill University)

SUPERVISOR: Professor M.F. Collins

NUMBER OF PAGES: xiv, 170

ABSTRACT

An experimental study of the dynamic properties of the quasi-one-dimensional magnetic materials CsMnBr_3 and $\text{CsMn}_{0.89}\text{Fe}_{0.11}\text{Br}_3$ has been carried out. In addition, some theoretical and computer simulation work was performed on aspects of the static behaviour of selected one-dimensional magnetic systems.

CsMnBr_3 is a one-dimensional magnetic insulator. Its magnetic behaviour can be described by a Heisenberg antiferromagnetic chain system with weak easy plane anisotropy. A truly one-dimensional system cannot sustain long-range order at any non-zero temperature, although short-range correlations can be strong at low temperatures. We used neutron scattering techniques to examine both the delocalized (spin wave) and localized (soliton) excitations of CsMnBr_3 in its paramagnetic phase at low temperatures. Our results of the spin wave response compare favourably with recent theory of co-operative excitations in the absence of long-range order. Our measurements of the soliton response is in qualitative agreement with the relevant theory. Soliton-like spin configurations could also be directly observed in the results of a Monte Carlo simulation on a system representative of CsMnBr_3 .

We also used the Monte Carlo method to examine static spin correlation lengths within the XY to Heisenberg crossover temperature regime in CsMnBr_3 .

We measured the magnetic excitation spectrum of the magnetic impurity chain system $\text{CsMn}_{0.89}\text{Fe}_{0.11}\text{Br}_3$ at low temperatures by neutron scattering techniques. The response was qualitatively different from either CsMnBr_3 or

previously studied magnetic vacancy chain systems and showed marked host mode-impurity mode interaction effects.

Finally we utilized the computational ease afforded by one dimension to examine the strengths of biquadratic exchange interactions in selected Mn^{+2} chain systems, including CsMnBr_3 .

ABSTRACT FOR THE NON-SPECIALIST

This thesis contains several studies of some special magnetic materials at low temperatures. In certain classes of materials, magnetic moments form at the atomic level in the solids. These magnetic moments can be thought of as tiny bar magnets located on the individual atoms. At high temperatures these atomic magnets flip about wildly and do not seem to take any notice of how the magnets on neighbouring atoms are behaving. At low temperatures, however, the direction any particular magnet points is very sensitive to the arrangement of the directions which the magnets close by to it are pointing. In many magnetic materials a preferred direction for the atomic magnets to point appears at sufficiently low temperatures and a magnetic structure is said to have formed. If the temperature is raised the magnets are thermally jostled about and the magnetic structure will eventually break down. However this thermal jostling of the atomic magnets occurs only by certain types of motion of the magnets known as normal modes. The experimental sections in this thesis concern themselves with examining these normal modes in the magnetic materials CsMnBr_3 and $\text{CsMn}_{0.89}\text{Fe}_{0.11}\text{Br}_3$.

These two materials are interesting because the atomic magnets contained in them are arranged in straight lines. For this reason they are referred to as one-dimensional magnetic materials. This is in contrast to most normal magnetic materials where the atomic magnets fill up three-dimensional space evenly. When the atomic magnets are arranged in straight

lines, the ways in which the magnetic structure is broken down, the normal modes, become extremely efficient. So much so in fact, that a true magnetic structure can only form at absolute zero temperatures where no thermal jostling at all is present.

Because the atomic magnets are arranged in straight lines it is also easier to imagine the possible orientations of the magnets along the lines than it is when the magnets fill up three-dimensional space evenly. This is because there are fewer dimensions to worry about. We have taken advantage of this greater simplicity in trying to model some of the magnetic behaviour of these materials. This has been done both by theoretical calculations and by use of a computer.

The thesis is thus made up of both experimental and theoretical types of investigations of one-dimensional magnetic materials.

ACKNOWLEDGEMENTS

I would like to express my appreciation for the guidance and support given to me over the course of these studies by my research supervisor, Dr. Malcolm Collins. Malcolm provided an exciting atmosphere of being able to contribute to scientific understanding, while demonstrating a very pleasant approach to the pursuit of this understanding.

I would like to thank Dr. Bill Buyers for his support and interest in all of our research, and in particular for his involvement in the work on $\text{CsMn}_{0.89}\text{Fe}_{0.11}\text{Br}_3$. In addition I would like to thank Bill for his hospitality during my stays in Deep River.

Drs. Izabela Sosnowska, Carl Stager and John Greedan all took an active interest in this research and I am grateful for their contributions.

It was a pleasure to work at the N.S.S.P. Branch of Chalk River Nuclear Laboratories largely due to being surrounded by the very knowledgeable scientific and technical staff. These gentlemen were Drs. Gerald Dolling, Tom Holden, Eric Svensson, Peter Martel, Peter Gerlach and Soo Kim as well as Messrs. Harold Nieman, Don Tennant, Alan Hewitt, Jim Evans and Mel Potter. I would also like to thank Mrs. Anne-Marie Van Dine for her help at the Branch.

The expert technical assistance I received at McMaster from Messrs. Jim Couper, Jim Garrett, Frank Gibbs and Gord Hewitson was greatly appreciated.

The people who found themselves in and around Senior Sciences 440 during the course of this work added a lot to the enjoyment of my stay at McMaster. These people included Chris Peters, Andy Duft, Roger Patterson,

Mike Coombes, Frank Marsiglio, Walter Stephan, Andy Duncan, Lynne Soderholm, Sonja Eicher, Brian Allore, Jake Vanderwal, Zhibing Hu, Isobel Davidson, Mahboob Ashraf and Channon and Marsha Price. Similarly my stays at Deep River were more enjoyable due to the presence of Mike Hogan, Rose Morra, Rose Morrelli, Martin Dove, Colin Broholm and Tom and Jenny Jackman.

I am especially indebted to Karen Hughes for her friendship and many helpful discussions over the course of this work.

I would like to thank Mrs. Helen Kennelly for the expert typing of this manuscript.

Finally, I would like to thank Atomic Energy of Canada Limited for providing experimental facilities as well as allowing me generous access to their computer facilities. The financial support of the Natural Sciences and Engineering Research Council of Canada, Les Fonds F.C.A.C. (Quebec), the Ontario Graduate Scholarship program and McMaster University is gratefully acknowledged.

to my family

TABLE OF CONTENTS

<u>CHAPTER</u>		<u>PAGE</u>
1	INTRODUCTION	1
	1.1 Why is One-Dimensional Magnetism of Interest?	1
	1.2 The Direction of the Thesis	5
	1.3 The Character of CsMnBr_3 and $\text{CsMn}_{0.89}\text{Fe}_{0.11}\text{Br}_3$	7
2	NEUTRON SCATTERING	16
	2.1 The Neutron as a Probe of Condensed Matter	16
	2.2 The Neutron Scattering Cross-Section	17
	2.3 The Practice of Neutron Scattering	22
3	PARAMAGNETIC SPIN WAVES IN CsMnBr_3	34
	3.1 Introduction	34
	3.2 The Neutron Scattering Experiment	35
	3.3 Results and Low Temperature Analysis	35
	3.4 Results and the Generalized Langevin Equation Approach to Spin Dynamics	43
4	SOLITONS IN CsMnBr_3	57
	4.1 Introduction	57
	4.2 Solitons in Condensed Matter	61
	4.3 Theoretical Treatment of the Anisotropic Heisenberg Antiferromagnetic Chain	66
	4.4 The Neutron Scattering Experiment	69
	4.5 Results and Discussion	77

<u>CHAPTER</u>		<u>PAGE</u>
5	SPIN WAVES AND LOCAL MODES IN $\text{CsMn}_{0.89}\text{Fe}_{0.11}\text{Br}_3$	90
	5.1 Introduction	90
	5.2 The Neutron Scattering Experiment	96
	5.3 Single Ion Analysis	105
	5.4 Discussion	113
6	THE MONTE CARLO METHOD	117
7	BIQUADRATIC EXCHANGE FROM SUSCEPTIBILITY DATA IN CLASSICAL ONE-DIMENSIONAL HEISENBERG SYSTEMS	125
	7.1 Introduction	125
	7.2 The Classical Heisenberg Chain	127
	7.3 The Classical Heisenberg Chain with Both Bilinear and Biquadratic Exchange	129
	7.4 Monte Carlo Treatment of CsMnBr_3	135
	7.5 Discussion	140
8	CROSSOVER BEHAVIOUR AND SOLITONS IN AN ANISOTROPIC HEISENBERG CHAIN	144
	8.1 Introduction	144
	8.2 Static Spin Correlations	145
	8.3 Spin Configurations and Out-of-Easy-Plane Solitons	153
9	CONCLUDING REMARKS	164
	BIBLIOGRAPHY	166

LIST OF FIGURES

<u>Figure</u>		<u>Page</u>
A1	The crystal structure of CsMnBr_3 and $\text{CsMn}_{0.89}\text{Fe}_{0.11}\text{Br}_3$	8
A2	The mosaic spreads of the CsMnBr_3 and $\text{CsMn}_{0.89}\text{Fe}_{0.11}\text{Br}_3$ samples	15
B1	A schematic diagram of the McMaster triple axis spectrometer at Chalk River	23
B2	A photograph of the author at the McMaster triple axis spectrometer	25
B3	The physical origin of the Bragg reflection condition	31
B4	Examples of spurious scattering events	33
C1	The measured spin wave dispersion for CsMnBr_3 at 15K with the results of zero temperature spin wave theory	36
C2	Constant Q scans at $(0.6, 0.6, 1.0)$ and $(0.1, 0.1, 1.0)$ for CsMnBr_3 at 21K	39
C3	The magnetic zone mixing argument for spin wave energy widths	42
C4	Constant Q scans at $(0, 0, \tau.15)$ for CsMnBr_3 as a function of temperature. Also plotted is theory treating paramagnetic spin waves in a Heisenberg antiferromagnet	49
C5	Constant Q scans at $(0, 0, 1.2)$ for CsMnBr_3 as a function of temperature. Also plotted are theoretical results from treatments of paramagnetic spin waves	51

<u>Figure</u>		<u>Page</u>
C6	Constant Q scans at (0,0,1.3) for CsMnBr ₃ as a function of temperature. Also plotted are theoretical results from treatments of paramagnetic spin waves	52
C7	Constant Q scans at (0,0,1.1) as a function of temperature for CsMnBr ₃	54
D1	A physical picture of a Sine-Gordon soliton, contrasted with that of a dissipative wave	60
D2	Spin configurations taken up by soliton bearing magnetic systems	63
D3	The spin configuration taken up by an antiferromagnetic chain system with easy-plane anisotropy, in the presence of an out-of-easy-plane soliton	65
D4	The scattering geometries involved in determining $S^{xx}(q_z, \omega)$ and $S^{zz}(q_z, \omega)$	71
D5	The constant energy scans shown relative to the spin wave response of CsMnBr ₃	72
D6	Typical inelastic constant energy scans at $\hbar\omega = 0.5$ meV and temperatures of 15K and 47K	75
D7	Typical inelastic, constant energy scans at T = 15K and $\hbar\omega = 1.0$ meV and 1.25 meV	76
D8	The measured values of $S^{xx}(Q_z, \omega)$ and $S^{zz}(Q_z, \omega)$ at 15K as a function of energy transfer for CsMnBr ₃	78
D9	The integrated intensity of $S^{zz}(Q_z, \omega)$ at 15K is compared with the same due to the noninteracting soliton model	81

<u>Figure</u>		<u>Page</u>
D10	The lineshape of $S^{ZZ}(Q_z, \omega)$ at 15K is compared with the predicted lineshape of the noninteracting soliton model	82
D11	The observed integrated intensity of $S^{ZZ}(Q_z, \hbar\omega = 0.5 \text{ meV})$ as a function of temperature	
D12	The apparent temperature dependence of the soliton mass	87
D13	The lineshape of $S^{ZZ}(Q_z, \hbar\omega = 0.5 \text{ meV})$ is shown as a function of temperature along with the lineshape predicted by the modified soliton theory	89
E1	A schematic diagram of the magnetic sites in a magnetic vacancy chain system as well as a magnetic impurity chain system	92
E2	Inelastic scattering at $Q = (-.15, -.15, 1.0)$ and $Q = (-.15, -.15, 1.05)$ at $T = 18\text{K}$ in $\text{CsMn}_{0.89}\text{Fe}_{0.11}\text{Br}_3$	98
E3	Inelastic scattering at $Q = (-.75, -.75, 1.15)$, $Q = (0, 0, 1.15)$ at 18K as well as $Q = (0, 0, 1.15)$	99
E4	Inelastic scattering at $Q = (0, 0, 1.2)$ at $T = 18\text{K}$ and 25K in $\text{CsMn}_{0.89}\text{Fe}_{0.11}\text{Br}_3$	100
E5	Inelastic scattering at $Q = (0, 0, 1.3)$ and $Q = (-.75, -.75, 1.3)$ at $T = 18\text{K}$ as well as $Q = (0, 0, 1.3)$ at $T = 25\text{K}$ in $\text{CsMn}_{0.89}\text{Fe}_{0.11}\text{Br}_3$	101
E6	Inelastic scattering at $Q = (0, 0, 1.4)$ and $Q = (0, 0, 1.5)$ at $T = 18\text{K}$ in $\text{CsMn}_{0.89}\text{Fe}_{0.11}\text{Br}_3$	102
E7	The dispersion of magnetic excitations in $\text{CsMn}_{0.89}\text{Fe}_{0.11}\text{Br}_3$ at $T = 18\text{K}$	104

<u>Figure</u>		<u>Page</u>
E8	Qualitative level scheme for Fe^{+2} in $\text{CsMn}_{0.89}\text{Fe}_{0.11}\text{Br}_3$	107
E9	The interacting mode model for $\text{CsMn}_{0.89}\text{Fe}_{0.11}\text{Br}_3$ is shown	115
G1	The experimental susceptibility of three $S = 5/2$ Heisenberg chain compounds as a function of reduced temperature	128
G2	The theoretical treatments of the susceptibilities of TMMC and MMC are compared to experiment	132
G3	Theoretical and Monte Carlo simulation results of the susceptibility of CsMnBr_3 are compared with experiment	133
G4	Typical data from the Monte Carlo simulation for two temperatures	138
G5	Results of the Monte Carlo treatment of CsMnBr_3 as a function of biquadratic exchange strength is compared to experiment at $T = 20\text{K}$	139
H1	Representative data from the numerical calculation of $(-1)^n \langle S_i^\alpha S_{i+n}^\alpha \rangle$ for in-plane and out-of-plane correlations	148
H2	Values of $\sqrt{\langle (S^\alpha)^2 \rangle}$ extracted from the simulation as a function of temperature	150
H3	Values of $\xi_\alpha(T)$, the correlation lengths, as a function of temperature, extracted from the simulation	151
H4	Out-of-easy-plane static correlation functions $\langle S_i^z S_{i+n}^z \rangle$ for $n = 4, 5$ and 6 as a function of temperature	154

<u>Figure</u>		<u>Page</u>
H5	Spin configurations as a function of temperature within the X₁ to Heisenberg crossover regime	155
H6	The section of the T = 12.5K spin configurations which exhibits the two out-of-easy-plane solitons	159
H7	Spin configurations at T = 5K exhibiting an out-of-easy-plane, but non-soliton, fluctuation	163

LIST OF TABLES

<u>TABLE</u>		<u>PAGE</u>
A1	Experimental Parameters which Determine the Resolution Function	29
B1	Hamiltonian Matrix for Fe^{+2} in $\text{CsMn}_{0.89}\text{Fe}_{0.11}\text{Br}_3$	111
B2	Eigenvectors and Eigenvalues for Fe^{+2} in $\text{CsMn}_{0.89}\text{Fe}_{0.11}\text{Br}_3$	112a,b
C1	Flow Diagram of Computer Program for Monte Carlo Simulation.	121

CHAPTER 1

INTRODUCTION

1.1 Why is One-Dimensional Magnetism of Interest?

A co-operative system is comprised of many constituents all of which are somehow coupled to each other, and their behaviour is governed by their collective motion and normal modes. There are many examples in nature of such systems; however due to the relative simplicity of the manner in which the constituents are coupled as well as the rich variety of co-operative behaviour possible, magnetic materials have become prototypical co-operative systems.

The constituents in magnetic materials are the magnetic moments formed by the unpaired atomic electrons at the atomic sites in solids. These moments can interact with each other via several exchange mechanisms as well as via the real magnetic dipole interactions. The type of exchange interactions present in a material depend on the electronic environment present in the material. Insulators, with no free, mobile electrons can support only the direct exchange and superexchange mechanisms. These both require the overlap of the magnetic electron wavefunctions with either the magnetic electron wavefunction of a neighbouring atom, or the electron wavefunctions of an intervening diamagnetic atom, respectively. Thus these interactions tend to be very short range; usually nearest neighbour interactions are sufficient to understand the phenomena.

Magnetic phenomena in metals are complicated by two features. Firstly the magnetic moments themselves can be thought of as localized at atomic sites only in special cases (such as some "well behaved" rare earth metals and alloys). In other cases the same electrons responsible for magnetism are also involved in conduction. Secondly the presence of the conduction electrons means that exchange interactions can be of much longer range than in insulators.

The moment formation problem in metals notwithstanding, we would expect the statistical mechanics of magnetism in insulators to be an easier challenge than that in metals. This is because, for the same type of system, there are fewer variables of relevance in the insulator problem due to the short range of the interactions.

The Heisenberg Hamiltonian,

$$H = \sum_{i,j} J(i,j) \underline{S}_i \cdot \underline{S}_j \quad (1.1)$$

or some modification thereof, is frequently used successfully in understanding magnetic systems. The contribution any one magnetic moment or spin, \underline{S}_i , makes to the Hamiltonian in such a model depends on the relative orientation of this spin to all the other spins, \underline{S}_j , for which the exchange constant, $J(i,j)$, is appreciable. It is these relative orientations which the statistical-mechanical treatment of this system must consider. Clearly if the range of interactions is shorter, then there are fewer relative orientations of interest in the problem, and this should simplify the treatment of the problem.

By the same token, if the spatial dimensionality of the system is reduced then there will be fewer variables of interest. In the extreme case

of a one-dimensional system with short-range interactions there will be only two neighbours and the theoretical treatment of this co-operative system should be as tractable as possible. This is indeed the case as there have been developed several exact solutions to the static behaviour, or thermodynamics, of certain one-dimensional models. The treatments of the dynamics (the spectrum of fluctuations or excitations from the ground state) of these systems have not afforded exact solutions. However this problem is still simpler than its higher dimensional counterparts and this allows considerably more scrutiny of the premises of the theory.

In addition the fluctuations of the system take on a much greater importance in understanding the phenomena of the one-dimensional system. This is because a disturbance (i.e. fluctuation, impurity etc.) at any one site is much more disruptive to the flow of information or correlations in one dimension than in higher dimensions. Information propagation in two and three-dimensional systems has many paths around any one particular constituent in the co-operative system. In one dimension with short range interactions, information propagation from one side of the system to the other involves every constituent in the system. Hence a fluctuation at any one site can disrupt the flow of the information and break up the correlations along the chain very effectively.

The importance of the fluctuations or excitations in these systems has the consequence that a truly one-dimensional system with short-range interactions does not display long-range order at any finite temperature. This is in contrast to most "normal" (i.e. three-dimensional) magnetic materials which display long-range magnetic order over an extended tempera-

ture range. The absence of long-range order means that theoretical treatments involving the presence of an order parameter cannot be used, and this greatly complicates the treatment of the excitations. For example linear spin-wave theory relies on the presence of a magnetization or sublattice magnetization and so should not be applicable. In addition it represents a failure of the standard mean field theory technique. Mean field theory essentially ignores, or averages over the fluctuations in a system. Thus, as mean field theory fails, the fluctuations should be dealt with explicitly in order to understand this magnetic behaviour. Again this is in contrast to three-dimensional magnetic materials in which much of the phenomena can be reasonably described within a mean field theory context.

One-dimensional magnetism has been of interest to the experimentalist as well. Good quality single-crystals of magnetic materials whose magnetic properties are sufficiently anisotropic that they can be considered as being one-dimensional in the proper temperature regime, have existed for roughly fifteen years. A healthy push-pull relationship between theory and experiment has existed and continues to exist today in this field. Novel phenomena which are expected to be absent or marginal in three-dimensional magnetism have been seen to be markedly present in one-dimensional magnetism, and this is the main reason for interest in one-dimensional magnetism.

Excellent reviews of phenomena involved in one-dimensional magnetism are given by Birgeneau and Shirane (1978), Steiner et al. (1975) and articles contained in Bernasconi and Schneider (1981).

1.2 The Direction of the Thesis

This thesis represents a study of the dynamic and some static magnetic properties of CsMnBr_3 and $\text{CsMn}_{0.89}\text{Fe}_{0.11}\text{Br}_3$. These two materials will be described in detail in the next section. There is a very pronounced anisotropy in the strength of the magnetic interactions, and this allows us to consider them as quasi-one-dimensional magnetic systems.

The thesis contains two types of work. First, inelastic neutron-scattering studies of the magnetic dynamics of CsMnBr_3 and $\text{CsMn}_{0.89}\text{Fe}_{0.11}\text{Br}_3$ in their paramagnetic phases will be presented. Following a chapter which describes neutron scattering techniques and the formalism involved in magnetic inelastic neutron scattering, three neutron studies will be presented. Each of these is contained in its own chapter. These are "Paramagnetic Spin Waves in CsMnBr_3 " in Chapter 3; "Solitons in CsMnBr_3 " in Chapter 4; and "Spin Waves and Local Modes in $\text{CsMn}_{0.89}\text{Fe}_{0.11}\text{Br}_3$ " in Chapter 5.

Short accounts of this work have appeared or will appear in scientific publications. These publications are:

Chapter 3

1. M.F. Collins and B.D. Gaulin, 1984, *J. Appl. Phys.* 55, 1869.
2. B.D. Gaulin and M.F. Collins, 1984, *Can. J. Phys.* 62, 1132.
3. M.F. Collins and B.D. Gaulin, 1984, Magnetic Excitations and Fluctuations, Lovesey et al. (editors), p. 12, Springer-Verlag, Berlin.

Chapter 4

1. B.D. Gaulin and M.F. Collins, 1985, *Can. J. Phys.* 63, 1235.

Chapter 5

1. B.D. Gaulin, M.F. Collins and I. Sosnowska (to appear in *Physica B*).

The second type of work involves examining the static correlations and configurations of several quasi-one-dimensional magnetic insulators with particular emphasis on CsMnBr_3 . This work proceeds mainly by a classical Monte Carlo simulation. Chapter 6 of the thesis describes briefly the principles involved in the simulation itself, as well as some problems associated with the computer simulation. Then two results are presented in Chapters 7 and 8.

Chapter 7 concerns itself with the relevance of higher order, specifically biquadratic, exchange processes in several quasi-one-dimensional systems. Chapter 8 uses the Monte Carlo simulation to calculate the spin correlations in a model one-dimensional system. Spin configurations are also generated as a function of temperature and these results tie in with the neutron results on solitons in CsMnBr_3 presented in Chapter 4.

Once again short accounts of this work will appear in the scientific literature. These publications will be:

Chapter 7

B.D. Gaulin and M.F. Collins (to appear in Phys. Rev. B).

Chapter 8

B.D. Gaulin and M.F. Collins (to appear in J. Phys. C).

A short introduction to each topic is attempted at the beginning of each chapter.

1.3 The Character of CsMnBr₃ and CsMn_{0.89}Fe_{0.11}Br₃

CsMnBr₃ crystallizes in the hexagonal space group P6₃/mmc with lattice constants at T = 70K of c = 6.439 Å and a = 7.56 Å. A diagram of the crystal structure is shown in figure A1. As can be seen from the diagram, the crystal is essentially comprised of chains of Mn⁺² ions running along the hexagonal c-axis. Between any two Mn⁺² ions are a triad of Br⁻ ions. The Cs⁺ ions lie out in the cell and serve to isolate the chains from each other.

This material is electrically insulating and the unfilled d-shell at the Mn⁺² site gives rise to a localized magnetic moment. The Hund's rule ground state which corresponds to the Mn⁺² electronic configuration yields an S = 5/2, L = 0 moment at the Mn⁺² site. These moments can interact relatively strongly via the superexchange mechanism utilizing the intervening triad of diamagnetic Br⁻ ions along the chain. Interactions between Mn⁺² moments on neighbouring chains involve a much longer and more complicated superexchange path and hence these interactions are much weaker than those along the chain. The ratio of the strengths of the interactions along to between the chains is believed to be ~ 470:1 (Breitling et al., 1977), and this is the origin of the material's one-dimensional nature.

Of course at sufficiently low temperatures these weak interchain interactions will precipitate a phase transition to a three-dimensional magnetically ordered phase. For CsMnBr₃ this occurs at 8.3K (Eibshutz et al., 1972). Above this temperature CsMnBr₃ behaves as a one-dimensional magnetic insulator. Spin wave energies in the three-dimensionally ordered state have been calculated by Oyedele and Collins (1978) and measured by Breitling et al., (1977).

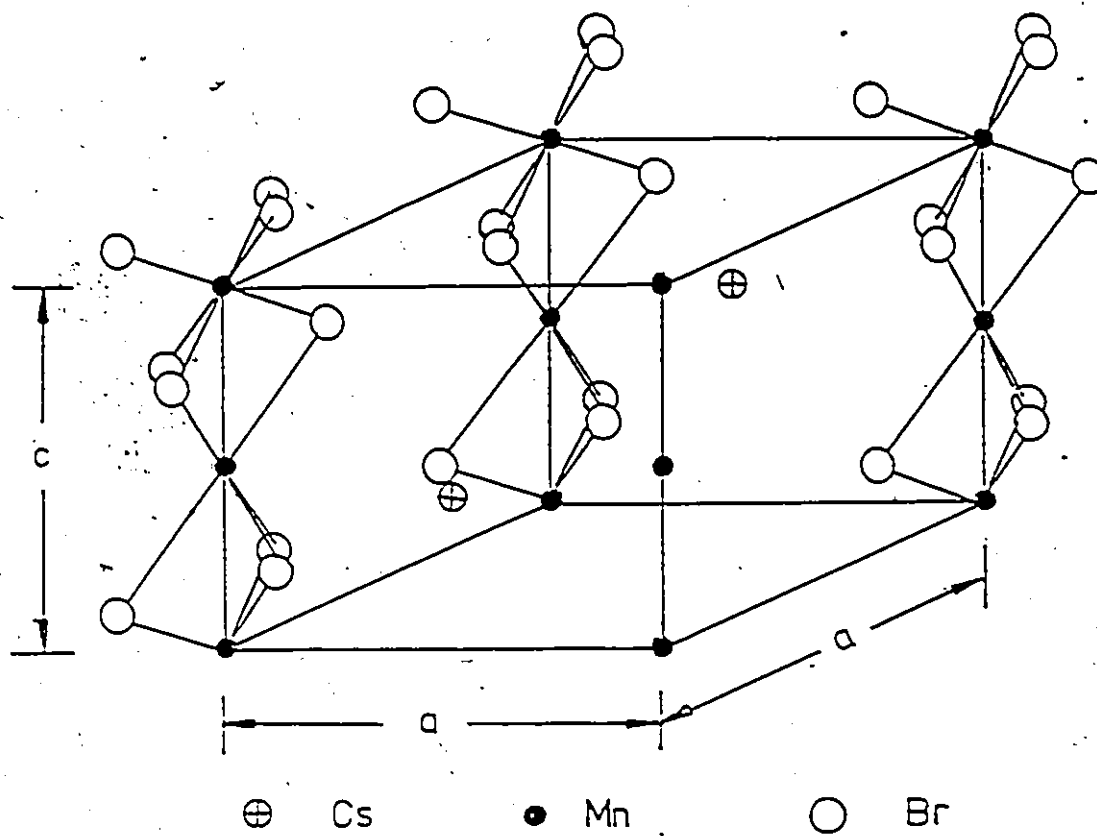


Figure A1: The crystal structure of CsMnBr_3 and $\text{CsMn}_{.89}\text{Fe}_{.11}\text{Br}_3$.

The $L = 0$ nature of the Mn^{+2} moment means that the interactions between the moments will be isotropic to a good approximation. This is because the moment only has a contribution from the internal spin magnetic moments of the electrons in the unfilled d-shell. These are not affected by the crystalline environment and thus in the absence of the exchange mechanism, there is no preferred direction or plane for the magnetic moment. Isotropy, or anisotropy, in the spin interactions is usually discussed in terms of the following general Hamiltonian:

$$H = - 2J \sum_i [S_i^x S_{i+1}^x + S_i^y S_{i+1}^y + |\gamma| S_i^z S_{i+1}^z] \quad (1.2)$$

One can see that equation (1.2) is a special case of (1.1), the Heisenberg Hamiltonian in one dimension, with nearest neighbour interactions only.

For the moment let us consider $|\gamma| = 1$. Then it is clear that if $J > 0$ the magnetic system can lower its energy by having all spins align parallel to each other, and these are referred to as ferromagnetic interactions. If $J < 0$ the magnetic system can lower its energy by having nearest neighbour spins align antiparallel to each other and these are referred to as antiferromagnetic interactions.

Now let us consider the antiferromagnetic case $J < 0$. If $\gamma = 1$, then each of the spin components S^x, S^y, S^z (where x, y and z are orthogonal axes) contribute equally to the energy of the system and the interactions are termed isotropic or Heisenberg-like. Should we have $\gamma < 1$ then two of the components will be more important to the energy of the system than the third,

S^z , component and the interactions will exhibit XY or planar anisotropy. Should we have $\gamma > 1$ then one component of spin, S^z , is more important to the energy than the other two and the interactions will exhibit Ising or unidirectional anisotropy. Clearly the greater the difference of γ from unity the more pronounced the anisotropy will be; however the anisotropy will always manifest itself at sufficiently low temperatures.

Now returning to our discussion of CsMnBr_3 , the leading order exchange interactions between Mn^{+2} moments along the chain are antiferromagnetic. The very weak exchange interactions between Mn^{+2} ions on adjacent chains are also antiferromagnetic. These interactions are actually electrostatic in origin, that is, they are the consequence of the Pauli principle (Fermi statistics) on the electrostatic energy of two Mn^{+2} configurations overlapping on a diamagnetic Br^- atomic configuration. In addition to this isotropic or Heisenberg-like exchange interaction, there is a real magnetic interaction. These are the magnetic dipole interactions of the form:

$$H_d \propto \frac{1}{r_{ij}^3} \{ \underline{S}_i \cdot \underline{S}_j - 3(\underline{S}_i \cdot \hat{r}_{ij})(\underline{S}_j \cdot \hat{r}_{ij}) \} \quad (1.3)$$

As real magnetic interactions, these interactions will be much weaker than the exchange interactions (at least along the chain). However the second part of the equation introduces some anisotropy into the system. This interaction falls off with distance only as r^3 , and thus in general it is a long range interaction. However in one dimension this is not very important as the strength of the second nearest neighbour interaction is 1/8 of the first nearest neighbour interaction strength. In three dimensions the long range nature of the dipoles does introduce difficulties.

The leading order exchange interaction acts so as to align nearest neighbours antiparallel to each other. The dipolar interactions then act to establish an easy plane perpendicular to the chain axis, or \hat{r}_{ij} in equation (1.3). Thus the low temperature paramagnetic "structure" of this system consists of a Néel type configuration of spins lying within a plane perpendicular to the chain axis. Two simplified Hamiltonians will be used to describe CsMnBr_3 in this thesis. They are equivalent at low temperatures and the difference is not thermodynamically relevant at high temperatures.

$$H_1 = -2J \sum_i \underline{S}_i \cdot \underline{S}_{i+1} + A \sum_i (S_i^z)^2$$

$$H_2 = -2J \sum_i \underline{S}_i \cdot \underline{S}_{i+1} + \delta \sum_i S_i^z S_{i+1}^z$$

Relevant parameters for CsMnBr_3 are $J = -0.88$ meV and $\delta = 0.03$ meV, which corresponds to $|\gamma| = .982$ in equation (1.2). The material $(\text{CH}_3)_4\text{NMnCl}_3$, better known as TMMC, is very similar to CsMnBr_3 and has been studied extensively. It is also essentially comprised of Mn^{2+} ions arranged along chains and the two compounds have very similar nearest neighbour $\text{Mn}^{+2}-\text{Mn}^{+2}$ separation distances along the chain. We frequently refer to work on TMMC throughout the thesis.

As was previously mentioned, exact solutions exist for the static behaviour of certain one-dimensional models. We will make great use of one of these in examining both the statics and dynamics of CsMnBr_3 . This is Fisher's solution (Fisher, 1964) of the one-dimensional classical Heisenberg model, with nearest neighbour interactions only.

The model Hamiltonian is that of equation (1.2) with $|\gamma| = 1$ and the spin magnetic moments are now classical vectors, \underline{S}_i , which can take on

any orientation in space. This is relevant for CsMnBr_3 (or at least aspects of its behaviour) due to the relatively weak anisotropy in the spin interactions ($|\gamma| = .982$) as well as the relatively large $S = 5/2$ moment present at the Mn^{+2} site. The correspondence principle asserts that one should recover classical mechanics from quantum mechanics as the quantum numbers of a system in question become large. The $S = 5/2$ quantum number may not appear that large, however with $(2S+1) = 6$ possible orientations with respect to some axis of quantization it is a reasonable approximation to treat the system as classical.

Fisher solved for the thermodynamics of his model classical Hamiltonian by allowing the preceding spin along the chain \hat{S}_{j-1} , to define the polar axis for \hat{S}_j (where $\hat{S}_j = S_j/|S|$). This allowed him to calculate both the partition function

$$Z_N = \int \frac{d\Omega_0}{4\pi} \int \frac{d\Omega_1}{4\pi} \cdots \int \frac{d\Omega_N}{4\pi} \exp[K \sum_i S_i \cdot S_{i+1}]$$

and the static spin pair correlation function

$$\langle S_i^z S_{i+l}^z \rangle = 3Z_N^{-1} \int \frac{d\Omega_0}{4\pi} \cdots \int \frac{d\Omega_N}{4\pi} S_i^z S_{i+l}^z \times \exp[K \sum_i S_i \cdot S_{i+1}]$$

where

$$K = 2J^z/kT$$

He then solved for the various thermodynamic properties of interest including the susceptibility.

$$\chi_N = g^2 \mu_B^2 N S(S+1) \left(\frac{1}{3kT} \right) (1+u)/(1-u)$$

where $u = \coth\left(\frac{1}{x}\right) - x$

and $x = \frac{kT}{(2JS(S+1))}$

as well as the correlation length along the chain

$$\xi = \ln\left[\coth\left(\frac{1}{x}\right) - x\right]$$

in units of the Mn^{+2} - Mn^{+2} separation distance, where the correlation length is defined by

$$\langle S_i \cdot S_{i+l} \rangle \sim \exp\left(-\frac{l}{\xi}\right)$$

This quantity gives a characteristic distance beyond which correlations can be thought of as being weak or absent. At low temperature ξ goes as $\frac{1}{T}$, which explicitly shows the absence of long range order (non-infinite correlation length) at all temperatures above absolute zero.

Thorpe solved exactly for the static properties of the random classical Heisenberg chain containing two types of moments and three different nearest neighbour exchange interactions (Thorpe, 1975). We shall make some use of this in our study of $CsMn_{0.89}Fe_{0.11}Br_3$. This material, grown by ourselves using Bridgeman techniques, is described in more detail in Chapter 5. Eleven percent of the Mn^{+2} have been replaced by Fe^{+2} , compared to $CsMnBr_3$. To the best of our knowledge, the substitution is random along the chain. The concentration gradient of the Fe^{+2} impurities along the length of the crystal was determined by an absorption study performed on

79

small selected pieces of the crystal at the Institute for Materials Research, at McMaster University. Our results show that the concentration gradient over the full length of the single crystal used, is less than 1.5%.

The mosaic spreads of both CsMnBr_3 and $\text{CsMn}_{0.89}\text{Fe}_{0.11}\text{Br}_3$ single crystals are shown in figure A2. These were both obtained by examining the 002 Bragg reflections of neutrons by each crystal at the McMaster spectrometer (E-2), N.R.U. reactor, Chalk River. As can be seen from this diagram, the quality of the $\text{CsMn}_{0.89}\text{Fe}_{0.11}\text{Br}_3$ crystal is better than that of the CsMnBr_3 crystal. The CsMnBr_3 single crystal is made up of three large single crystals, very closely aligned, as well as other smaller pieces also closely aligned. One of these large pieces is much bigger than the other two. The mosaic spread of the crystal is then $\sim 2^\circ$ (FWHM). The $\text{CsMn}_{0.89}\text{Fe}_{0.11}\text{Br}_3$ single crystal is comprised of two very closely aligned single crystals, one of which is much larger than the other. The mosaic spread of this crystal is $\sim 0.5^\circ$ (FWHM).

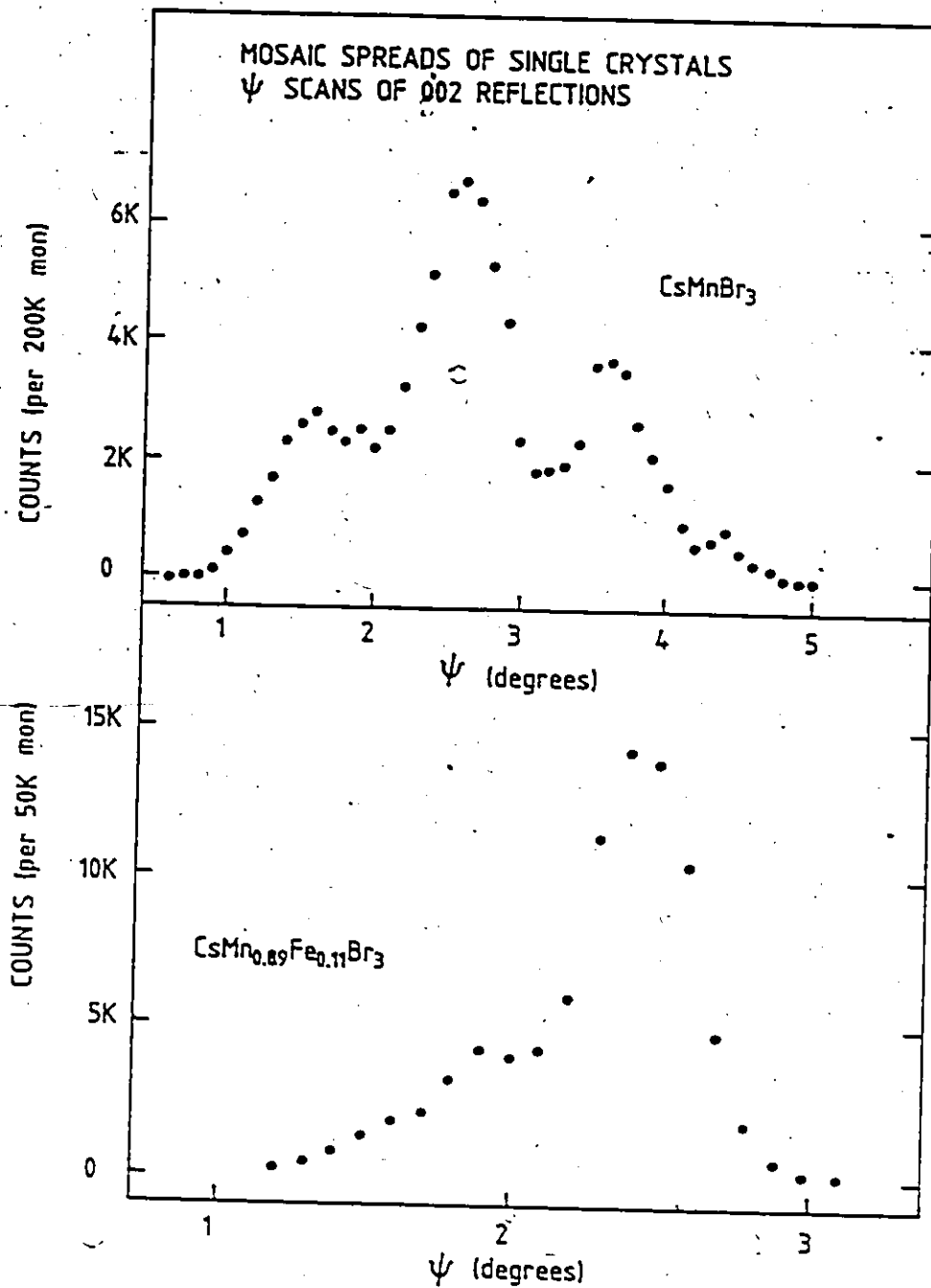


Figure A2: The mosaic spread of the two samples CsMnBr_3 and $\text{CsMn}_{0.89}\text{Fe}_{0.11}\text{Br}_3$. The CsMnBr_3 sample has an effective mosaic of $\sim 2^\circ$ while the superior quality $\text{CsMn}_{0.89}\text{Fe}_{0.11}\text{Br}_3$ crystal has a mosaic spread of $\sim .5^\circ$

CHAPTER 2
NEUTRON SCATTERING

2.1 The Neutron as a Probe of Condensed Matter

Since relatively strong sources of neutrons became available following the Second World War (via the development of nuclear reactors), the neutron has become the most powerful probe for exploring many interesting properties of condensed matter. To understand why this is so, we must consider three basic properties of the neutron. The neutron is a nucleon which carries no electric charge. It has a magnetic dipole moment of $\mu_n = -1.91 \mu_N$, where μ_N is the nuclear magneton. Finally, its rest mass is such that its de Broglie wavelength satisfies the equation $E = 81.80/\lambda^2$ with E in meV and λ in Å.

As a nucleon with no charge the neutron will interact weakly with condensed systems. To a good approximation, it will interact only via a very short range nuclear interaction with the nuclei in the target, or magnetically with magnetic moments in the condensed system. This implies two things. Firstly, a neutron beam will bathe the entire target system, as opposed to preferentially interacting with the surface as do most other probes. Secondly, the subsequent analysis can, for the most part, concern itself with single scattering events only.

The relationship between the neutron's energy and its wavelength means that neutrons of thermal (~ 25 meV) energies (as are copiously

produced in reactors) have wavelengths of the order of angstroms and frequencies in the terahertz region. These length and time ($2\pi/\omega$) scales are extremely well matched to those of spatial and temporal correlations in condensed matter. By using what are now standard moderation techniques (hot and cold sources), the energy spectrum of neutrons emerging from the reactor can be moved up and down to some extent, allowing the frequency range of 10^{10} to 10^{14} hertz and corresponding wavelength range of 30 to $.5 \text{ \AA}$ to become available for experiment. The new generation of spallation neutron sources (Rutherford Laboratory, U.K. and Los Alamos) should extend the frequency scale at the high or epithermal end considerably. Thus neutron scattering techniques can contribute to the understanding of static and dynamic correlations in condensed matter, both atomic and magnetic, on a very wide length and time scale.

2.2 The Neutron Scattering Cross-Section

The theory of neutron scattering has been very well treated by several authors (Squires, 1978 and Lovesey, 1984) and only those elements of the theory pertinent to understanding the experiments will be discussed here. We are interested in the magnetic correlations in several materials, but let us first consider two limiting cases of scattering; coherent and incoherent scattering.

For the most part we examine in this work the normal modes of simple magnetic systems where the degree of magnetic order is sufficiently high so as to give rise to the concept of an excitation from a co-operative ground state. The co-operative nature of the system means that wavevectors can be associated with the spatial correlations in the system and a magnetic

Brillouin zone remains a useful concept. We then expect the magnetic neutron scattering from this system to exhibit pronounced interference effects from the different correlated constituents of the co-operative system. This type of scattering is referred to as coherent, and well-defined structure appears in the wavevector dependence of the scattering.

Within the same sample the neutrons will interact with the target nuclei. This interaction depends partly on the interaction between the neutron magnetic moment and the nuclear spin (if there is one). Let us ignore the presence of isotopes of the elements in the samples. At any temperatures of interest here, these nuclear spins will be disordered and thus part of the nuclear scattering will show no interference effects. Any material with constituent nuclei with non-zero nuclear spin will display this nuclear incoherent scattering, which of course will have no or very little wavevector dependence associated with it.

Consider now the cross section for neutron scattering by an arrangement of magnetic moments on a Bravais lattice with the moment given by g_J times the total angular momentum J . The cross-section is given by

$$\begin{aligned} \frac{\partial^2 \sigma}{\partial \Omega \partial E'} &= \frac{(\gamma r_0)^2}{2\pi h} \frac{k'}{k} N \left\{ \frac{1}{2} g_J F(Q) \right\}^2 \sum_{\alpha\beta} (\delta_{\alpha\beta} - \hat{Q}_\alpha \hat{Q}_\beta) \\ &\times \sum_{\underline{\ell}} \exp(i\underline{Q} \cdot \underline{\ell}) \int_{-\infty}^{\infty} \langle \exp(-i\underline{Q} \cdot \underline{u}_0(0)) \exp(i\underline{Q} \cdot \underline{u}_\ell(t)) \rangle \\ &\times \langle J_0^\alpha(0) J_\ell^\beta(t) \rangle \exp(-i\omega t) dt \end{aligned}$$

In this expression r_0^2 and γ are constants such that $(\gamma r_0)^2 = .292$ barns/sr. The N magnetic sites are at equilibrium positions \underline{l} with possible displacements from equilibrium, $\underline{u}_l(t)$, at time t .

The wavevector transfer of the scattering event is defined as the vector difference between initial and scattered neutron wavevector; $\underline{Q} = \underline{k}^0 - \underline{k}^1$. It is often convenient to consider the wavevector transfer relative to the magnetic or nuclear zone centre. This reduced wavevector $\underline{q} = \underline{Q} - \underline{\tau}$, where $\underline{\tau}$ is a reciprocal lattice vector, enters naturally in most theories due to the periodicity of the lattice. The energy transfer of a scattering event is defined by the difference between incident and scattered neutron energies, $\hbar\omega = E_i - E_f$.

$F^2(\underline{Q})$ is the magnetic form factor and represents the Fourier transform of the spatial distribution of the scattering centre. A term such as this is common to all scattering cross-sections and in our case the scattering centre is the distribution of magnetic (unpaired) d-electrons at the Mn^{+2} or Fe^{+2} sites. This quantity falls off with increasing $|\underline{Q}|$ and the measurable magnetic response is limited to the relatively small $|\underline{Q}|$ regime.

If we neglect the effects of having the atoms not at their equilibrium sites, and replace the total angular momentum $\underline{J}_l^\alpha(t)$ by $\underline{S}_l^\alpha(t)$ (as we will be mainly interested in spin only systems) we can write the cross-section as

$$\frac{\partial^2 \sigma}{\partial \Omega \partial E^2} = C \frac{k^1}{k^0} F^2(\underline{Q}) \sum_{\alpha\beta} (\delta_{\alpha\beta} - \hat{Q}_\alpha \hat{Q}_\beta) S^{\alpha\beta}(\underline{Q}, \omega)$$

with

$$S^{\alpha\beta}(\underline{Q}, \omega) = \sum_{\underline{l}} \int_{-\infty}^{\infty} \exp(i\underline{Q} \cdot \underline{l}) \exp(-i\omega t) \langle S_0^{\alpha}(0) S_{\underline{l}}^{\beta}(t) \rangle dt$$

The physics of the system under investigation is contained in the dynamic pair correlation function $S(\underline{Q}, \omega)$ or its Fourier transforms. It is at this level that theory and experiment will normally be compared.

We restrict our consideration to the usual condition that $S^{\alpha\beta}(\underline{Q}, \omega)$ is zero for $\alpha \neq \beta$, where α and β are orthogonal axes (x,y,z). The effect of the Lorentz factor, $\sum_{\alpha\beta} (\delta_{\alpha\beta} - \hat{Q}_{\alpha} \hat{Q}_{\beta})$, is to pick out those dynamic correlation functions $\langle S_0^{\alpha}(0) S_{\underline{l}}^{\alpha}(t) \rangle$, for which α is perpendicular to the wavevector of the scattering event. This is to say we observe the spectrum of spin fluctuations lying in a plane perpendicular to \underline{Q} . Thus we can write

$$\frac{\partial^2 \sigma}{\partial \Omega \partial E'} = C \frac{k^1}{k^0} F^2(\underline{Q}) \sum_{\alpha \perp \underline{Q}} S^{\alpha\alpha}(\underline{Q}, \omega)$$

If the system has eigenstates, $|n\rangle$ of its Hamiltonian with energies $\hbar\omega_n$, which are known either exactly or approximately we can write

$$S^{\alpha\alpha}(\underline{Q}, \omega) = Z^{-1} \sum_{m,n} \exp(-\hbar\omega_n/kT) \langle n | S^{\alpha}(\underline{Q}) | m \rangle \\ \times \langle m | S^{\alpha}(-\underline{Q}) | n \rangle \delta(\omega - \omega_n + \omega_m)$$

where Z is the partition function and $S^{\alpha}(\underline{Q})$ is the Fourier transform in space of the spin operator.

In some cases the eigenstates and eigenvalues are not known even approximately and this treatment is inappropriate. If a sufficient amount

of information regarding the correlations in the system is known, theories can still be successful in describing the experiment by using a phenomenological equation of motion. This is the route we have used, for example, in describing our spin wave measurements in the paramagnetic regime of CsMnBr_3 by a generalized Langevin equation approach to the dynamics of this system.

Another approach is, in some approximate way, to solve for the equation of motion of some components of spin. The dynamic spin pair correlation function may then be calculated classically by summing or integrating over all relevant variables (which may include velocities, for example) weighted by the usual Boltzmann factor. This can then be Fourier transformed to produce $S^{\alpha\alpha}(Q, \omega)$. This method is used in our examination of the out-of-easy plane soliton response in CsMnBr_3 .

Before leaving this section we should mention that an equivalent description of the scattering (which is sometimes more useful) can be made in terms of the imaginary, or energy absorbing, part of the generalized susceptibility. It is related to $S^{\alpha\alpha}(Q, \omega)$ by the fluctuation-dissipation relation which connects the spectrum of fluctuations in a system to the possible dissipation or energy absorbing processes in that system. Thus we can write

$$S^{\alpha\alpha}(Q, \omega) = - \frac{\chi''(Q, \omega)}{\pi(1 - \exp(-\hbar\omega/kT))}$$

The imaginary part of the susceptibility is related to the real part of the susceptibility by a Kramers-Kronig relation and the limit of Q and ω going to zero in the real part of the susceptibility yields the static

susceptibility. A useful comparison of static susceptibility and neutron measurements can be made (although it is more complicated than that sketched here) using this result (Jackman, 1983).

In addition to the coherent magnetic scattering there will also be coherent nuclear scattering due to the normal modes of the lattice, the phonons. This scattering can be distinguished from the magnetic scattering in several ways. Firstly, while the intensity of the magnetic scattering falls off with increasing $|Q|$ due to the form factor, that of one-phonon scattering will increase as $(\hat{\epsilon} \cdot Q)^2$, where $\hat{\epsilon}$ is the eigenvector of the particular phonon. In addition for antiferromagnets, the magnetic Brillouin zone is a different size than the nuclear zone. Finally, the translational order of the nuclear lattice is usually broken up thermally on a different temperature scale from that of the magnetic lattice. For example in the crystals considered in this work, magnetic correlations are lost for temperatures greater than $\sim 100\text{K}$ while the crystals melt at roughly 900K . Hence temperature dependent scattering (in the neutron energy loss mode) below say 100K can be identified as magnetic in origin.

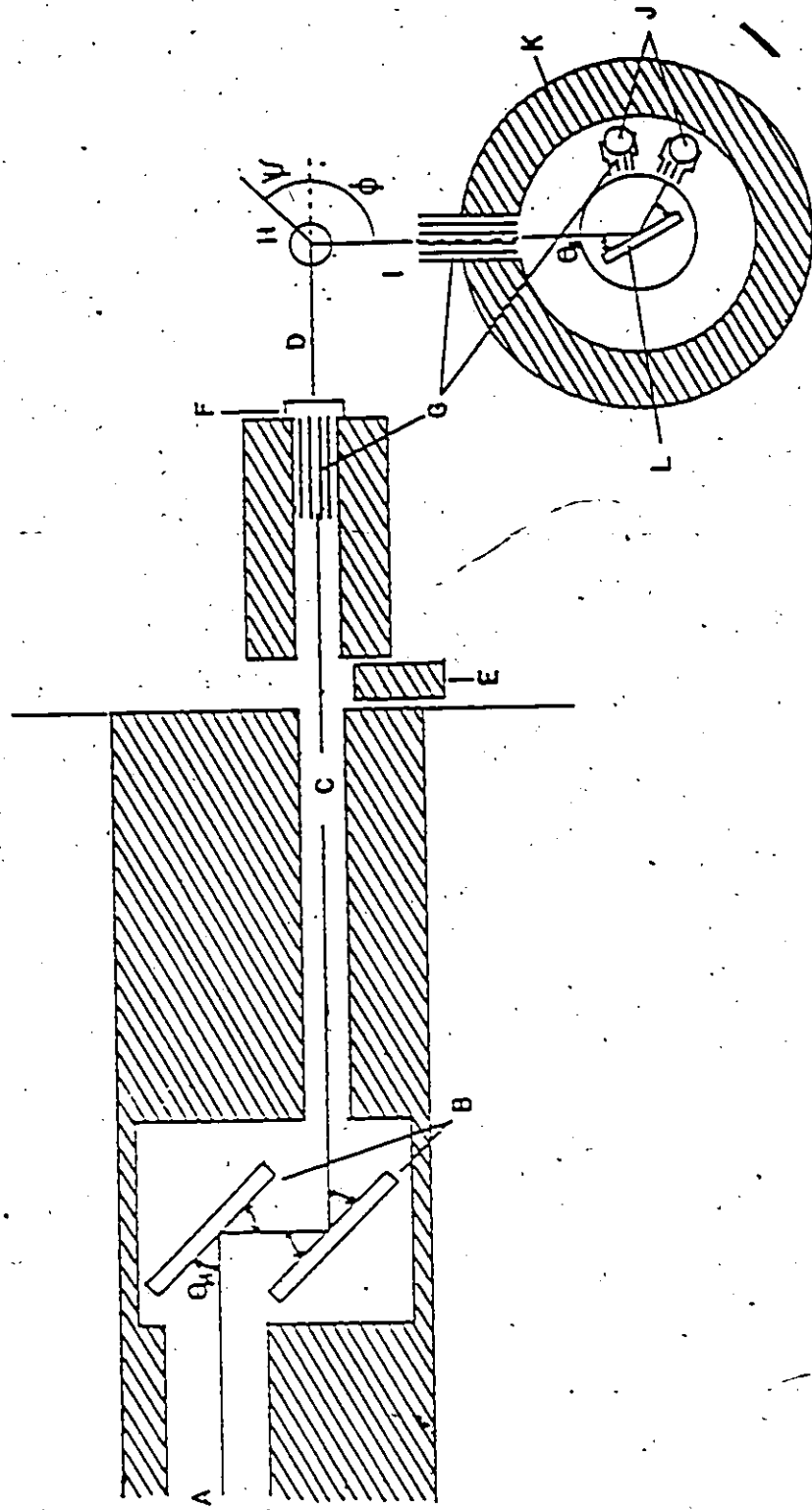
2.3 The Practice of Neutron Scattering

The two quantities of interest in characterizing a scattering event are the momentum transfer, $\hbar Q$, and the energy transfer, $\hbar\omega$ of the event. The neutron triple axis spectrometer, shown in schematic form in figure B1 is a spectrometer designed to allow a systematic study of selected regions of Q and ω space. This particular figure corresponds to a double monochromator spectrometer. The McMaster spectrometer (E-2) at the N.R.U. reactor, Chalk River, is such a spectrometer. A photograph of the spectro-

Figure B1: Schematic of McMaster triple-axis spectrometer.

- A hole in reactor wall
- B double crystal monochromator
- C monochromatic beam
- D beam incident on specimen
- E beam gate
- F fission chamber monitor
- G Soller-slit collimators
- H sample angling apparatus
- I counter angling apparatus
- J helium counters
- K parafin and cadmium shielding barrel
- L analysing crystal

This figure was taken from Locke (1981)



meter in operation is shown in figure B2. The more popular form of this spectrometer has only a single monochromator.

The spectrometer makes use of the Bragg reflection condition,

$$n\lambda = 2d\sin\theta$$

in order to select neutrons of a particular wavelength and direction. The physical origin of this condition is shown in figure B3.

Referring to figure B1 one can see that the spectrometer will accept a "white" (ie a Maxwellian distribution of neutrons centred on the energy corresponding to the temperature of the moderator) beam of neutrons moving in the proper direction towards the first monochromating single crystal. Neutrons of wavelength $n\lambda$ will be diffracted by atomic planes of spacing d in the first crystal. The second crystal is set so as to accept the neutrons diffracted from the first at the proper angle θ_m (for $n\lambda$ neutrons) and reflect this in a similar way towards the sample. At each stage in the path of the neutrons, collimators, or soller slits (guides with walls lined with neutron absorbing material) can be inserted to better define the beam's direction. At this point the incident neutron's energy (neglecting $n \neq 1$) and momentum have been established.

The beam then impinges on the sample which, in the case of single crystal studies, is mounted on a rotatable table with the sample's crystallographic axis in some known position relative to the direction of the incident beam. After interacting with the sample the scattered neutron will go off in arbitrary directions, however the detector arm of the spectrometer is set so as to accept neutrons scattered in the horizontal plane at angle ϕ to the incident direction. This beam of scattered neutrons may be passed through soller slits and then allowed to impinge on a single

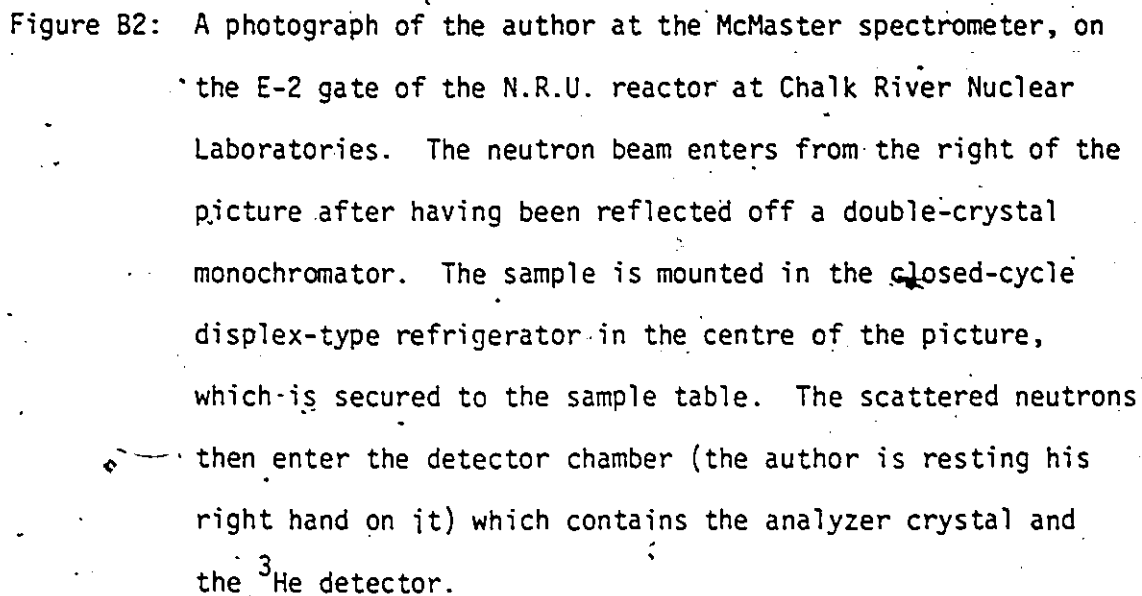


Figure B2: A photograph of the author at the McMaster spectrometer, on the E-2 gate of the N.R.U. reactor at Chalk River Nuclear Laboratories. The neutron beam enters from the right of the picture after having been reflected off a double-crystal monochromator. The sample is mounted in the closed-cycle displacer-type refrigerator in the centre of the picture, which is secured to the sample table. The scattered neutrons then enter the detector chamber (the author is resting his right hand on it) which contains the analyzer crystal and the ^3He detector.



8601-17675-1

ALUMINUM RESEARCH CO. LTD. - RESEARCH CO.
SHEPPARD AVENUE EAST
TORONTO, CANADA

crystal analyser at angle θ_A to some appropriate set of planes with spacing d_A in the analysing crystal. A high efficiency He^3 neutron detector will be set so as to accept neutrons of energy $n\lambda'$ diffracted from the crystal. The angle the detector must be set at, relative to the direction of the transmitted neutron beam, is $2\theta_A$ in order to satisfy the Bragg condition. This then establishes (again neglecting $n \neq 1$ in the Bragg condition) the scattered neutron beam's energy and momentum. Thus by adjusting the angles in the scattering geometry ($\theta_m, \phi, \psi, \theta_A$ and $2\theta_A$) a particular Q and ω can be investigated in a crystal. Usually the single crystal sample is aligned in such a way that the scattering plane (typically horizontal), defined as the plane spanned by k^0 and k^1 , contains relevant high symmetry crystallographic directions of the sample.

Information regarding the physics of the system under study is then derived from the relative intensities of scattered neutrons measured at different positions in Q and ω space for some set incident number of neutrons, or monitor count. This monitor count is performed by passing the incident beam through a low-efficiency fission neutron counter. As ideally the efficiency of the fission counter is proportional to $1/v^0 \propto 1/k^0$, if the measurements are made by keeping $|k^1|$ constant (as are all those reported here), the prefactor $\frac{k^1}{k^0}$ in the cross section yields only a constant and these relative intensities give relative strengths of $F^2(Q) \sum_{\alpha \perp Q} S^{\alpha\alpha}(Q, \omega)$.

Two methods for systematically getting this information are commonly used. The first and most common method is constant Q . Here the scattering geometry is manipulated such that the energy transfer is mapped out for some fixed point in Q space. Clearly not all of energy transfer space can

be covered for some fixed Q and fixed constant scattered neutron energy (a constant incident energy). The amount of this parameter space which is of interest to the experimenter influences his choice of spacing for both monochromator and analyser as these determine possible allowed wavelengths of neutrons such that the triangle $Q = k^0 - k^1$ can be formed.

The second method is the Constant Energy method in which the scattering geometry is manipulated such that some region in Q space is examined for a given energy transfer. Once again parameter space is limited by the condition that a closed triangle satisfying $Q = k^0 - k^1$ must be formed for any scattering event.

An important consideration in the design of any experiment is the resolution of the spectrometer and how it can be manipulated. We usually speak loosely in terms of specific wavelengths of the neutrons and precise angles of incidence relative to some planes in a perfect crystal. However due to a mosaic spread in all the crystals involved in the experiment (analyser, monochromator and sample) and to the divergence in angles that a neutron path may follow from one interaction to another in the spectrometer, both the wavevector and energy transfer of a scattering event in a real spectrometer are accepted within some characteristic range, $Q_0 \pm \Delta Q$ and $\omega_0 \pm \Delta\omega_0$.

These characteristic ranges can be manipulated in several ways. Use of a smaller constant scattered energy (for example) increases the energy resolution of a given measurement. Crystal monochromators and analysis making use of planes with larger d spacings can be used to achieve this end. Also the angular divergence of some path in the spectrometer can be re-

stricted by using narrower sollar slits to define the beam direction. It is also important to note that improved resolution of a measurement comes at the expense of time required to get the same integrated intensity. Therefore tight collimation and small mosaic spreads in the crystals may impede the experimenter in his attempts to understand the physical system. The choice of components in the spectrometer should be matched to the problem under investigation and to which regions of Q and ω space are of interest.

These effects have been considered in detail (Cooper and Nathans, 1967). The treatment that results is that the intensity of scattered neutrons is related to the cross section by a convolution with the resolution function, $R(Q_0 + \Delta Q, \omega_0 + \Delta\omega)$, of the spectrometer which depends on all the previously mentioned parameters. Thus the relevant quantity to compare with experiment is not the theoretical cross section, but

$$I(Q_0, \omega_0) = \iiint R(Q_0 + \Delta Q, \omega_0 + \Delta\omega) S(Q_0 + \Delta Q, \omega_0 + \Delta\omega) \partial \Delta Q \partial \Delta \omega$$

Table B1 contains the values of the experimental parameters entering in the resolution calculation for each of the experiments.

Consideration must also be addressed to the Bragg condition being satisfied for all neutrons of wavelength $n\lambda$ with $n > 1$, as well as the possibility of contributions to the measured spectrum where the scattering event in either the monochromator or analyser is not an elastic Bragg event. These are both common problems in practice.

The first of these, as pictured in figure B3, varies in importance

TABLE A1
EXPERIMENTAL PARAMETERS WHICH DETERMINE THE
RESOLUTION FUNCTION

Crystal	Scattering plane	d-spacing	Mosaic spread
Monochromator	Cu 220	1.2781	.33°
Analyser	Graphite 002	3.35	.42°
CsMnBr ₃	-	-	~ 2°
CsMn _{0.89} Fe _{0.11} Br ₃	-	-	~ .5°

	Collimation	
	Horizontal	Vertical
in pile	$\alpha_0 = 5.7^\circ$	$\beta_0 = 5.74^\circ$
mono-specimen	$\alpha_1 = .7^\circ$	$\beta_1 = 1.72^\circ$
specimen-anal.	$\alpha_2 = .7^\circ$	$\beta_2 = 1.72^\circ$
anal.-detector	1) $\alpha_3 = 4.76^\circ$	$\beta_3 = 28.65^\circ$
	2) $\alpha_3 = 2.36^\circ$	$\beta_3 = 28.65^\circ$

- 1) All experiments except those on CsMn_{0.89}Fe_{0.11}Br₃
- 2) CsMn_{0.89}Fe_{0.11}Br₃ experiments.

according to where the first order ($n=1$) neutron wavelength is, relative to the distribution in wavelengths of neutrons impinging on the crystal. The conditions $\frac{\lambda}{2}$, $\frac{\lambda}{3}$ etc. correspond to $4E$, $9E$, etc., thus if the number of neutrons with energy larger than the first order neutrons is a monotonically decreasing function of energy, then there will be many more first order neutrons compared with higher order neutrons. If this is not the case, then it becomes a more serious problem.

Some materials will transmit most neutrons incident on them within some relatively narrow energy range and be quite opaque for most other energies. Pyrolytic graphite is one such material with a neutron "window" at about 14.5 meV. When a beam of neutrons of constant energy is desired, (as our experiments with constant scattered neutron energy) such a material can be placed in the beam to eliminate contributions to the measured intensity due to λ/n with $n > 1$ wavelength neutrons.

The second of these considerations, pictured in figure B4, will enter whenever one is interested in the diffuse (ie. non-elastic) response of the sample. The origin of this problem is that any processes involving two elastic events plus one diffuse event in the three crystals (monochromator, analyser and sample) will contribute roughly the same intensity. Analysis always assumes the elastic events do not occur in the sample. However should conditions for a Bragg scatter in the sample either preceded by a diffuse scatter in the monochromator or followed by a diffuse scatter in the analyser which then allows this process to be counted occur, then the analysis may become confused. The most likely cause of a diffuse scattering is an incoherent nuclear elastic event. This process has little Q or directional dependence, does not change the energy of the

BRAGG REFLECTION CONDITION

$$n\lambda = 2d \sin\theta$$

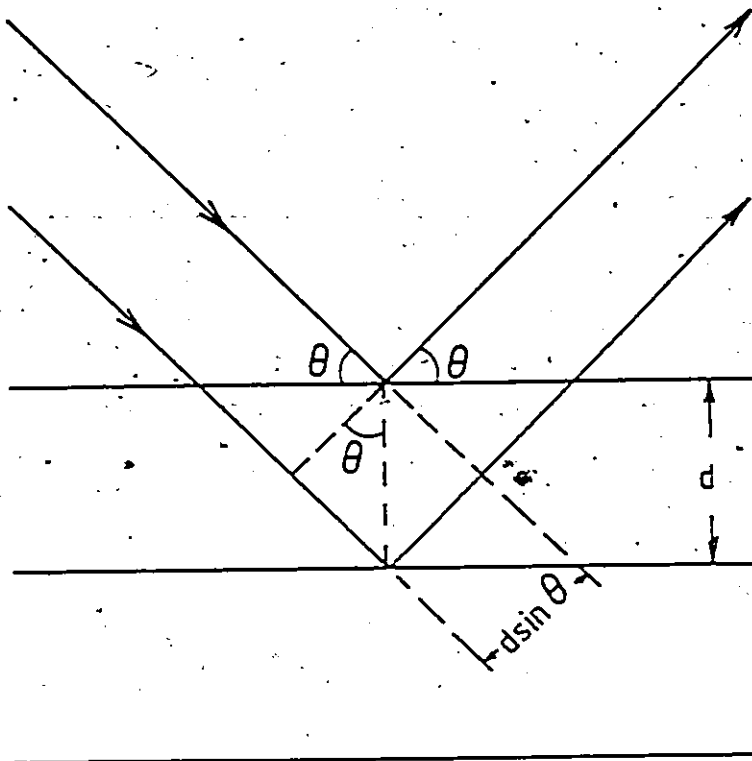


Figure B3: The Bragg reflection condition for neutrons scattered off atomic planes with spacing d between them is shown. Constructive interference occurs when the phase difference between the waves, $2d \sin \theta$, equals some integer times the wavelength. It is clear that λ/n neutrons will also be reflected by higher order (ie. $n > 1$) processes.

incident neutron and can be relatively intense. Events of this type can be identified by a diagram as figure 84, and it depends on a coincidence of parameters in the scattering geometry. Thus by changing the constant scattered energy value this type of event should disappear.

Considerations of the type mentioned above are not prohibitive to any experiment, but they must be kept in mind when analysing data.

SPURION SCATTERING EVENTS

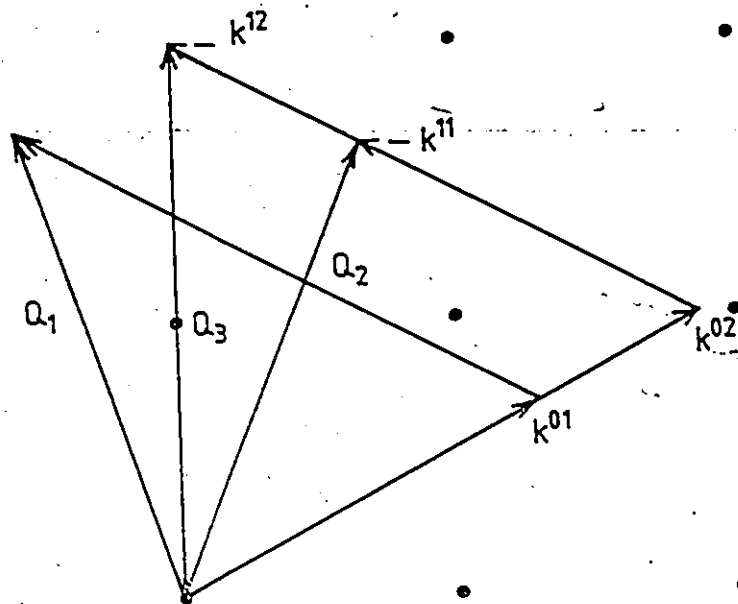


Figure B4: Two scattering events which yield spurious scattering are shown. In one case an attempt to observe scattering at $Q_1 = \underline{k}^{01} - \underline{k}^{12}$ is complicated by incoherent elastic scattering at the monochromator which yields a spurion at $Q_3 = \underline{k}^{02} - \underline{k}^{12}$. The second case shows an attempt to observe scattering at $Q_2 = \underline{k}^{02} - \underline{k}^{11}$ which is complicated by incoherent elastic scattering at the analyser which also yields a spurion at Q_3 .

CHAPTER 3

PARAMAGNETIC SPIN WAVES IN CsMnBr_3

3.1 Introduction

The low temperature phase of most magnetic materials is one which the magnetic moments in the system align together such that there is a net magnetization or sublattice magnetization present in the absence of an applied field. The excitations from this magnetically ordered ground state are usually called spin waves or magnons. These spin waves physically correspond to the coherent superposition of a single spin deviation from the order parameter vector (magnetization) over the entire crystal. As has already been mentioned, the pathological nature of the excitations and fluctuations in a truly one-dimensional system is sufficient to prevent the appearance of long-range order, and thus an order parameter, at any temperature above absolute zero. For this reason, the discovery of well defined normal modes across most of the magnetic Brillouin zone in $(\text{CH}_3)_4\text{NMnCl}_3$ (TMMC) (Hutchings et al., 1972) and CsNiF_3 (Steiner and Dornier, 1973) was initially somewhat of a surprise.

This section describes a neutron scattering study of the inelastic spectrum of CsMnBr_3 at low temperatures within the paramagnetic phase. The data are used to extract information as to the anisotropy of the spin interactions and to compare with recent theory which describes spin waves in the absence of long-range order.

3.2 The Neutron Scattering Experiment

Neutron measurements were made with the crystal mounted in a closed-cycle displax-type refrigerator with the $(hh\ell)$ plane in the scattering plane. Data were taken in the constant Q mode, primarily along $Q = (0,0,\ell)$ with ℓ running from 1.0 to 1.5. The scattered neutron energy was held constant at 14.65 meV, and a pyrolytic graphite filter was placed in the scattered beam to remove higher order contamination. The sample could be maintained at any temperature above a minimum of 15K.

At the lowest temperatures there were peaks in the neutron scattering which were essentially limited in their energy widths over most of the magnetic zone only by the resolution of the spectrometer. At small wave vectors ($q_c < 0.1$) the peaks took on considerable width and at the zone centre only a shoulder to the scattering is present. The energy attributed to the centre of these peaks is plotted against their reduced wave vector in figure C1.

3.3 Results and Low Temperature Analysis

Conventional spin wave theory is applicable for a fully ordered chain and this has been applied to the case of a one-dimensional system with nearest-neighbour antiferromagnetic exchange interactions and long-range dipolar interactions by Deitz et al. (1974). In one dimension the dipole sums converge rapidly and the predictions of this theory are plotted for CsMnBr_3 in figure C1. The theory produces two branches of excitation which are nearly degenerate except near the magnetic zone centre. The two branches correspond to fluctuations within and perpendicular to the easy plane, which, as was previously mentioned, is formed as a result

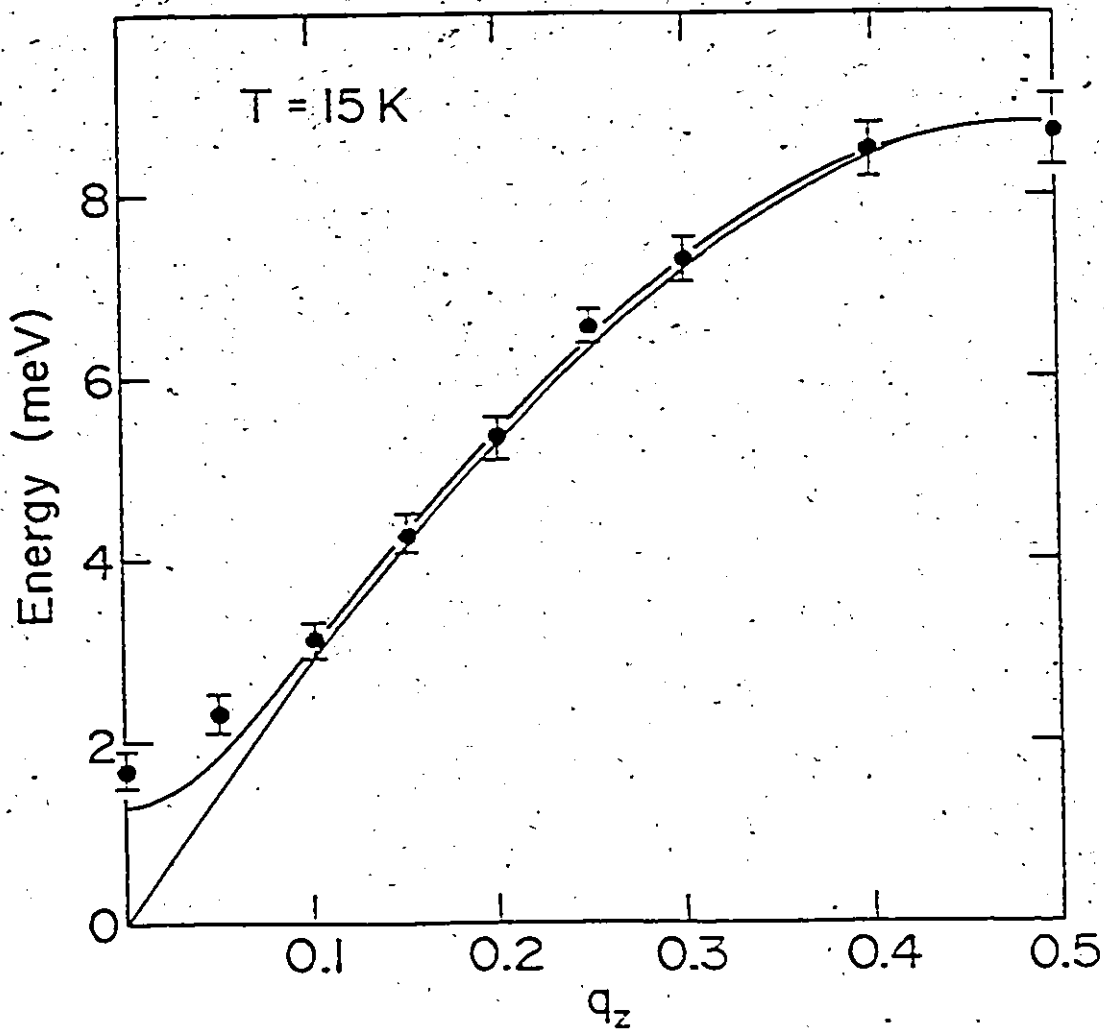


Figure C1: The measured spin wave dispersion of CsMnBr₃ at T = 15K is shown. The solid lines are the predictions of linear spin wave theory as derived by Walker et al (1972) for a classical one-dimensional magnetic system with Heisenberg exchange and dipolar interactions. The zero temperature theory is exact and predicts two branches of excitation corresponding to fluctuations within and perpendicular to the dipole-induced easy plane.

of this type of long-range interaction. A rotation of all the spins together within the easy plane costs zero energy, while a rotation out of the easy plane must still overcome the anisotropy energy associated with the dipolar forces. Thus the in-plane fluctuation branch goes to zero energy at zero wave vector while the out-of-plane branch goes to some finite energy at the zone centre.

Comparison between this zero-temperature theory and our experiment shows that the anisotropy energy gap at $q_c = 0$ is slightly larger than predicted by the dipole sums alone. The calculation predicts a zone centre energy of 1.2 meV while we measure an energy of 1.7 ± 0.2 meV. It is interesting to make this same analysis for TMMC. In this case the Mn-Mn distance along the chain is almost exactly the same as in CsMnBr_3 thus the strength of dipolar interactions should be almost the same. However for TMMC, the experiment (Heilmann et al., 1979) shows the zone centre mode at 0.8 ± 0.1 meV while the theory calculates a gap of 1.0 meV.

As Mn^{+2} corresponds to an S-state Hund's rule configuration, additional anisotropic interactions of the form $D \sum_i (S_i^z)^2$ are expected to be very small. Terms of this type have been considered for both CsMnBr_3 and TMMC by Edgar et al. (1980) and Kalt et al. (1983) respectively. In both cases they calculate positive values for D , although larger for CsMnBr_3 than for TMMC. This positive value for D tends to reinforce the dipolar easy plane and thus raise the energy of the zone centre gap to 1.5 meV in the CsMnBr_3 case and 1.1 meV for TMMC. This brings the expected gap energy for CsMnBr_3 within uncertainty of experiment but leads to an even greater discrepancy between theory and experiment for TMMC. It should be pointed

out however, that this last term in the Hamiltonian is hard to calculate with confidence as it is so small for the Mn^{+2} configuration.

The two modes are degenerate at the zone boundary with energy $4JS$ where J is the nearest neighbour exchange constant. Zero temperature analysis by Heilmann et al. (1981) showed that the gap energy at the zone centre for such a system is given approximately by

$$\Delta = 4JS \sqrt{\frac{D}{J}}$$

for anisotropy of arbitrary strength D in a Hamiltonian of the form

$$H = -2J \sum_i S_i \cdot S_{i-1} - D \sum_i S_i^z S_{i-1}^z$$

Thus our experiment yields the parameters J and D in the Hamiltonian

$$J = -0.88 \pm 0.01 \text{ meV}$$

$$D = 0.033 \pm 0.009 \text{ meV}$$

This D value is an effective planar anisotropy parameter which is set by the experimental spin wave energy at the zone centre.

Two constant Q scans at $Q = (0.6, 0.6, 1.0)$ and $Q = (0.1, 0.1, 1.0)$ are shown in figure C2. These are at the same one-dimensional wave vector ($Q_z = 1.0$) but they sample different weights of the in-plane and out-of-plane fluctuations. It is clear that the scan at $Q = (0.1, 0.1, 1.0)$ shows only a shoulder while that at $Q = (0.6, 0.6, 1.0)$ shows a sharper structure at roughly 1.7 meV. In addition there is more magnetic intensity present in the $Q_x = 0.6$ scan than in the $Q_x = 0.1$ scan despite the depression of the intensity by the magnetic form factor of the $Q_x = 0.6$

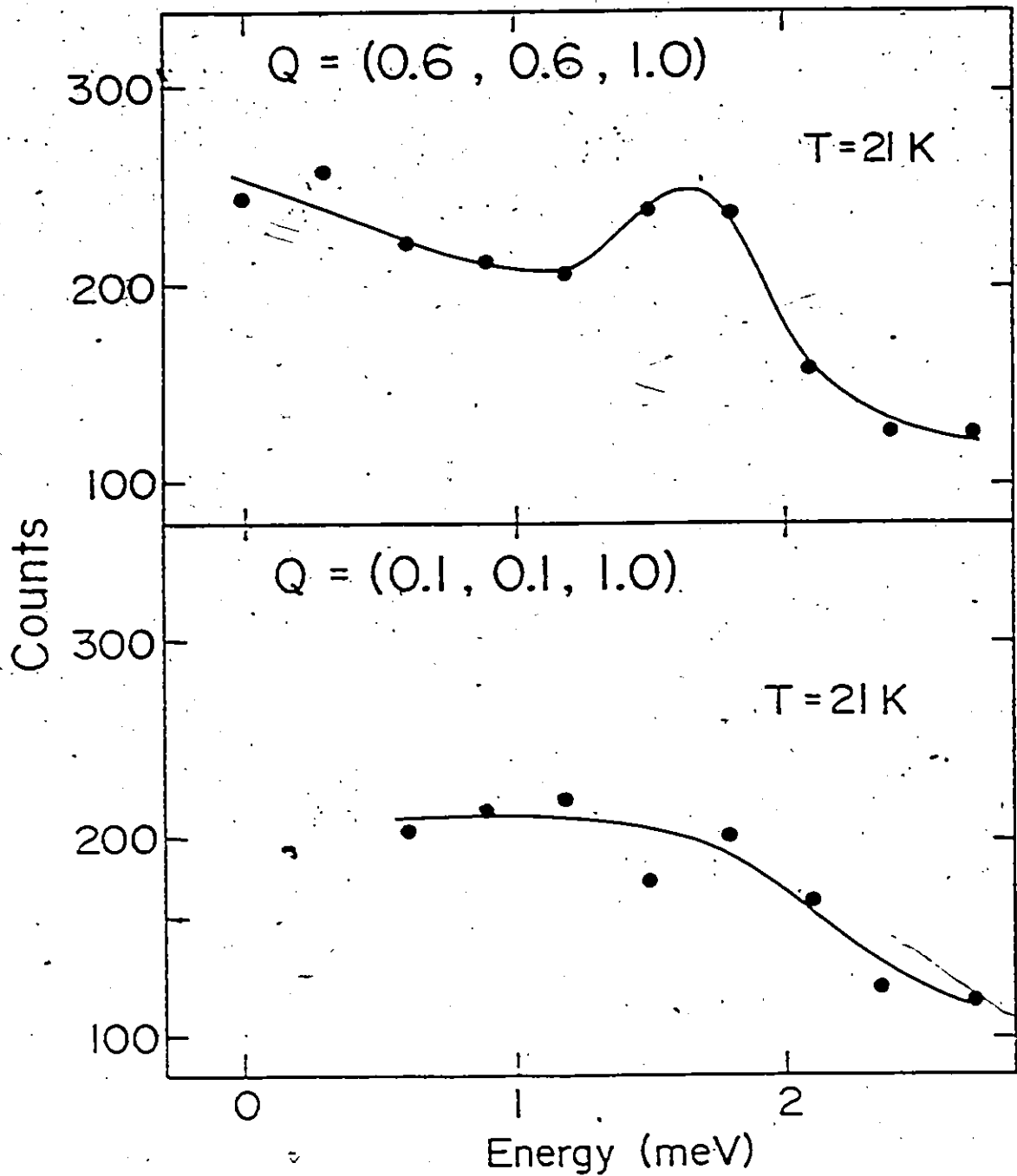


Figure C2: Constant Q scans at the magnetic zone centre ($Q_z = 1.0$) at $T = 21\text{K}$, are shown. The upper panel at $\underline{Q} = (0.6, 0.6, 1.0)$ shows more of a peaked structure than the $\underline{Q} = (0.1, 0.1, 1.0)$ scan and this we take as evidence of the out-of-easy plane polarization of this damped mode at ~ 1.7 meV.

scan. We take this as evidence that the shoulder and peak at the magnetic zone centre corresponds to a damped spin wave model which is preferentially out-of-plane, or zz , in polarization.

We do not observe the second predicted branch which goes to zero energy at zero wave vector and corresponds to fluctuations within the easy plane. Magnetic scattering is observed below the gap mode at 1.7 ± 0.2 meV at the zone centre but no peak or shoulder is found. This is not in disagreement with the ideas of theory, as this predicted mode is for $T = 0$ while our experiment is performed at $T = 15K$.

The spectrum of the two types of fluctuations are expected to display qualitatively different temperature dependence near the zone centre for two reasons. Firstly the in-plane correlations have a much larger characteristic length than do the out-of-plane correlations at low temperature; but this length is much more temperature dependent than for the out-of-plane case. This will be discussed in more detail in a subsequent section. More importantly however, their dispersion relations near the zone centre are very different with the out-of-plane fluctuations energy coming in flat at the zone centre while the in-plane fluctuations go to zero energy linearly with q_c .

The terms magnetic zone and zone centre have been (and will continue to be) used freely in the discussion. At finite temperature though the ideal system is paramagnetic and thus what we refer to as the zone centre is actually the maximum of $\chi(q)$ which occurs in sheets across $(h\ell)$ with ℓ odd. The correlations, while not of infinite range, are sufficiently long so that the concept of a magnetic zone remains valid. However we

must think of the zone as only being defined to within $1/\xi$ where ξ is the correlation length. We have already seen that Fisher's exact solution for ξ of the classical Heisenberg model in one dimension produces a $\xi \sim 1/T$ at small temperatures. Thus it is infinite in the limit of zero temperature (long range order) and hence the magnetic zone is exactly defined. At infinite temperature the correlation length is zero and the magnetic zone is not defined at all.

At low temperatures it is convenient to think of the spin wave response coming from a superposition of mismatched magnetic zones where the degree of mismatch is $1/\xi$. This is shown for each spectrum of fluctuations in figure C3. As the temperature is raised the mismatch increases and the intrinsic width of the neutron response as measured in a constant Q experiment would increase. However in the case of the out-of-plane spectrum at small mismatch, spin waves of the same energy are mixed together due to the flatness of the dispersion at the zone centre. Hence a sharper (relative to the in-plane spectrum) response is expected and it should give a better measure of the lifetime of the spin wave due to the thermal population of other excitations.

Now let us examine the spin waves in the middle of the zone. If we choose spin waves of wave vectors where the two branches are almost degenerate ($q_c > 0.15$) and examine the fluctuations within the easy plane ($Q \parallel c$) the dipolar anisotropy effects on the spin dynamics should be small. A detailed comparison between the theory of spin dynamics in a Heisenberg chain system and our neutron measurements would then be relevant. It is clear that this theory must be qualitatively different than conventional

MAGNETIC ZONE MIXING ARGUMENT FOR SPIN WAVE ENERGY WIDTHS

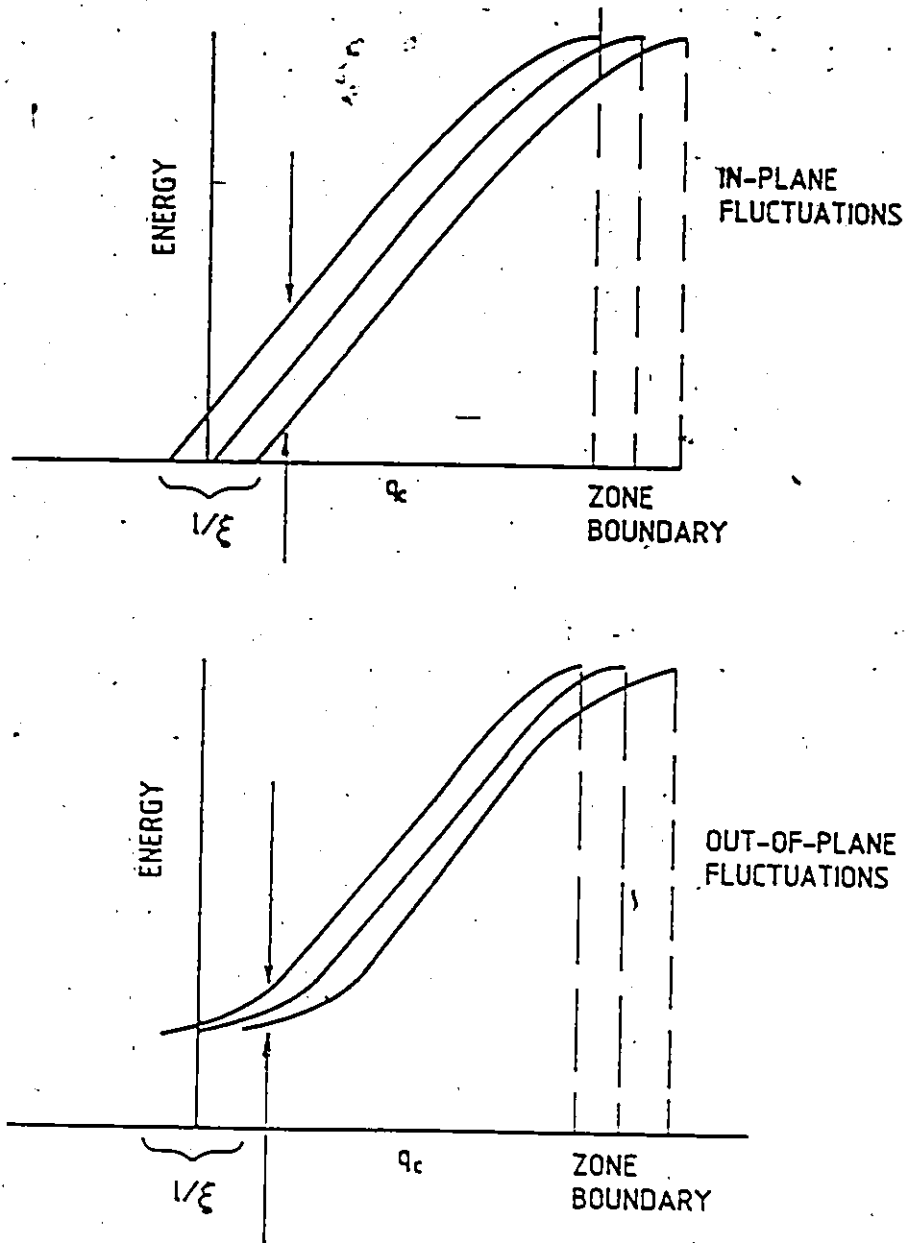


Figure C3: The diagram displays the argument by which the out-of-easy-plane fluctuations should appear sharper in energy than the in-plane fluctuations near the magnetic zone centre. Also as $\xi \sim 1/T$ at low temperature it is easily seen how all the spin waves broaden in energy as the temperature is raised.

linear spin wave theory as no order parameter vector about which the spins can oscillate (thinking classically) now exists.

3.4 Results and the Generalized Langevin Equation Approach to Spin Dynamics

The theoretical approach which we will apply to the problem of spin dynamics in the absence of an order parameter will be the generalized Langevin equation approach due originally to Mori (1965 a,b). It was applied first to magnetism by Lovesey and Merserve (1973) and to the one-dimensional Heisenberg chain by Lovesey (1974). It is sufficiently general though that it can be applied to many diverse problems such as density fluctuations in liquids (Lovesey 1973).

It is convenient to write the dynamic structure factor, $S^{\alpha\alpha}(\underline{Q},\omega)$, in terms of a function which has nice analytic properties, $F^{\alpha\alpha}(\underline{Q},\omega)$ (Marshall and Lowde, 1968). The two are related by

$$S^{\alpha\alpha}(\underline{Q},\omega) = \chi(\underline{Q}) \frac{\omega}{[1-\exp(-\omega/kT)]} F^{\alpha\alpha}(\underline{Q},\omega) \quad (3.1)$$

A phenomenological equation of motion is written for one component (which is arbitrary for a Heisenberg system) of the dynamic spin pair correlation function which is Fourier transformed in space

$$\frac{\partial S^{\alpha\alpha}(\underline{Q},t)}{\partial t} = - \int_0^t d\bar{t} K(\underline{Q},t-\bar{t}) S^{\alpha\alpha}(\underline{Q},\bar{t}) + f(\underline{Q},t)$$

This Langevin equation of motion is similar to what one might expect for a particle experiencing Brownian motion. That is that the variable under question, $S^{\alpha\alpha}(\underline{Q},t)$, is being randomly jostled about by some random force,

$f(Q,t)$, while it has some short time memory of correlations in its environment which are built into the theory by the as yet unspecified memory function $K(Q,t-\bar{t})$.

In terms of the relaxation function (the frequency Fourier transform of $F(Q,\omega)$), $F(Q,t)$ one can write

$$\frac{\partial F^\alpha(Q,t)}{\partial t} = - \int_0^t d\bar{t} K(Q,t-\bar{t}) F^\alpha(Q,\bar{t}) \quad (3.2)$$

which has the considerable advantage that it no longer involves the random force $f(Q,t)$.

The Laplace transform of equation (3.2) is particularly simple (dropping references to the arbitrary components).

$$\tilde{F}(Q,s) = \frac{F(Q,t=0)}{s + \tilde{K}(Q,s)} = \frac{1}{s + \tilde{K}(Q,s)}$$

The memory function, $K(Q,t)$, satisfies a similar equation of motion in terms of a higher order memory function which also satisfies this type of equation in terms of still higher order memory functions. The result is that a continued fraction expression for $\tilde{F}(Q,s)$ can be written

$$\tilde{F}(Q,s) = \frac{1}{s + \frac{K^{(1)}(Q,t=0)}{s + \frac{K^{(2)}(Q,t=0)}{s + \dots}}}$$

If all the $K^{(n)}(Q,t=0)$ functions can be constructed then $\tilde{F}(Q,s)$ is known and the scattering can be understood completely by using the relation

$$\pi F(Q, \omega) = \text{Re}\{\tilde{F}(Q, i\omega)\}$$

Clearly this analysis is limited by two factors. First, how many $K^{(n)}(Q, t=0)$ functions are known, and second how can this continued fraction expression be truncated. They are somewhat interdependent as the number of $K^{(n)}(Q, t=0)$ known will determine where the truncation must be made.

The short time expansion of $F(Q, t)$ can be written as

$$F(Q, t) = 1 - \frac{t^2 \langle \omega^2 \rangle}{2!} + \frac{t^4 \langle \omega^4 \rangle}{4!} - \dots$$

where $\langle \omega^n \rangle$ is the nth frequency moment of $F(Q, \omega)$ defined by

$$\langle \omega^n \rangle = \int_{-\infty}^{\infty} \omega^n F(Q, \omega) d\omega$$

Then the function $F^{(n)}(Q, t=0)$ can be expressed, in terms of $\langle \omega^n \rangle$. In turn the nth frequency moment is expressible in terms of products of up to the n spin static correlation functions (Marshall and Lowde, 1968). Ultimately the difficulty in calculating these static correlation functions is what limits the process.

For the classical Heisenberg chain the first three (non-zero) static correlation functions are known exactly at all temperatures. This forces the truncation to be at either the third or fourth level (or pole).

The relevant relations are:

$$K^{(1)}(Q, t=0) = \langle \omega^2 \rangle$$

$$K^{(2)}(Q, t=0) = \langle \omega^4 \rangle / \langle \omega^2 \rangle - \langle \omega^2 \rangle^2$$

$$K^{(3)}(Q, t=0) = \frac{\langle \omega^6 \rangle / \langle \omega^2 \rangle - \langle \omega^4 \rangle^2 / \langle \omega^2 \rangle^2}{-K^{(2)}(Q, t=0)}$$

Exact expressions for $\langle \omega^2 \rangle$ and $\langle \omega^4 \rangle$ are given in Lovesey (1974) and for $\langle \omega^6 \rangle$ in Tomita and Mashiyama (1972 and 1974). Approximate low temperature expressions are given for the moments through to $\langle \omega^{10} \rangle$ by H. de Raedt (1979). To avoid possible confusion we should point out that in this theoretical work the zero temperature zone boundary frequency of the spin waves is defined as $\omega_{ZB} = 4JS'$ with $S' = \sqrt{S(S+1)}$. Thus the exchange constant is not 0.88 meV but rather 0.74 meV. Of course this is a matter of definition only.

The other consideration is how the truncation of the continued fraction must be made. Lovesey (1974) proposes to replace $\tilde{K}^{(3)}(s)$ by $\tilde{K}^{(3)}(0)$ in the three pole truncation of the theory which then gives a closed form expression for $\bar{F}(Q, s)$ if a closed form for $\tilde{K}^{(3)}(0)$ is known. This approximation is justified if $\tilde{K}^{(3)}(s)$ is a slowly varying function of s or if $K^{(3)}(t)$ decays rapidly enough compared to the time scale of the spin dynamics.

The only exact information we know about the memory function is that it is a monotonically decreasing function of time and that it eventually goes to zero. That is, $|K(t)| \leq K(0)$ and $K(\infty) = 0$. Consistent with this, Lovesey proposed a Gaussian form for $K(t)$, which is

$$K(t) = K^{(1)}(Q, t=0) \exp\left\{-\frac{K^{(2)}(Q, t=0)t^2}{2}\right\}$$

This forces the truncation at the third level or pole to use

$$\tilde{K}^{(3)}(s) = \tilde{K}^{(3)}(0) = \left(\frac{\pi}{2} K^{(2)}(Q, t=0)\right)^{0.5}$$

The resulting expression for $F(Q, \omega)$ is

$$\pi F(Q, \omega) = \frac{K^{(1)}(Q, t=0)K^{(2)}(Q, t=0)}{[\omega(\omega^2 - K^{(1)}(Q, t=0) - K^{(2)}(Q, t=0))]^2 + \tilde{K}^{(3)}(0)[\omega^2 - K^{(1)}(Q, t=0)]^2}$$

and within these approximations the scattering is completely determined.

De Raedt and De Raedt (1977) and H. De Raedt (1979) propose a somewhat different truncation function and work to a higher level or pole expansion in the continued fraction. If we wish to work only with the exactly known static correlation functions then we need only their truncation functions or termination schemes at the third and fourth levels. This particular work is done in terms of the imaginary part of the generalized susceptibility, which was previously defined and the truncation functions used are

$$\tilde{K}^{(3)}(s) = (\langle \omega^4 \rangle / \langle \omega^2 \rangle)^{0.5}$$

$$K^{(4)}(s) = \left\{ \frac{\langle \omega^6 \rangle / \langle \omega^2 \rangle - 2\langle \omega^4 \rangle + \langle \omega^2 \rangle^2}{[\langle \omega^4 \rangle / \langle \omega^2 \rangle - \langle \omega^2 \rangle]} \right\}^{0.5}$$

The contention is made by De Raedt that an odd pole termination should produce a non-physical central mode in $S^{\alpha\alpha}(Q, \omega)$. Thus an even pole termination should be more desirable in describing the experiments. We will now

compare the neutron groups with the predictions of the three forms of the theory which we have just sketched. These are the three pole continued fraction expressions due to Lovesey as well as the three and four pole expressions due to the De Raedts.

Our experimental results for spin waves at $Q = (0,0,1.15)$, $Q = (0,0,1.2)$ and $Q = (0,0,1.3)$ are shown as a function of temperature in figures C4, C5 and C6. These wavevectors correspond to 30%, 40% and 60% of the way from magnetic zone centre to zone boundary respectively. As $Q \parallel c$ where c is the chain axis, all these measurements sample fluctuations within the easy plane. In addition all three are at sufficiently large wavevector that the energy difference between in and out of easy plane spin waves is very small. Finally it should be noted that as the temperatures of the measurements are just lower and larger than the characteristic temperature that defines the strength of the easy plane, $T = 20K \approx \hbar\omega(q=0)$, we expect then that the comparison to the theory of the dynamics of the Heisenberg chain is relevant. We will return to this point later.

The lineshapes of the neutron groups are seen to be quite sharp at our lowest temperature of 15K, with energy widths close to those determined solely by the spectrometer's resolution (~ 1 meV). The groups all broaden out markedly with increasing temperature and the peak of the distributions for the $Q_z = 1.2$ and 1.3 move to lower energy. The $Q_z = 1.15$ groups show very little temperature renormalization of their peak energies at all. Neutron groups for spin waves at $Q = (0,0,1.1)$, 20% of the way to the zone boundary, are shown in figure C7. Here this trend continues as the peak in the spin wave spectrum moves up in energy slightly from $3.0 \pm .2$ meV at 15K to $3.2 \pm .2$ meV at 35K. This change in energy is just

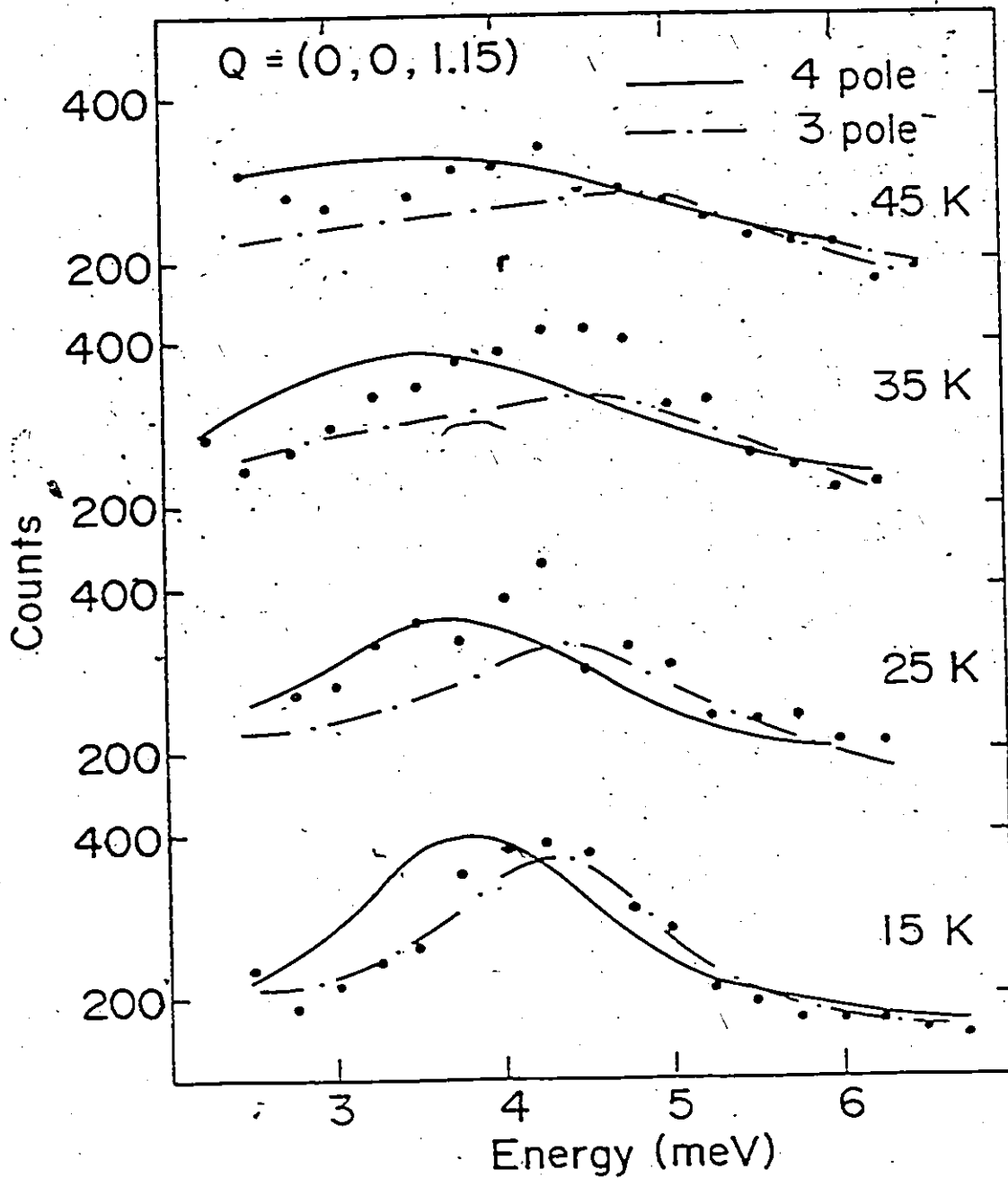


Figure C4: Constant Q scans at $Q = (0, 0, 1.15)$ as a function of temperature are compared with the predictions of Lovesey's three pole model and the De Raedts' four pole model of the dynamics of the classical Heisenberg spin chain.

within our experimental sensitivity. Neutron groups at $Q = (0,0,1.1)$ are too close to the anisotropy influenced zone center response though to be used for comparison to the theory of dynamics of the Heisenberg chain.

Upwards renormalization of the spin wave energy with temperature for low energy (zone centre) spin waves is consistent with this theory. This is due in part to the form of the dynamic structure factor equation (3.1). The theory solves for $F^{\alpha\alpha}(Q,\omega)$, which, for a given Q is some peaked function of ω . However if the peak in ω is sufficiently broad then the prefactor ω connecting $F(Q,\omega)$ and $S(Q,\omega)$ will distort the peak causing an increase in intensity on the high ω side of the peak. Hence if $F(Q,\omega)$ does not produce a peak which falls to lower ω quickly enough, the observed $S(Q,\omega)$ will display a peak moving to higher energy with increasing temperature. This behaviour has been observed for low q_c spin waves in TMMC (Hutchings et al., 1972).

The resulting theoretical curves for $S(Q,\omega)$ are plotted on top of the data in figures C4, C5 and C6. For the $Q = (0,0,1.2)$ and $Q = (0,0,1.3)$ neutron groups, the theories with third pole termination of the continued fraction due to Lovesey as well as the third and fourth pole terminations of the De Raedts are shown. For the $Q = (0,0,1.15)$ group only the three pole, Lovesey, termination and the four pole, De Raedt, terminations are shown. In all cases the lineshape produced by the theory is convoluted with the resolution function of the spectrometer according to the method of Cooper and Nathans (1967).

As the zone boundary spin wave frequency determines J , the only disposable parameter in the comparison is the intensity of the theoretical curve at one point and temperature. This is done by forcing all versions.

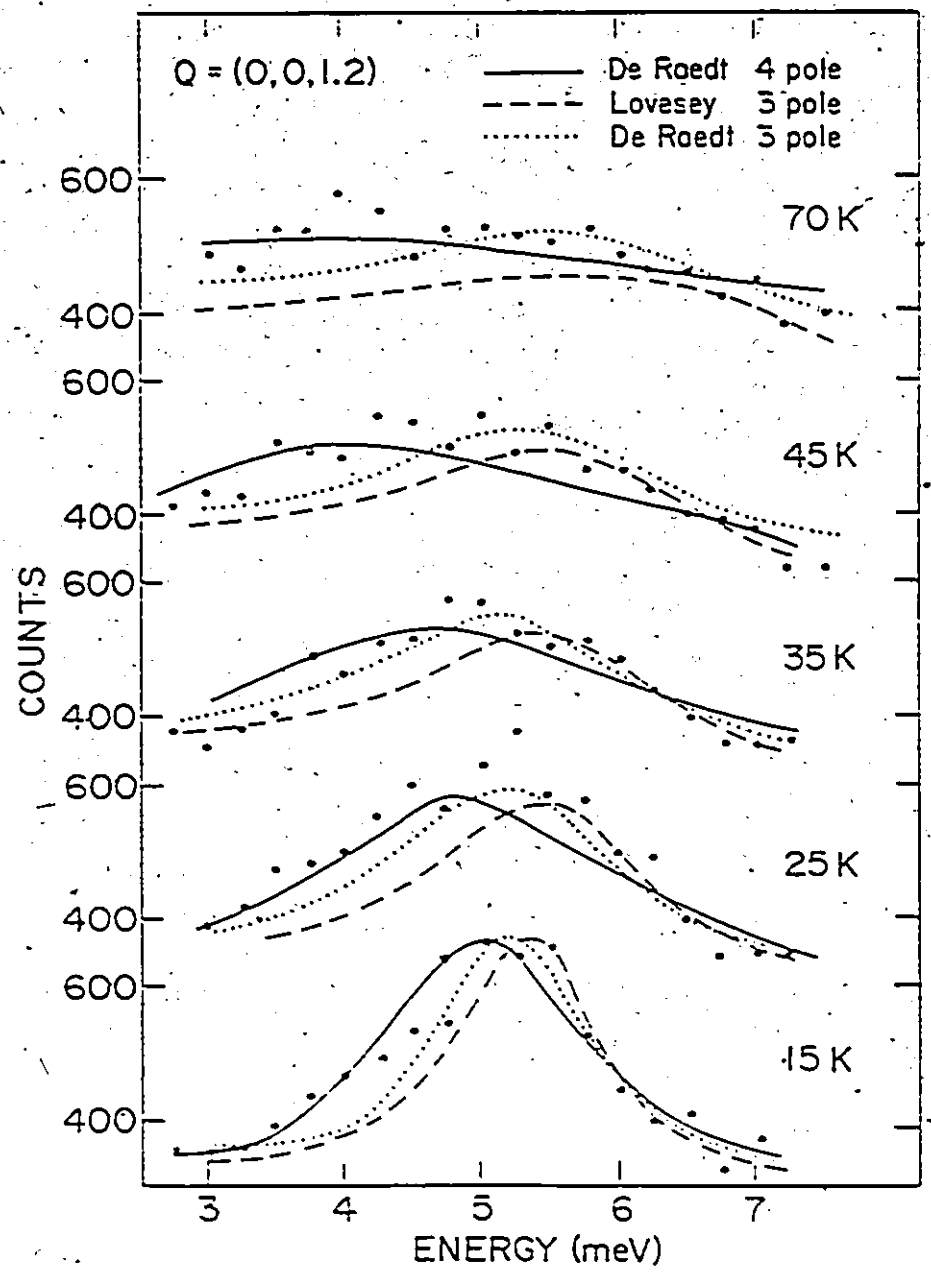


Figure C5: Inelastic scattering at $Q = (0,0,1.2)$ with temperatures of 15, 25, 35, 45 and 70K are compared with the predictions of the Lovesey three pole model and the De Raedt three and four pole models.

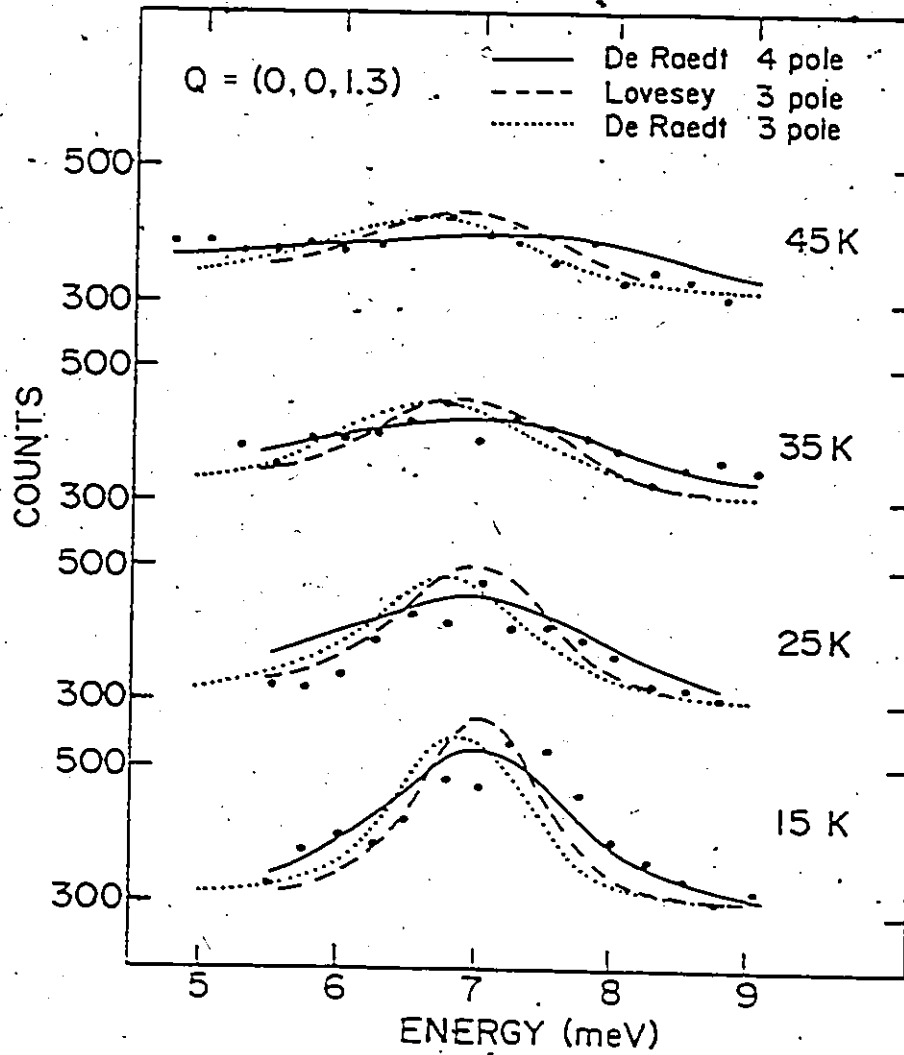


Figure C6: Inelastic scattering at $Q = (0,0,1.3)$ with temperatures of 15, 25, 35 and 45K are compared with the predictions of the Lovesey three pole and the De Raedt three and four pole models.

of the theory to produce the correct intensity of the peak in $S(Q,\omega)$ at $T = 15\text{K}$ and $Q = (0,0,1.2)$.

The analysis suggested by the De Raedts (De Raedt and De Raedt (1977) and De Raedt (1979)), produces integrated intensities for the neutron groups which do not vary with wavevector according to the exactly known $\chi(Q)$ (Fisher (1964)). At low temperatures in fact the integrated intensities are found to be independent of wavevector. This is clearly due to an omission of the $\chi(Q)$ factor in their analysis, which does not affect the peak positions, lineshape or intrinsic wavevector dependence on the intensities produced by their formalism. We have avoided this difficulty by fitting this intensity at $T = 15, Q = (0,0,1.2)$ and scaling the intensities of the other wavevectors by the exact form of $\chi(Q)$ for the classical Heisenberg antiferromagnetic chain.

Clearly there are discrepancies between the theory and the measured neutron lineshapes. However the theory does do several things well. It puts the low temperature peaks at roughly the correct energy. It produces roughly the right kind of low temperature width in energy (although this is largely determined by the resolution of the spectrometer). Finally it produces a peak which becomes overdamped and disappears on the correct temperature scale.

The peaks however do not renormalize necessarily in the correct direction (up or down in energy) with increasing temperature. Somewhat surprisingly the higher order termination, the four pole termination, does not produce a better representation of the data than the three pole version of the theory.

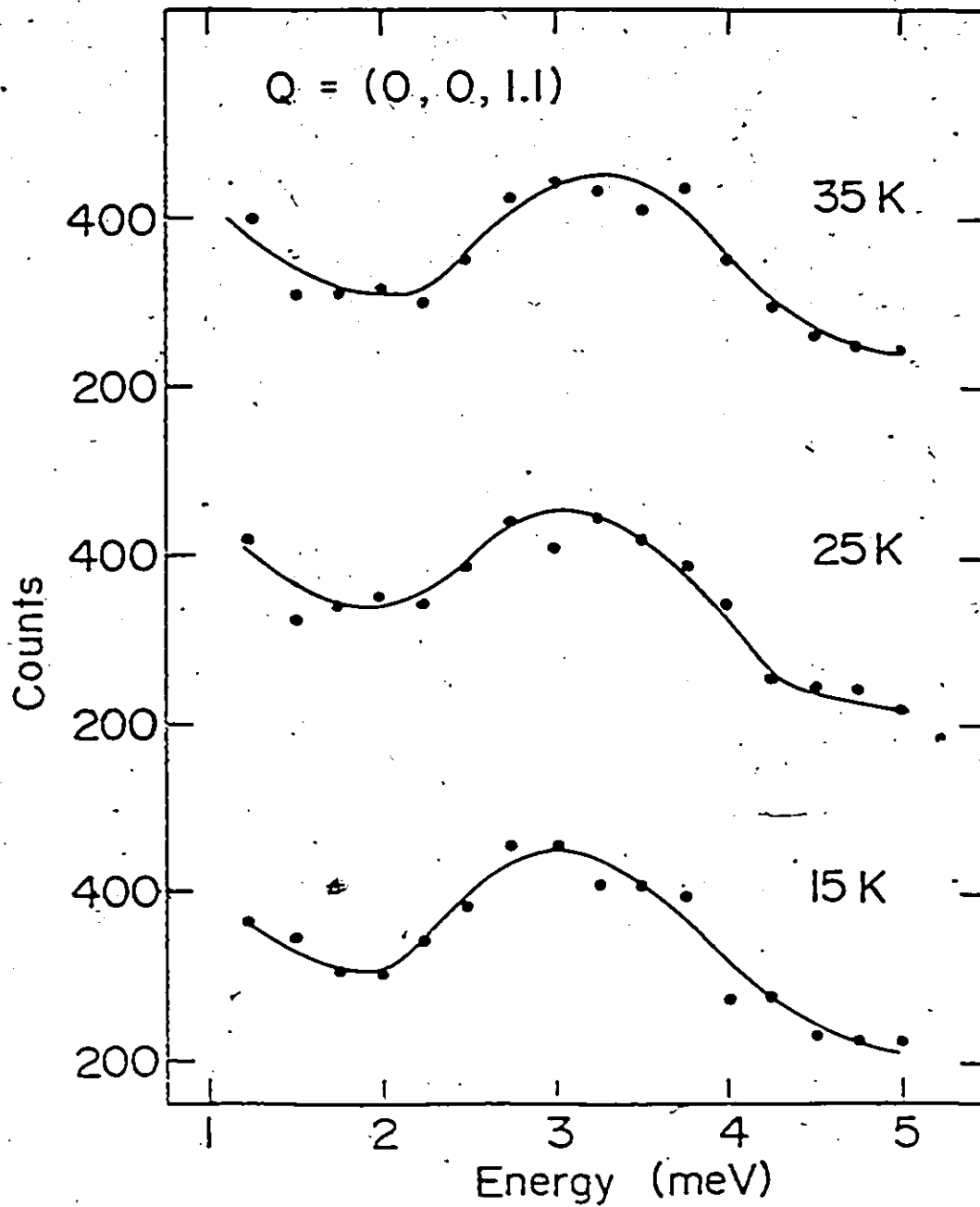


Figure C7: Inelastic scattering at $Q = (0, 0, 1.1)$ is shown as a function of temperature. The slight upwards renormalization of the spin wave energy with temperature is predicted by the generalized Langevin equation theory for low energy spin waves.

We conclude by stating that the qualitative behaviour of the system is reasonably well reproduced by the theory, although discrepancies in the quantitative comparison exist. The level of termination is found not to have much of an effect, at least within the level terminations examined here. The particular termination scheme used is thought to be at least as important. It should be kept in mind that the theory has no disposable parameters save for the intensity at one point in (Q, ω, T) parameter space.

We now turn to the question of the use of this theory in describing the inelastic spectrum of TMMC. It was generally thought previously that the generalized Langevin equation approach was not successful in describing the response of a real one-dimensional Heisenberg system. This was on the basis of comparison of the theory to results of measuring the neutron group linewidth of TMMC as a function of temperature (Hutchings and Windsor (1977)) as well as the measurement of the "critical wavevector" in TMMC as a function of temperature (Shirane and Birgeneau (1977)). The critical wavevector is the wavevector at which the spin wave response becomes overdamped, that is loses its peaked structure. The theory does not predict either of the experimental findings correctly and thus it comes as somewhat of a surprise as to how well it does in describing our data. We believe the answer is that, although these other experiments are definitive experiments on TMMC, they are not relevant for comparison with theory for the dynamics of a Heisenberg system. This is because they are at temperatures sufficiently low (mostly $T < 10K$) and at inappropriate wavevectors to sample Heisenberg-like fluctuations. The work by Hutchings and Windsor (1978) is at large reduced wavevectors but at low temperatures

and wavevectors far off the chain axis, thus picking up a substantial contribution of out-of-easy plane fluctuations in their intensity. The critical wavevector work is at low temperatures and very small reduced wavevectors where the effects due to anisotropy are greatest.

This is not to say that the theory describes the measured response of CsMnBr_3 completely. There are real discrepancies, but the qualitative comparison is quite reasonable and it is perhaps unrealistic to expect more considering how little information is built into the theory.

CHAPTER 4

SOLITONS IN CsMnBr_3

4.1 Introduction

The description of the paramagnetic spin waves in CsMnBr_3 in the preceding chapter represents the description of a spatially delocalized normal mode of the co-operative system. This is to say that the spin wave excitation is composed of the correlated motion of many of the constituent spins in the system at the same time. The only limit to how many spins are involved in this motion at any one time is the correlation length along the chain. In a system with long range magnetic order, the spin waves represent completely delocalized normal modes of the system. The classical description of such a spin wave is that of a single spin deviation (from order) coherently distributed over the entire crystal.

One may then ask the question: Is it possible to have an excitation of the entire system (involving all the constituent spins' motion) that is spatially localized at any one time? These are known to occur in a spatially inhomogeneous co-operative system such as a system with defects, but until recently, not in a homogeneous (or pure) system. The answer appears to be yes, but it requires the condition that a kink or twist must be put into the local order parameter. The absence of long range order does not preclude the existence of a local order parameter if short range correlations are sufficiently high within a given local area.

The physical picture is a moving domain wall connecting lower energy stable (or ground) states. The excitation (the domain wall) moves along the chain thereby involving all the spins in the motion. However, at any one time only some small numbers of spins is involved in the motion of this excitation.

As opposed to the spin wave, the moving domain wall is made up of many spin deviations distributed over a few spins at any one time. Thus, whereas the spin wave is a small amplitude or linear excitation, the moving domain wall is a non-linear excitation. In general this is not very good for the prognosis of understanding this excitation, because even if an equation of motion can be formulated it usually cannot be solved due to its non-linear nature. However there exists a class of non-linear differential equations of the form

$$\frac{\partial^2 \phi}{\partial t^2} - \frac{1}{c^2} \frac{\partial^2 \phi}{\partial z^2} = \omega^2 \frac{\partial V}{\partial \phi}$$

that have exact solutions for many choices of $V(\phi)$. These are equations of motion for soliton bearing systems. A constraint must be placed on the form of the potential term $V(\phi)$. This is that $V(\phi)$ must have more than one minimum. Clearly not all equations satisfying this constraint have been investigated. The one that will be relevant in the remaining discussion is referred to as the Sine-Gordon equation. In this case $V(\phi)$ has an infinite sequence of degenerate ground states. The Sine-Gordon equation of motion is

$$\frac{\partial^2 \phi}{\partial t^2} - \frac{1}{c^2} \frac{\partial^2 \phi}{\partial z^2} = \omega^2 \sin \phi$$

The physics of this equation of motion is best considered with reference to figure D1. The system is described by assigning a value to ϕ for every point (continuously) along the chain, z . The behaviour of ϕ is governed by how it moves on its energy surface $V(\phi)$. For the diagram $V(\phi) = -\cos\phi$, and the ground state of the system is represented by having ϕ take on values for every point along the chain such that it lies in the valley of the corrugated energy surface $V(\phi)$.

If we wish to create a local excitation which departs from the ground state at a particular point and returns to a ground state at some other point, then there are two ways we can do this. These are referred to as the dissipative wave and the soliton. In the case of the dissipative wave, ϕ takes on values at some point z_1 , such that it no longer lies in the valley of the energy surface but climbs up the side of this surface. There it executes arbitrary motion without crossing over the energy hump to the next valley of $V(\phi)$, and at some point, z_2 , it returns to the same valley and holds this value for all other points on the chain. In the case of the soliton, ϕ takes on values such that it leaves the valley of $V(\phi)$ at some point z_1 . It then takes on values such that it climbs up the side of the energy surface, crosses over the energy hump, and returns at some point, z_2 , to values such that it lies in the adjacent valley of $V(\phi)$ to the one in which it started.

It is well known that any localized disturbance can be made up of an infinite sum of its Fourier components. If left to develop in time, each of these components will evolve at a characteristic velocity. This

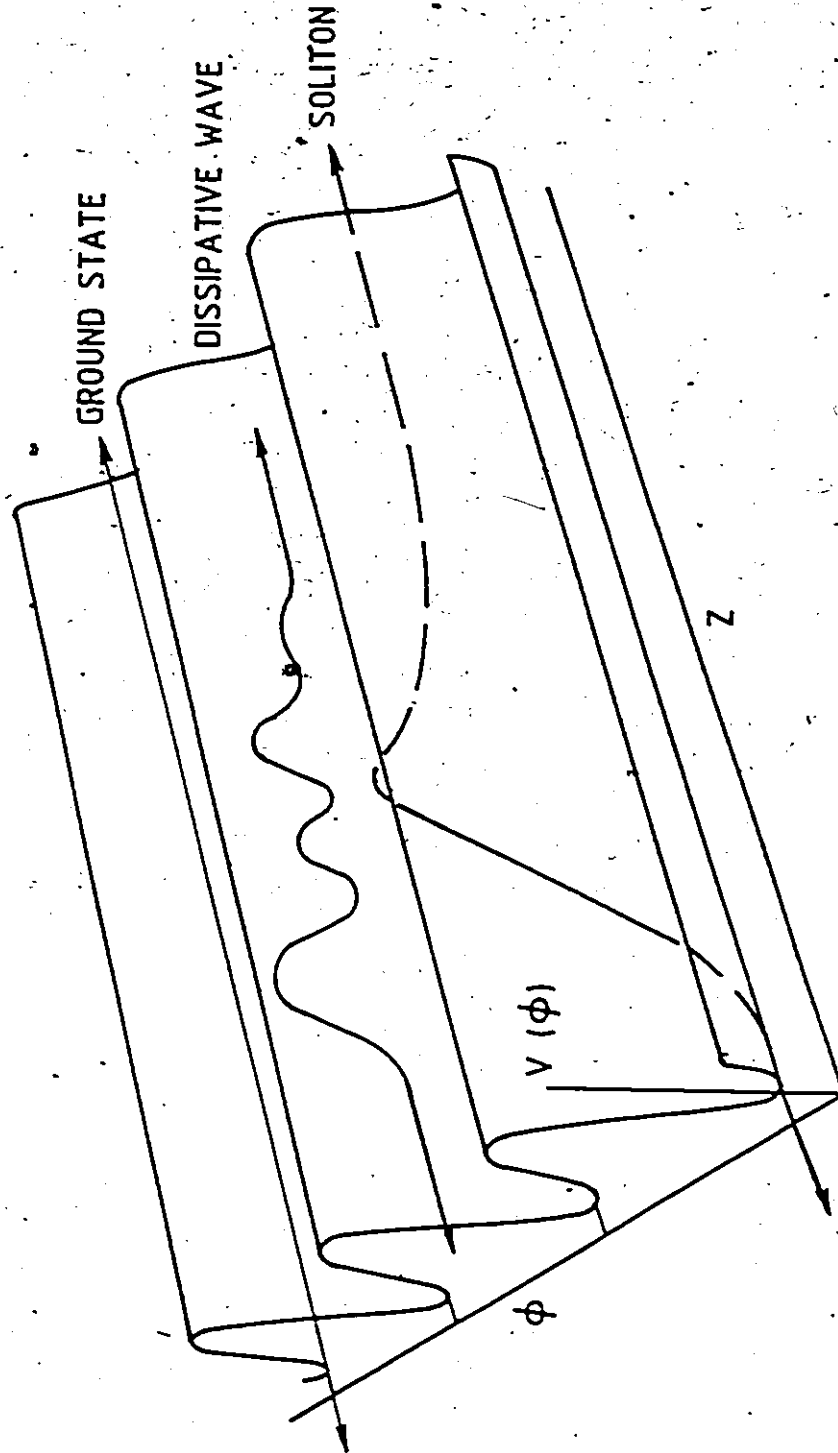


Figure D1: A physical picture of solitons can be arrived at by using the above pedagogical model taken from Rebbi (1979). The soliton bearing system is completely described by assigning some value to ϕ for every point along the chain, z . The behaviour of the system is governed by the topology of the potential term $V(\phi)$. This particular topology is particular to a Sine-Gordon system.

then gives rise to dissipation or "spreading out" of a disturbance as the fast Fourier components evolve more quickly than the slower ones. This can be pictured for figure D1 by imagining each configuration of the system to be represented by a rope lying on a corrugated surface. The time evolution of such a system can be imagined by thinking of grabbing either end of the rope and pulling. In the case of the dissipative wave the result would be that one would take up the slack of the rope and the configuration would end up looking much like the ground state. The localized excitation would have dissipated.

The same process could be imagined for the soliton. However, the boundary conditions of one end lying in one valley and the other in an adjacent valley of the surface, preclude the localized excitation from dissipating regardless how hard the rope is pulled. This is because at some point the rope must cross from one valley to another.

Physical descriptions of the physics of solitons, with particular emphasis to particle physics are given in Rebbi (1979). An excellent review of solitons in condensed matter physics is given in Bishop et al. (1980). Specific discussions of solitons in condensed matter physics are contained in Bernasconi and Schneider (editors, 1981) and Lovesey et al. (editors, 1984).

4.2 Solitons in Condensed Matter

The soliton was put forward as an excitation of the strongly fluctuating condensed system first by Krumhansl and Schrieffer (1975). The relevant ideas had previously been introduced in several other areas of physics. The first concrete suggestions for which systems may bear

solitons and the direct calculation of observables, was due to Mikeska (1978). In this work he considered the ferromagnetic chain system with easy plane anisotropy and a field applied within the easy plane.

In the intervening time between 1978 and the present, comprehensive experimental investigations have been undertaken of several candidates for soliton bearing systems CsNiF_3 , TMMC, CsCoBr_3 and CsCoCl_3 as well as the polymer polyacetylene. For the magnetic systems the most detailed information on the spin dynamics due to the presence of solitons comes from neutron scattering results. CsNiF_3 is an $S=1$ ferromagnetic chain system with a relatively strong (compared with either CsMnBr_3 and TMMC) easy plane anisotropy at low temperatures. A Sine-Gordon soliton is expected to result from the application of a magnetic field within the easy plane (Mikeska, 1978). The motion of the spins along the chain as a soliton passes by is depicted in figure D2. The spins lie within the easy plane and point along the field direction on either side of the soliton. The spins rotate by 2π within the easy plane as the soliton passes. Initial neutron work (Kjems and Steiner, 1978) was complicated by the presence of two magnon scattering (Reiter, 1981). However later work identified a soliton signature which required the presence of some out-of-easy plane fluctuations (Kakurai et al., 1984). In addition interesting soliton stability phenomena were investigated as a function of field (Kumar, 1982).

The application of a magnetic field within the easy plane of TMMC also results in a Sine-Gordon soliton. These spin dynamics, which are the antiferromagnetic analogue of those just described for the ferromagnet CsNiF_3 , are also shown in figure D2. In this case the spins rotate within the easy plane by π so that each sublattice of spins exchanges orientation

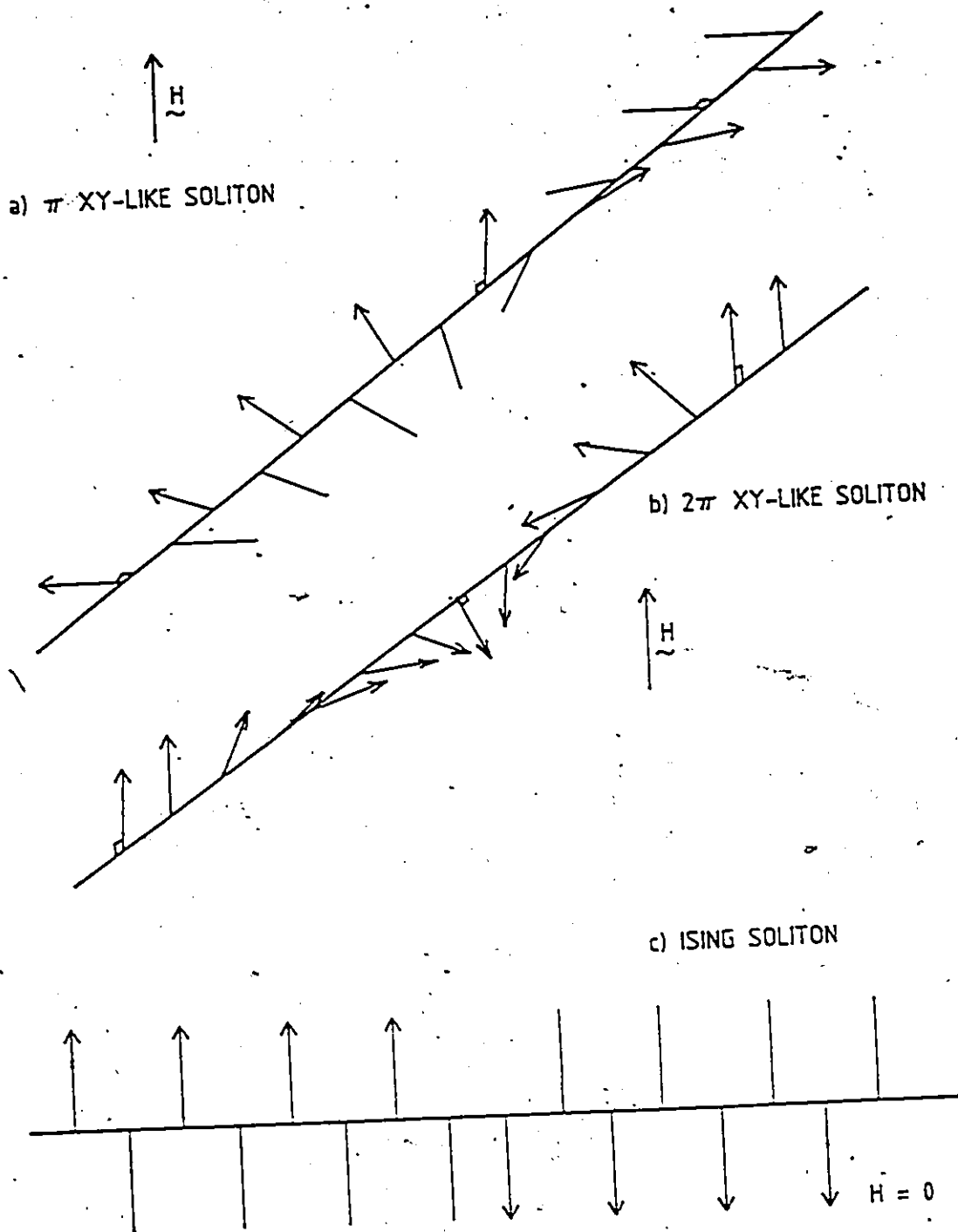


Figure D2: Spin configurations taken up by soliton bearing systems. The π XY-like soliton has been observed in TMMC. The 2π XY-like soliton (with slight modifications) has been seen in CsNiF_3 while Ising-like solitons have been seen in CsCoCl_3 .

before and after the soliton. The ground state configuration of the spins on either side of the soliton is that of both sublattices spin-flopped perpendicular to the field direction within the easy plane. Clear signatures for the presence of solitons in this system have been observed in neutron scattering results (Regnault et al. 1982 and Boucher et al., 1985).

CsCoBr_3 and CsCoCl_3 represent Ising-like antiferromagnetic chain systems with $S = \frac{1}{2}$. As such they can exhibit infinitely narrow solitons in the absence of any applied field as shown in figure D2. The equations of motion for the spin dynamics do not map onto a soliton bearing equation of motion but are rather "topological" solitons which represent propagating domain walls connecting ground states. These propagating modes were investigated in detail theoretically by Villain (1975) and experimentally by Nagler et al. (1982).

The soliton of interest to ourselves in CsMnBr_3 and zero field is depicted in figure D3. The motion of spins coming out of the easy plane, can be mapped onto a Sine-Gordon equation of motion (Mikeska, 1980). The spins come out of the easy plane, reach full deflection out of the plane and then return to the easy plane such that the two sublattices have interchanged positions within the easy plane. As, in this system, there is isotropy within the easy plane, there appears at first sight to be an analogy between these solitons and the "pulse" solitons of the purely Heisenberg chain (Tjon and Wight, 1977). However this is not the case, as the method of arriving at this soliton solution is exactly the same as for the CsNiF_3 and TMMC cases in applied fields. This is to map the spin dynamics of some spin component (or related quantity) onto a Sine-Gordon equation of motion.

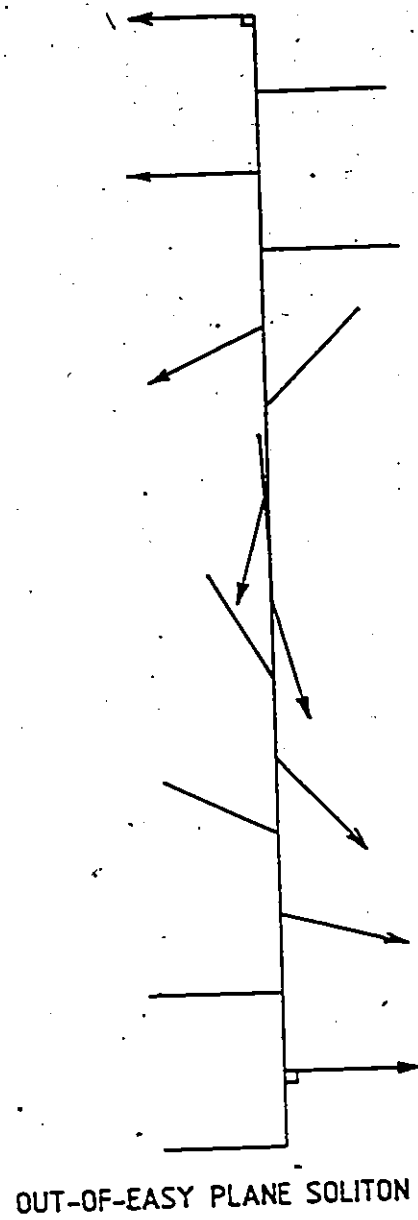


Figure D3: The spin configuration, taken up by an antiferromagnetic chain system with easy-plane anisotropy, due to the presence of an out-of-easy-plane soliton. This mode, predicted by Mikeska (1980), is the subject of our investigation of CsMnBr_3 . The easy plane is perpendicular to c .

4.3 Theoretical Treatment of the Anisotropic Heisenberg Antiferromagnetic Chain

The ultimate aim of this treatment, due to Mikeska (1980), is to map the equation of motion for a parameter of the system onto a Sine-Gordon equation. In order to do this, approximations for treating the real quantum mechanical spins as classical vectors and treating the discrete lattice as a continuum field must be made.

The Hamiltonian is

$$H = -2J \sum_i \vec{S}_i \cdot \vec{S}_{i+1} + A \sum_i (S_i^z)^2 \quad (4.1)$$

The relevant parameters for CsMnBr_3 are $4JS = 8.75$ meV and $\sqrt{A/J} = .19$

The classical spin field can be written in terms of four parameters; $\Theta(z,t)$, $\theta(z,t)$, $\Phi(z,t)$, $\phi(z,t)$. This is as

$$S_{\substack{\text{even} \\ \text{odd}}}(z,t) = \pm S \{ \sin(\Theta \pm \theta) \cos(\Phi \pm \phi), \sin(\Theta \pm \theta) \sin(\Phi \pm \phi), \cos(\Theta \pm \theta) \} \quad (4.2)$$

Four parameters are necessary to account for differences between the Néel state (all nearest neighbour spins being antiparallel) and the real low temperature ground state.

The continuum approximation is appropriate when the spatial variation of the spins is not large, which should apply at low temperatures. Explicitly the continuum approximation means that expansions making use of

$$\left(a \frac{\partial}{\partial z}\right) \ll 1 ; \quad \Theta \ll 1 ; \quad \phi \sin \Theta \ll 1 \quad (4.3)$$

can be made, where a is the Mn-Mn separation distance along the chain.

Applying these expansions (4.3) to the results of substituting (4.2)

into (4.1) gives a continuum Hamiltonian of

$$H = C + |J|s^2 \int \frac{dz}{a} \left\{ \left(\frac{\partial \theta}{\partial z} \right)^2 + 4\theta^2 \right. \\ \left. + \sin^2 \theta \left[\left(\frac{\partial \phi}{\partial z} \right)^2 + 4\phi^2 \right] + \frac{A}{|J|} [\cos^2 \theta + \theta^2 (1 - 2\cos^2 \theta)] \right\} .$$

The equations of motion for the four parameters can then be derived from the principal Poisson bracket for the polar representation of a spin vector. This is (Villain, 1974)

$$\{S_n^z, \phi_m\} = \delta_{nm}$$

The resulting equations of motion are then examined for permanent profile solutions. These are solutions which depend not on space and time independently, but rather on $s = z - ut$ where u is a characteristic velocity. In addition boundary conditions consistent with a ground state-localized disturbance-ground state configuration are imposed. These are

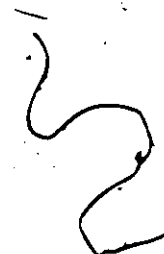
$$\sin \theta \quad (\text{at infinity}) = 1$$

$$\frac{\partial \phi}{\partial s} \quad (\text{at infinity}) = 0$$

With this taken into account a Sine-Gordon equation of motion results for the parameter $\eta = \pi - 2\theta$

$$\left(1 - \frac{u^2}{c^2}\right) \frac{\partial^2 \eta}{\partial s^2} = m^2 \sin \eta$$

The space time solutions to these equations of motion are



$$\begin{aligned} \cos\theta(z,t) &= \operatorname{sech}\left[\left(1 - \frac{u^2}{c^2}\right)^{-0.5} m(z-ut-z_0)\right] \\ \phi(z,t) &= \phi_0 + \pi \operatorname{sign}(z-z_0-ut)/2 \end{aligned} \quad (4.4)$$

Ignoring the small angles ϕ and θ , the dynamic configurations of the chain so described correspond to a localized disturbance moving with velocity u , centred at $z = z_0 + ut$. On either side of this "kink" is a well ordered Néel-type ground state configuration of spins lying within the easy plane. The disturbance is a large fluctuation of the S^z component of the spin field separating ground state configurations which are π out of phase with respect to each other. The parameter m enters the theory as the parameter which characterizes this soliton bearing system. As such it is referred to as the soliton "mass" and it is given by $m = \sqrt{A/J}$. The energy of this configuration is $4JS^2 m \left(1 - \frac{u^2}{c^2}\right)^{-0.5}$.

In order to make contact with experiment we need to know the Fourier transform (FT) in both space and time of the relevant dynamic spin pair correlation function.

$$\text{FT} \langle S_i^z(t) S_0^z(0) \rangle \sim \text{FT} \{ (-1)^n \langle \cos\theta_n(t) \cos\theta_0(0) \rangle \}$$

At low soliton velocities, u , this calculation is analogous to that for the S^{xx} dynamic structure factor $\chi''(H)$ for the planar antiferromagnet in a symmetry breaking field applied within the easy plane (Mikeska, 1980).

Hence we have

$$\begin{aligned} S_r^{zz}(q_z, \omega) &= (8B / (c q_z \cosh^2 L)) \exp(-8\beta m) \\ &\times \exp(-4\beta m \omega^2 / (c^2 q_z^2)) \end{aligned} \quad (4.5)$$

In this expression the distance between nearest neighbour spins, $(c/2)$, has been set equal to unity so that

$$q_z = |\hat{z} \cdot (\pi\hat{z} - Q)|$$

with $\hat{z} \cdot Q$ in units of $2/c$ and $\tilde{c} = 4JS$, $\beta = |J|S^2/2kT$ and $L = (\pi q_z/2m)$.

It should be noted that the theory treats the soliton as a localized excitation connecting ground states and thus ignores all interaction effects with either spin waves or additional solitons.

4.4 The Neutron Scattering Experiment

The strategy for extracting a signature of the presence of solitons in CsMnBr_3 from a neutron scattering experiment depends on four characteristics of the excitation. The motion of the spins as a soliton passes by is to undergo a large fluctuation in their out-of-easy plane or S^z components. Next, the soliton involves a large change in angular momentum from the ground state, and thus the neutron cannot create or destroy a soliton as it can (for example) a spin wave since the neutron is a spin $1/2$ particle. Further, this implies the measured response will depend on the population of solitons present at a given temperature and thus the scattering should be thermally activated. This is only true within the non-interacting soliton picture. Finally, the form of the $S^{zz}(q_z, \omega)$ dynamic structure factor shows that the soliton response is peaked about the magnetic zone centre, $q_z = 0$.

The first two of these characteristics introduce some experimental difficulty. As the soliton response occurs in the $S^{zz}(q_z, \omega)$ structure factor, the out-of-easy-plane fluctuations must be separated from the in-plane fluctuations. This can be accomplished by making two measurements over the same range of q_z and ω values but at sufficiently different Q

vectors that each measurement samples a different combination of in-plane fluctuations, $S^{XX}(q_z, \omega)$, and out-of-plane fluctuations, $S^{ZZ}(q_z, \omega)$. A subtraction algorithm can then be employed to determine the two dynamic structure factors. The experimental problem is due to the phenomena of self-absorption in the sample. This is that in different scattering geometries the rate of absorbing neutrons from the beam by the nuclei in the sample will in principle be different for a non-spherical sample. Therefore the sample in the two different scattering geometries may be exposed to different effective neutron fluxes, or alternatively, the sample will present a different effective volume to the experiment in different geometries. This is clearly more important for samples with high absorption cross sections, however it must (and will be) considered when the absolute magnitudes of two measurements are directly compared or subtracted.

The fact that the neutron cannot create or destroy a soliton means that the response will be centred on zero energy transfer. The experimental problem here is that the scattering intensity due to nuclear incoherent events also appears in an intense, approximately gaussian distribution of scattering centred on zero energy transfer. This scattering appears in all of reciprocal space as it is incoherent, and it must be separated from the magnetic scattering of interest.

Our solution to these problems is shown in figures D4 and D5. Constant energy scans for energies below the spin wave branch with zone centre energy of 1.7 meV, were made across the magnetic zone centre. Two such measurements were made as shown in figure D4. One at wavevectors

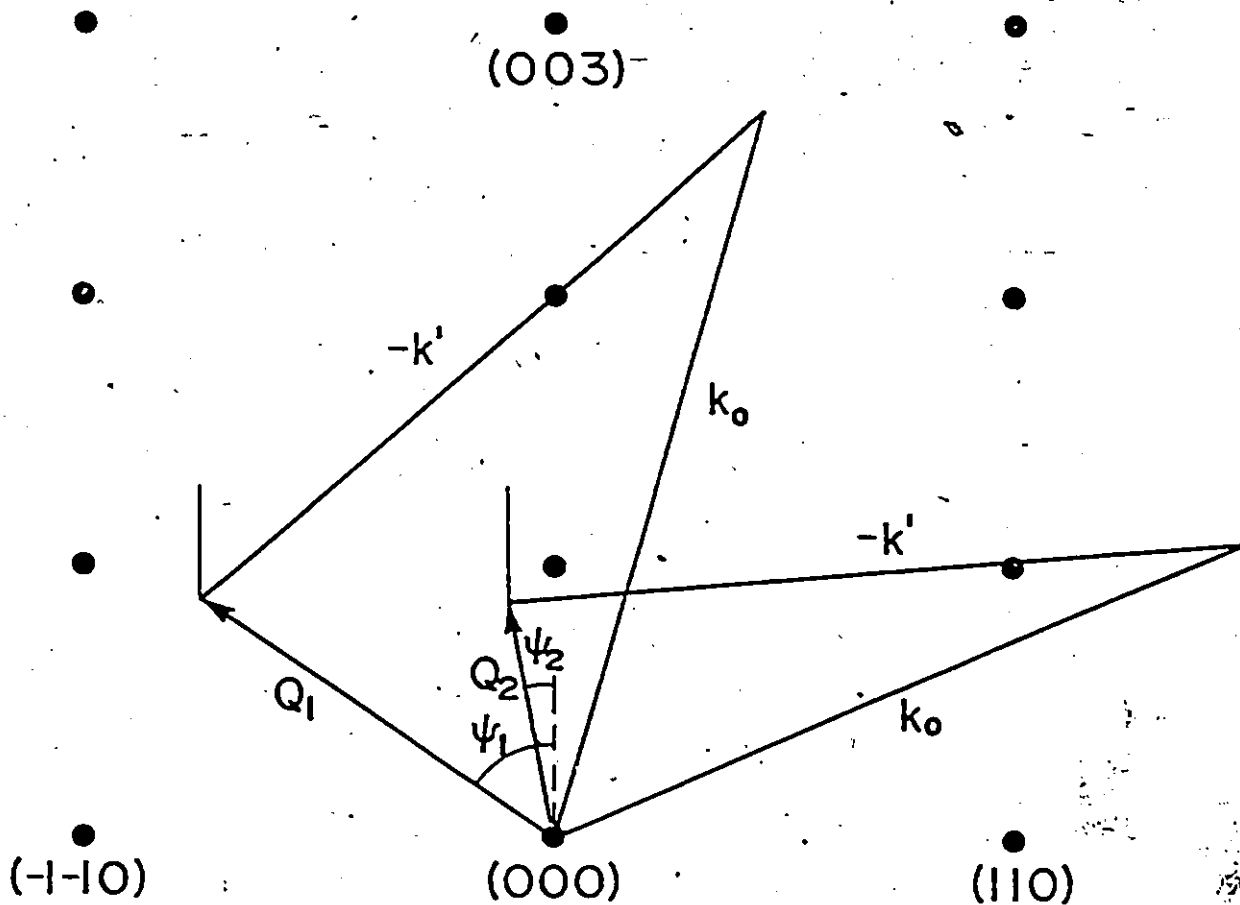


Figure D4: The scattering geometries (to scale) involved in measurements at $\underline{Q}_1 = (-0.75, -0.75, 0.85)$ and $\underline{Q}_2 = (-0.1, -0.1, 0.85)$. The thin lines emanating from \underline{Q}_1 and \underline{Q}_2 are typical paths the constant energy scans would take. ψ_1 and ψ_2 are the angles between the relevant \underline{Q} and the hexagonal axis that determine the relative strength of in-plane and out-of-plane correlations in the scattering.

CONSTANT ENERGY SOLITON SCANS RELATIVE TO
SPIN WAVE RESPONSE FOR CsMnBr_3

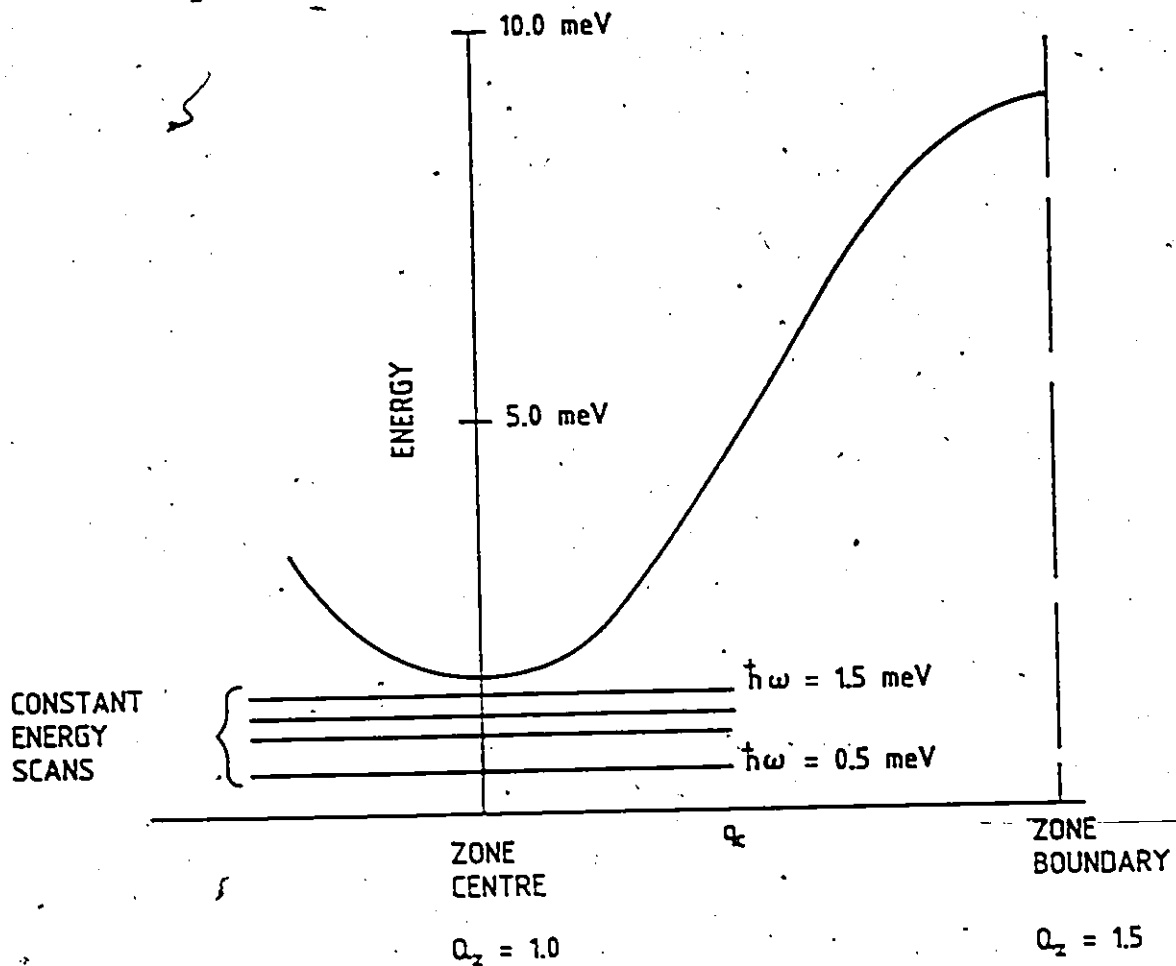


Figure D5: The constant energy scans are shown relative to the spin wave response of CsMnBr_3 . The out-of-easy-plane spin wave response does not extend below ~ 1.5 meV. In-plane fluctuations are present below this branch, but the response does not show an inelastic peak in either constant Q or constant energy scans.

$Q_1 = (-0.75, -0.75, Q_z)$ and another at $Q_2 = (-0.1, -0.1, Q_z)$ and both at the same set of constant energy transfers. This means that both examine the spin fluctuations at small energy transfers and across the magnetic zone centre ($Q_z = 1.0$) but each measures a different combination of in-plane and out-of-plane fluctuations. These particular wavevectors were chosen for the relatively "clean" background (absence of strong spurious etc.) as well as that they are at sufficiently different Q while still being at values of $|Q|$ such that the magnetic form factor does not adversely affect the intensity of the scattering too much.

Constant energy scans were employed so that the scans could ride on top of the incoherent nuclear intensity, which depends only weakly on Q , and then pick up the magnetic scattering as we scanned across the magnetic zone centre at $Q_z = 1$. The alternative is to perform two measurements, one with and one without magnetic scattering in constant Q scans. The intense nuclear incoherent scattering would then have to be subtracted out. This was felt to be an inferior method, as the scattering to be subtracted is both intense and has marked energy space structure to it.

These scans were performed at temperatures above 15K. Once again the sample was mounted in a displax type closed cycle refrigerator with the $(h h \ell)$ plane lying in the scattering plane. Other experimental details are given in table A1.

The scattering cross section can then be written as

$$\frac{\partial^2 \sigma}{\partial \Omega \partial E'} \sim F^2(Q) [(1 + \cos^2 \psi) S^{xx}(q_z, \omega) + \sin^2 \psi S^{zz}(q_z, \omega)] / 2$$

where ψ is the angle between the chain axis and Q_z . The magnetic form factor for Mn^{+2} is known (Bacon, 1962). We can then write

$$\begin{aligned} \text{Int}(Q_x = -0.1) &\sim F^2(Q) S^{xx}(q_z, \omega) \\ \text{Int}(Q_x = -0.75) &\sim V_{\text{eff}} F^2(Q') \{ (1 + \cos^2 \psi') S^{xx}(q_z, \omega) \\ &\quad + \sin^2 \psi' S^{zz}(q_z, \omega) \} / 2 \end{aligned} \quad (4.6)$$

In writing this we have approximated $\psi(Q_x = -0.1) = 0$ and have allowed for the effect of self absorption by including an effective volume factor in the $Q_x = -0.75$ intensity. As already mentioned the CsMnBr_3 single crystal is cylindrical in shape with the cylindrical axis being approximately parallel to the c axis. Knowing the geometry of the crystal, we now have a consistency check on the effective volume factor. A neutron trajectory across the crystal in the $Q_x = -0.75$ geometry goes through more of the crystal than a trajectory in the $Q_x = -0.1$ geometry. Thus the chances of absorption are greater in the $Q_x = -0.75$ geometry and consequently this should be compensated for; thus $V_{\text{eff}} \geq 1$. However, examination of the nuclear incoherent background in the vicinity of these geometries shows no tendencies of this kind. This was also checked on scans made on the same crystal and a different spectrometer (Chalk River's N-5 Spectrometer). Thus $V_{\text{eff}} = 1$ was assumed in all subsequent analysis.

Typical raw data of the constant energy scans are shown in figures D6 and D7. The data was fitted to an analytic expression for a Gaussian peak near $Q_z = 1.0$ (representing the magnetic intensity) plus a background.

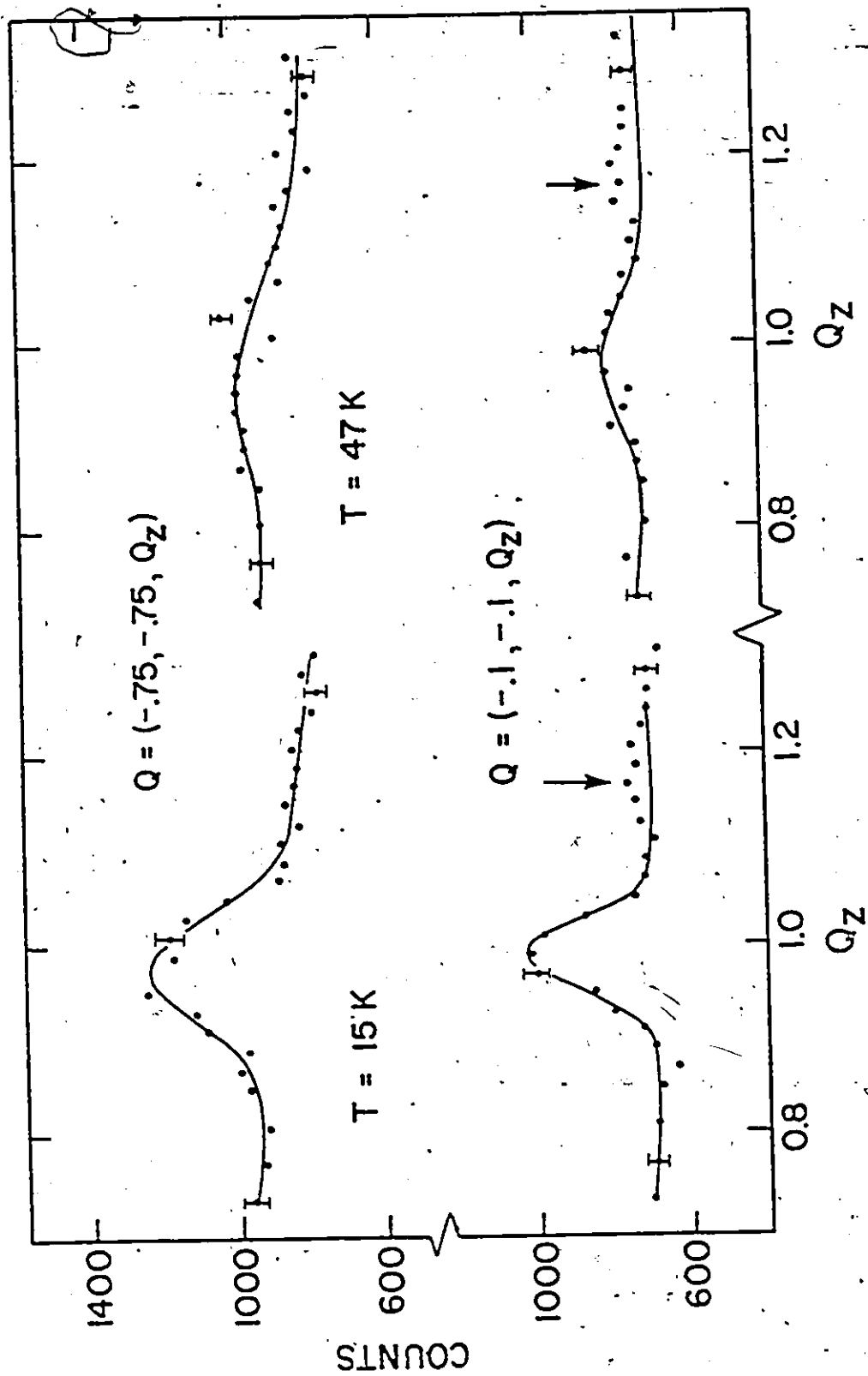


Figure D6: Typical inelastic, constant-energy scans at $\hbar\omega = 0.5$ meV. The lines drawn are fits to the data for a Gaussian peak plus background as described in the text. The arrows present in the lower scans at $Q_z = 1.17$ indicate scattering which originates from a spurious effect involving an 002 Bragg reflection and an incoherent process. Its weight was suppressed in the fit.

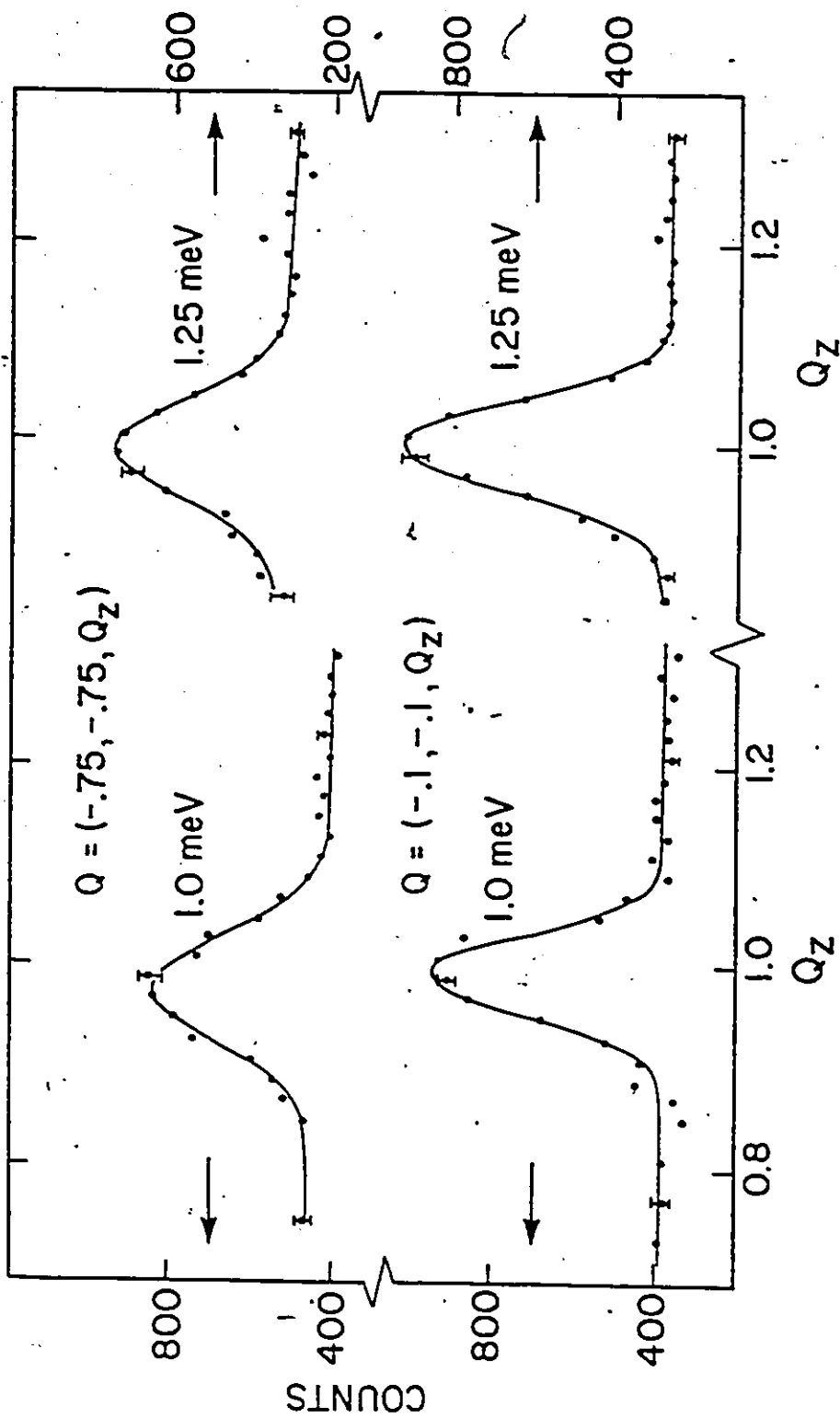


Figure D7: Typical inelastic, constant-energy scans at $T = 15\text{K}$ and $\hbar\omega = 1.0\text{ meV}$ and $\hbar\omega = 1.25\text{ meV}$. The lines drawn are fits to the data for a Gaussian peak plus background as described in the text.

It is thus of the form

$$\text{Int} = A + B(Q_z - Q_0) + c(Q_z - Q_0)^2 + D \exp(-E(Q_z - Q_0)^2)$$

The fitted curves are also plotted on the relevant figures with the raw data. It is these smooth curves that are manipulated further in all subsequent analysis.

Figure D6 shows the two scans at 15K and again at 47K. The marked drop off in intensity of the gaussian part of the scattering demonstrates that it is magnetic in character, as no lattice property varies on this temperature scale.

It is easily seen that by using equations (4.6) we can arrive at the desired separation of polarizations.

$$S^{ZZ}(q_z, \omega) = [2 \text{Int}(Q_x = -0.75, \omega) F^{-2}(Q') - (1 + \cos^2 \psi) \text{Int}(Q_x = -0.1, \omega) F^2(Q)] / \sin^2 \psi$$

$$S^{XX}(q_z, \omega) = \text{Int}(Q_x = -0.1, \omega) F^{-2}(Q)$$

where the contributions to the intensity due to background are not included.

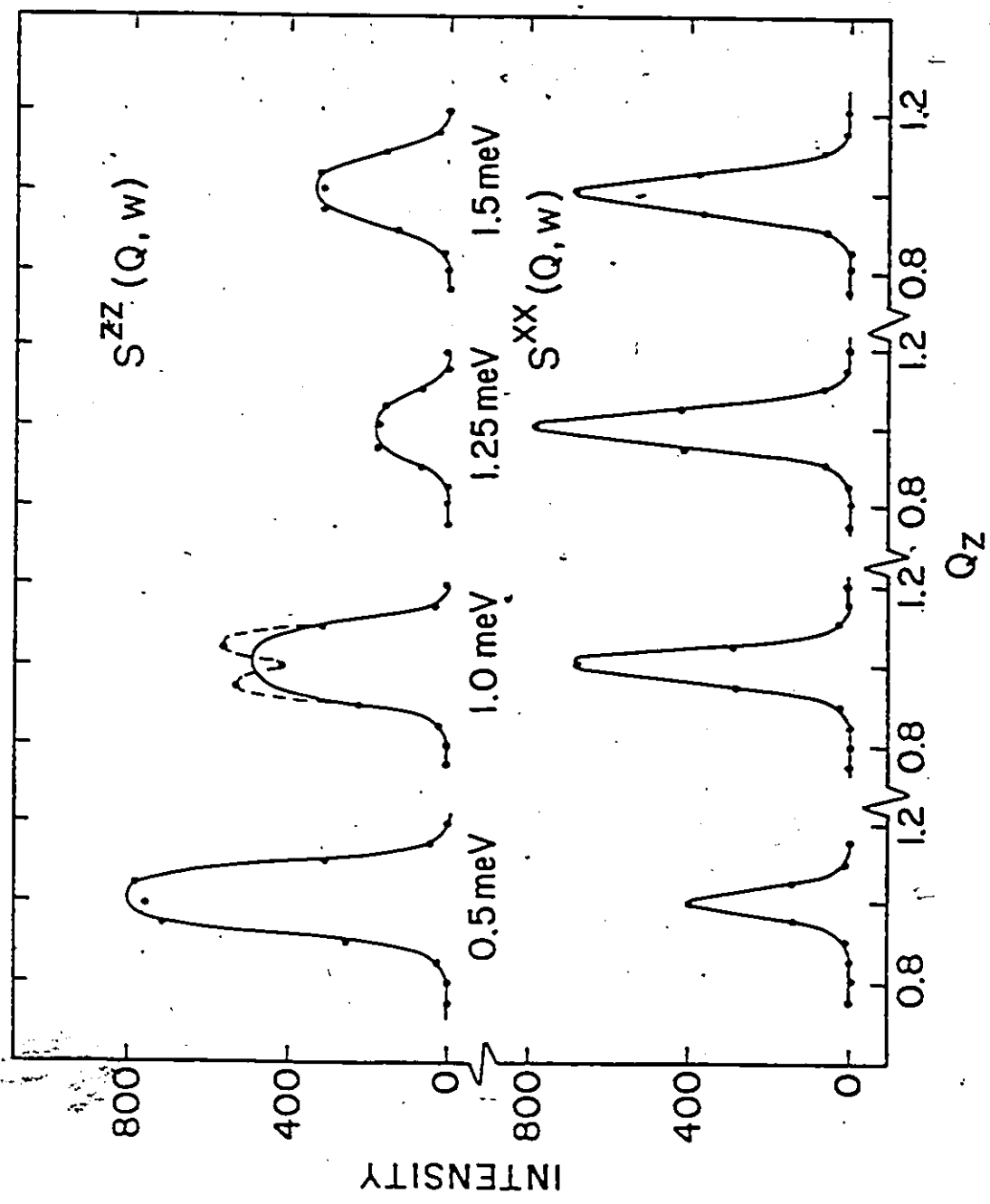
4.5 Results and Discussion

a) Low Temperature Results (T = 15K)

The intensities at 15K of the separated polarizations of the dynamic structure factor, $S^{ZZ}(Q_z, \omega)$ and $S^{XX}(Q_z, \omega)$ are shown as a function of energy transfer in figure D8. It is clear that there are strong qualitative differences between the energy dependencies of the polarizations. The S^{ZZ}



Figure D8: $S^{ZZ}(Q_z, \omega)$ and $S^{XX}(Q_z, \omega)$ are shown as a function of energy at 15K. They are both drawn on the same scale and the lines are guides to the eye. The strong qualitative differences in the energy dependencies are clear. The rise in intensity at $\hbar\omega = 1.5$ meV for $S^{ZZ}(Q_z, \omega)$ is due to a damped spin wave at 1.7 meV and at the zone centre.



intensities fall off sharply with increasing energy transfer from 0.5 meV to 1.25 meV. Over the same region in S^{xx} the intensity increases monotonically.

As demonstrated in Chapter 3 of this thesis a damped zone-centre spin wave is present at 1.7 ± 0.2 meV. This spin wave was shown to be preferentially S^{zz} in polarization. Therefore the rise in intensity of S^{zz} at an energy of 1.5 meV is consistent with the approach to this spin wave from below in energy. This same study showed that an additional spin wave branch, primarily S^{xx} in polarization, should exist below the observed branch at low temperatures. At 15K, though, this branch is expected to be over-damped for small wavevectors. The behaviour observed in the S^{xx} intensity for energies of 1.5 meV and below could arise from this over-damped mode.

The non-interacting soliton theory provides a good qualitative description of the observed behaviour of S^{zz} below 1.5 meV. The theory provides intensity in the S^{zz} polarization alone which falls off sharply with both increasing q_z and energy; exactly what is observed. As has already been mentioned, the analysis on other candidates for magnetic soliton bearing systems, TMMC and CsNiF_3 has been complicated by the demonstration (Reiter, 1981) that multi-spin wave processes can produce a neutron response very similar to what is expected from solitons. This is because both the soliton response and the multispin wave response are polarized along the equilibrium spin direction. In the present case the equilibrium spin direction lies somewhere within the easy plane while the soliton response is polarized perpendicular to this plane. Hence they cannot be confused.

Let us now compare our measured $S^{ZZ}(Q_z, \omega)$ at 15K and below 1.5 meV with the non-interacting soliton theory quantitatively. Figure D9 shows the integrated intensity of our measured $S^{ZZ}(Q_z, \omega)$ plotted against the numerical integration over q_z of Mikeska's expression, equation (15). The overall peak of the theoretical curve has been adjusted to best fit our three data points. It can be seen that the theory overestimates the intensity at $\hbar\omega = 0.5$ meV and underestimates the intensity at $\hbar\omega = 1.0$ meV but correctly predicts the trend of the results.

In figure D10, the detailed lineshape of the theory (the solid line) is compared with our measured lineshape. The theory contains no adjustable parameters as even the scale is set by the choice of scale for the integrated intensity. The lineshape of the theory contains a sharp double-peak structure which is not seen in the experiment. This is not surprising as the experimental resolution has not been taken into account and would not be expected to follow such sharp features.

The treatment of the resolution in this case is difficult because of the subtraction of the two sets of data. There is not a theoretical lineshape for S^{XX} in this region and thus, two convolutions of theory are not possible. We have attempted to treat the resolution of the spectrometer in an approximate manner by considering the effect to be the convolution of the soliton cross section at the scattering geometry which receives the S^{ZZ} contribution. That is that $Q = (-0.75, -0.75, Q_z)$ alone. This is to say we have neglected the effect of making the subtraction of the convoluted S^{XX} response. Hence the resolution should be somewhat further worsened although we should have considered the most important part. This convolution was performed according to the method of Cooper and Nathans (1967).

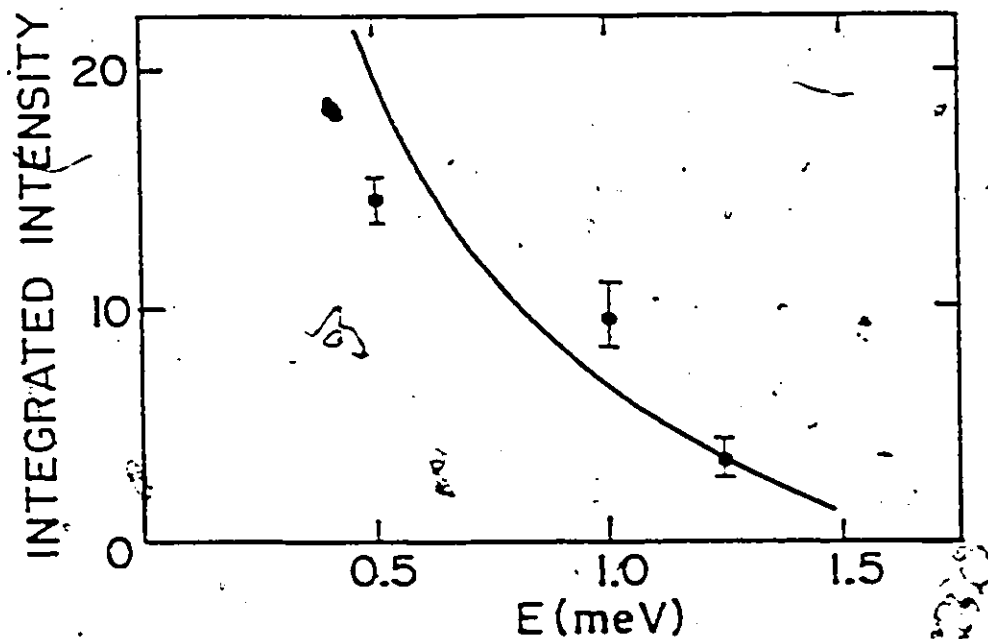


Figure D9: The integrated intensity of the measured $S^{ZZ}(Q_z, \omega)$ at 15K is compared with the same for the non-interacting soliton model due to Mikeska. There are no adjustable parameters in the theory, save for the vertical scale which was set to best describe our data.

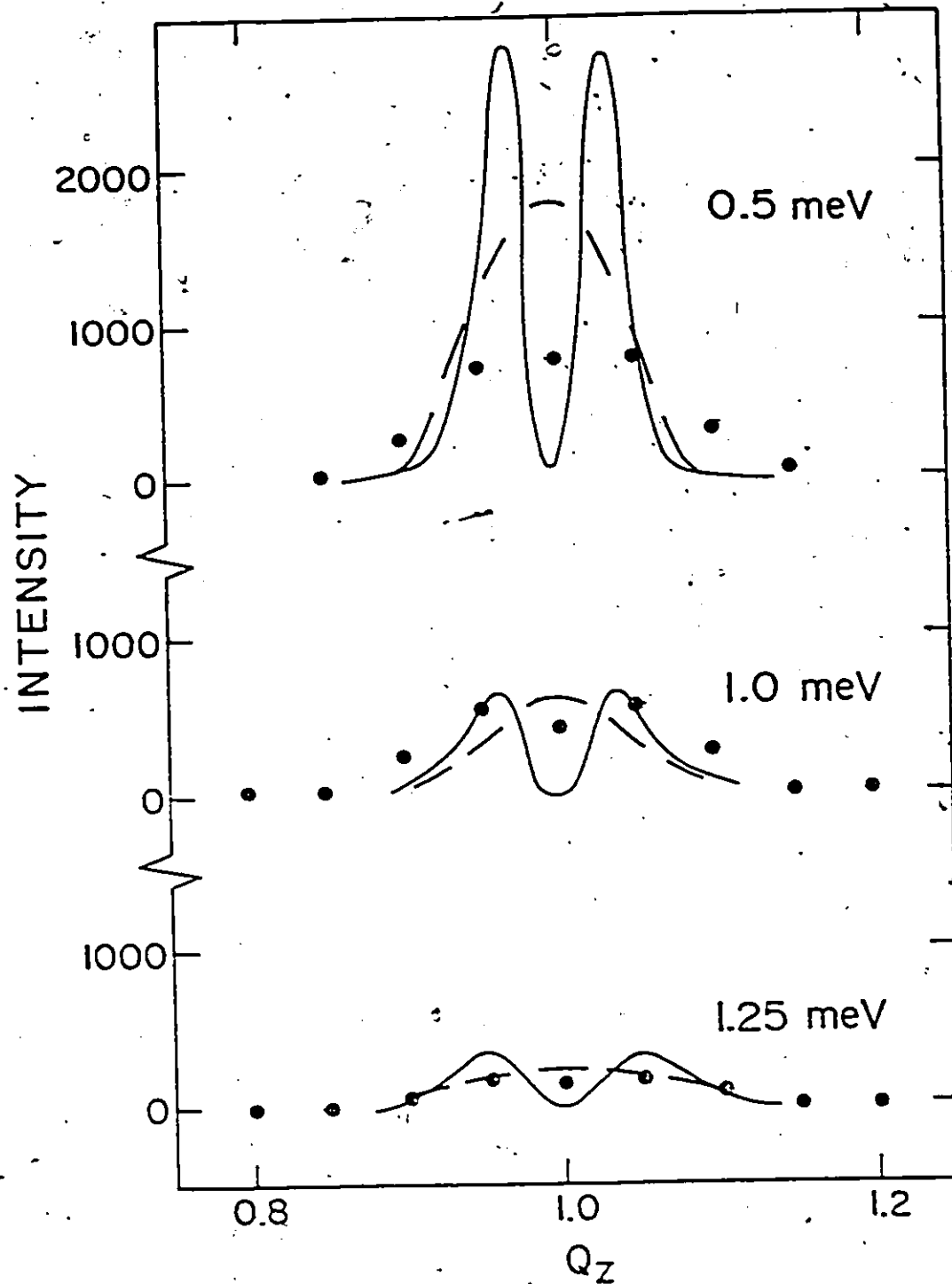


Figure D10: The line shape of our measurements of $S^{ZZ}(Q_z, \omega)$ at 15K is compared with the predicted line shape of the non-interacting soliton theory due to Mikeska (the solid line). The broken line is the convolution of Mikeska's predictions with the resolution function of our spectrometer. The overall scale for the theoretical results is predetermined when the scale of the integrated intensity in figure D9 is set.

The resulting comparison of the convoluted cross section with our data is also shown in Figure D10 with the dashed line being the convoluted cross-section. Again the overall scale of the theory is set by the scale of the integrated-intensity plot. We see immediately that the double-peak structure is no longer present and the comparison to the theoretical lineshape is reasonable.

The measured width (in Q space) is still slightly wider than the convoluted theory predicts. There are two possible causes. First, there is the possible effect of the subtraction on the resolution, and second the intrinsic lineshape may differ from the prediction of the non-interacting theory.

Although the former will certainly contribute to some extent, the latter appears to contribute as well. This is based on the discrepancies also present in the integrated intensity plot. These discrepancies would likely arise from interactions with delocalized excitations (spin waves, undamped and otherwise) such that the true description of the system is not that of a moving kink connecting two ground states but rather a moving kink connecting two small-amplitude excited states.

Despite this, the model does three things well in describing the data at 15K. The trend of the integrated intensity as a function of energy transfer is correct. The width of the response in Q space is approximately correct. Finally the polarization of the response, S^{ZZ} , is correct. These successes of the non-interacting soliton model in describing our data are impressive.

b) Elevated Temperatures ($T > 15K$)

The temperature dependence of the integrated intensity of $S^{ZZ}(q_z, \omega = 0.5 \text{ meV})$ is shown in figure D11. The peak intensity of the lineshape decreases monotonically with increasing temperature while the width increases monotonically over the same range. Thus the integrated intensity of the peak decreases only slightly over this range in temperature.

Examination of the expression for $S^{ZZ}(q_z, \omega)$, equation (4.5), shows that this behaviour cannot be described by the non-interacting soliton model. The intensity is predicted to vary as $T^{-1} \exp(-cT^{-1})$. Hence there should be a sharp rise in intensity with temperature.

The non-interacting soliton picture can be disrupted in two ways with increasing temperature. Firstly the approximation of the dipolar anisotropy as a single ion term which causes the creation of an easy plane will break down as the correlation length along the chain decreases. However as most of the strength of the dipole sum along the chain comes from first nearest neighbours, this will not break down until relatively high temperatures. Secondly the soliton will interact with a thermal bath of other solitons and, most importantly, spatially delocalized spin waves. The statistical mechanics of interacting Sine-Gordon solitons has been studied theoretically (Sasaki, 1984), but this is expected to be less important than the effects of the spin waves, as the solitons are spatially localized and thus can avoid each other much of the time.

The dynamic consequences of the soliton-spin wave interaction have been examined for the ferromagnetic chain in an applied field. It was previously known that the spin waves are in modified plane-wave states due

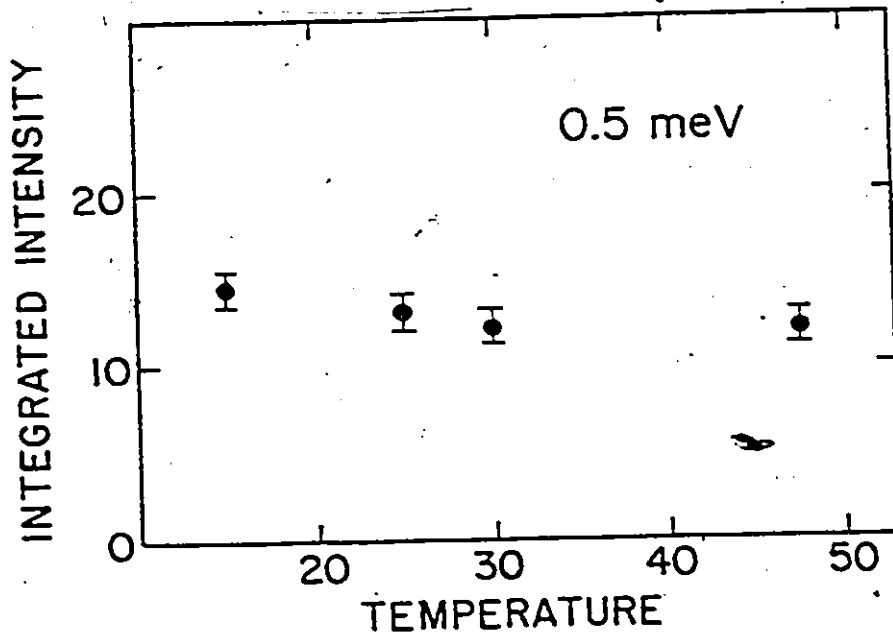


Figure D11: The observed integrated intensity of $S^{ZZ}(Q_z, \hbar\omega = 0.5 \text{ meV})$ is shown as a function of temperature (in Kelvin).

to the presence of the static soliton (Rubinstein, 1970). The spin waves then act to inhibit the central peak due to the soliton response and Allroth and Mikeska (1980) calculate a temperature damping of the non-interacting soliton-induced central peak that is linear in temperature. The case of the antiferromagnetic chain has not been considered.

While it is encouraging that spin wave-soliton interactions can dampen the consequences of the central peak's temperature dependence, and thus better describe our findings, it is clear that a damping proportional to temperature is too little to produce an approximately flat dependence of the integrated intensity, with temperature. We have, therefore, chosen perhaps the simplest phenomenological approach possible which is to give a temperature dependence to the parameter characterizing the soliton-bearing system, the soliton mass, m .

The integrated intensity can be fitted at each temperature by varying the soliton mass and the resulting temperature dependence of the soliton mass is as shown in figure D12. It is seen that the mass rises almost linearly with temperature. It should be recalled that the soliton mass is given by the ratio of the spin wave energy at the zone centre to that at the zone boundary and that the low wavevector spin waves renormalize upwards (De Raedt and De Raedt, 1977, and Chapter 3, this thesis) with temperature before they damp out altogether. The zone boundary spin waves on the other hand show little temperature dependence at all. Thus an upwards renormalization of the mass is consistent with this result.

A comparison is made between the theoretical lineshape, convoluted with experimental resolution, using the temperature dependent soliton mass

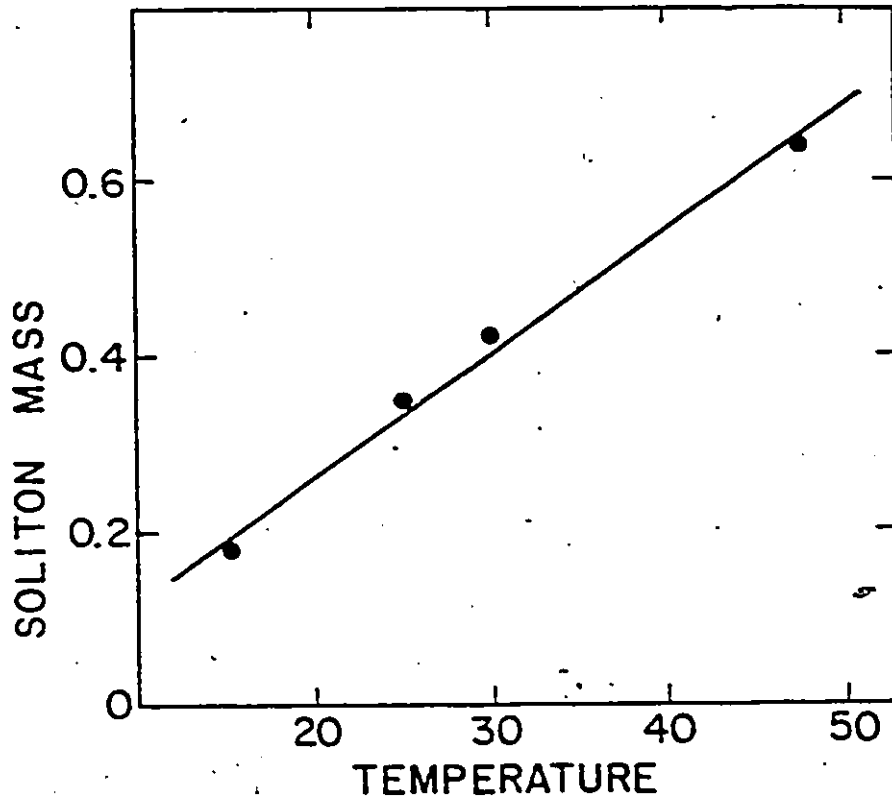


Figure D12: The apparent temperature dependence of the soliton mass is shown. This temperature dependence was ascribed to the mass in order to describe the temperature dependence of $S_{ZZ}(\mathbf{Q}_z, \hbar\omega = 0.5 \text{ meV})$ shown in figure D11. An upward renormalization of the soliton mass with increasing temperature is consistent with the upward renormalization of the spin wave energy near the zone centre.

and our measurements in figure D13. The agreement between the two is clearly good.

This concludes the description of our neutron investigations of solitons in CsMnBr_3 . However Monte Carlo simulation work in Chapter 8 will provide a different perspective on the relevance of solitons in an anisotropic Heisenberg chain system. This later section will address points on the viability of the soliton model in different ranges of temperature, as well as the question of stability.

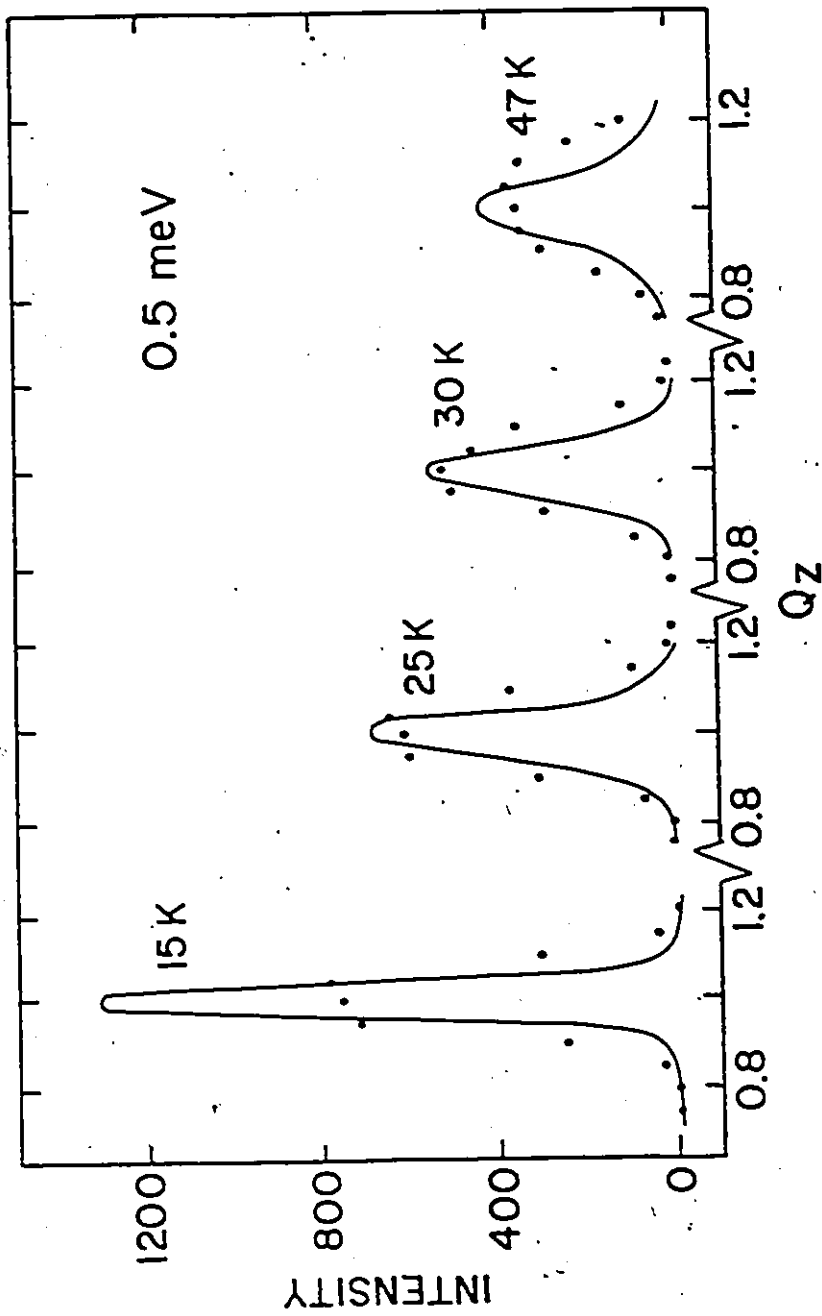


Figure D13: A comparison is made between the line shape of $S^{zz}(Q_z, \hbar\omega) = 0.5 \text{ meV}$ and the modified soliton theory convoluted with the spectrometer resolution, as a function of temperature. The vertical scale for the theory is set by requiring agreement with the integrated intensity as shown in figure D11.

CHAPTER 5

SPIN WAVES AND LOCAL MODES IN $\text{CsMn}_{0.89}\text{Fe}_{0.11}\text{Br}_3$

5.1 Introduction

It has long been apparent that the presence of impurities in magnetic systems produces interesting physics (Cowley and Buyers, 1972; Birgeneau et al., 1984). The range of co-operative phenomena found in these systems is quite impressive. Areas of interest have included percolation of correlations (Cowley et al., 1980), competing interactions and anisotropies (Fishman and Aharony, 1978), and much recent work on quenched random fields (Yoshizawa et al., 1982 and Aharony, 1985).

The presence of impurities in one-dimensional magnetic insulators produces particularly pronounced effects. This is for essentially the same reasons as why thermal fluctuations are so important in one dimension; that is because for short-range interactions and a one-dimensional system there is only one possible path from one side of the sample to the other. Therefore, for example, the percolation limit for magnetic vacancies is full concentration. This is to say that any magnetic vacancies at all will preclude the possibility of long range order even at zero temperature, and the system is broken up into isolated finite patches.

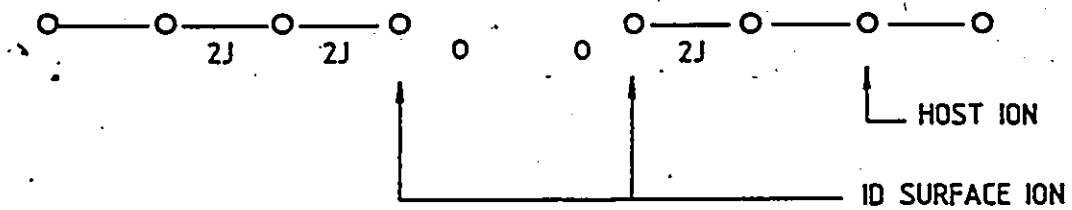
Each magnetic site feels a mean exchange field from only two nearest neighbours. This is as opposed to two and three-dimensional systems where the number of magnetic sites contributing to the mean exchange field on any one particular magnetic site is considerably higher. This leads to

strong host-mode-impurity-mode coupling effects which are not seen in higher dimensions. This has consequences on the experiment to be presented here for $\text{CsMn}_{0.89}\text{Fe}_{0.11}\text{Br}_3$. It means that simple theoretical approaches, such as the single ion approach, will not provide an adequate description of the dynamics of the impurity and host moments. In spite of this, this is specifically what we will use to start to analyse our data. We will then explicitly see the breakdown of the single ion approach and infer strong host-mode-impurity-mode coupling from this analysis. As such the theoretical analysis contained in this chapter is less complete than in any other part of this thesis. However, the observed behaviour is qualitatively very different from either "pure" CsMnBr_3 or any magnetic vacancy or "weak link" one-dimensional system, and therefore is interesting in its own right.

Two one-dimensional impurity systems have been previously studied by neutron scattering techniques. These are the quasi-classical Heisenberg system $(\text{CD}_3)_4\text{Mn}_x\text{Cu}_{1-x}\text{Cl}_3$ (Endoh et al., 1981) and the quantum Ising-like system $\text{CsCo}_x\text{Mg}_{1-x}\text{Cl}_3$ (Nagler et al., 1984). In the latter case the Mg^{+2} ion is strictly diamagnetic and hence the system is a collection of isolated patches. In the former case the Cu^{+2} ion carries a small moment and thus it represents a "weak link" system, although much of its behaviour can be understood in terms of diamagnetic impurities.

In $\text{CsCo}_x\text{Mg}_{1-x}\text{Cl}_3$ there is no impurity mode as the impurity is a magnetic vacancy; while in $(\text{CD}_3)_4\text{Mn}_x\text{Cu}_{1-x}\text{Cl}_3$ the impurity mode would be expected to be very weak. However there would be expected to be a one dimensional "surface" mode present in both cases. This is shown schematically in figure E1. The magnetic host ion (either Mn^{+2} or Co^{+2}) bordering on a vacancy would feel a different mean exchange field than a host ion sur-

MAGNETIC VACANCY SYSTEM



MAGNETIC IMPURITY SYSTEM

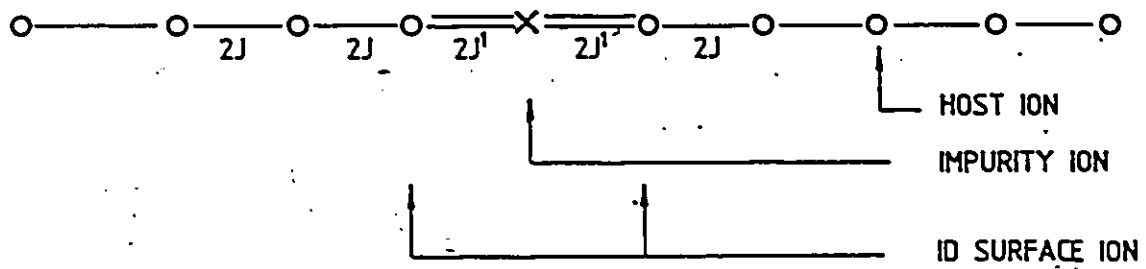


Figure E1: A schematic diagram showing the two magnetic environments of the magnetic vacancy system and the three magnetic sites of the magnetic impurity system. $\text{CsMn}_{0.89}\text{Fe}_{0.11}\text{Br}_3$ is a magnetic impurity system.

rounded by other host ions. In fact the one-dimensional surface ion would feel one half the mean exchange field felt by the host ions. We may then expect two branches of excitations to be present. One of these would be a host mode resembling the spin wave spectrum of the pure system, while the other would be a new surface mode. If the single ion fluctuations of these two types of magnetic sites (host and surface) do not interact with the other mode appreciably, then we would expect the magnetic zone boundary excitation frequency ratio (for host to surface) to be two to one.

The experimental picture is very interesting. A surface mode was found by Nagler et al. at roughly one half the zone boundary spin wave frequency in $\text{CsCo}_x\text{Mg}_{1-x}\text{Cl}_3$, while no additional mode was found at all for the $(\text{CD}_3)_4\text{Mn}_x\text{Cu}_{1-x}\text{Cl}_3$ case by Endoh et al. What, at first glance, appears to be very different behaviour in the two compounds can actually be understood by considering the host-mode-surface mode coupling and how the host mode dispersion depends on spin dimensionality. For the pure Heisenberg antiferromagnetic chain the spin wave dispersion is $\hbar\omega = 4JS \sin(q_c\pi)$ where q_c goes from zero to 0.5 on going from the magnetic zone centre to zone boundary. Therefore in $(\text{CD}_3)_4\text{Mn}_x\text{Cu}_{1-x}\text{Cl}_3$ the single ion fluctuation of a surface Mn^{+2} spin can lower its energy considerably by coupling to zone centre host spin waves. In this one dimensional case this coupling will be very strong as the fluctuation of the surface Mn^{+2} spin represents the disruption of half of the mean field felt by its nearest neighbour host Mn^{+2} spin. Physically this means that the surface spin cannot fluctuate without the host spins rotating with the fluctuation, thereby driving this surface mode frequency below the lowest host mode frequency to zero. This

does not occur in higher dimensions as the host mode-surface (or impurity) mode coupling is much weaker. This is because the fluctuation of a surface magnetic moment in higher dimensions represents the disruption of only a small fraction of the mean exchange field felt by its nearest neighbour host magnetic moments.

The same phenomenon occurs in the Ising-like system $\text{CsCo}_x\text{Mg}_{1-x}\text{Cl}_3$, however the host spin wave dispersion for a purely Ising system is flat at $\hbar\omega = 4JS$. This is modified somewhat in $\text{CsCo}_x\text{Mg}_{1-x}\text{Cl}_3$ by transverse spin contributions in the Hamiltonian, however the qualitative idea is the same; there is a large spin wave gap even at the zone centre. This means that the surface mode cannot lower its energy by coupling to low energy zone centre host spin waves as in $(\text{CD}_3)_4\text{Mn}_x\text{Cu}_{1-x}\text{Cl}_3$, because there are none. Thus the surface mode indeed appears at roughly one half the zone boundary host spin wave energy.

The point of this discussion is that the strong host mode-impurity mode coupling present in the Heisenberg-like impurity chain system invalidated the single ion description of the surface mode. As the single ion approach treats the modes as non-interacting, the failure of this approach is evidence in itself for this strong coupling.

The subject of our experimental investigation is $\text{CSMn}_{1-x}\text{Fe}_x\text{Br}_3$ with $x = 0.11$. The crystal was described in Chapter 1 and can be thought of as being made up of chains of magnetic sites along the hexagonal c direction, 89% of which are occupied by Mn^{+2} with 11% Fe^{+2} randomly interspersed. In this case the impurity itself, Fe^{+2} , is believed to carry a large magnetic moment on it. Thus the physics of this system should be qualitatively different than that of the two systems previously described. A qualitative single ion picture of this system produces three branches of excitation;

one corresponding to the host Mn^{+2} mode, one to the Mn^{+2} surface mode and one to the impurity Fe^{+2} mode. This is shown also schematically in figure E1.

An investigation of the single ion properties of Fe^{+2} in almost exactly the same crystalline environment as the present case has been carried out for $RbFeBr_3$ (Lines and Eibschutz, 1975). This study found that Fe^{+2} in this environment exhibits relatively strong easy-plane anisotropy due to its orbitally unquenched angular momentum. Numerical values were produced for the single ion parameters appropriate to Fe^{+2} in this environment, and we will make use of these in our present study.

A static susceptibility study of this crystal has been carried out in collaboration with C.V. Stager. The data are consistent with an anti-ferromagnetic Mn-Fe interaction on the basis of a comparison to an exact treatment of the static behaviour of the classical impure chain (Thorpe, 1975). The strength of this interaction is difficult to ascertain from this measurement. Possible Fe-Fe interactions are even harder to determine; but these are not important in our study due to the small proportion of Fe moments which would find themselves bordering another Fe moment in this crystal.

With this in mind, we can write the Hamiltonian for this system as

$$H = - 2 \sum_i J(i, i+1) S_{-i} \cdot S_{-i+1} + |\Delta| \sum_i (L_i^z)^2 + |\lambda| \sum_i (S_{-i} \cdot L_{-i}) \quad (5.1)$$

In this expression

$$J \text{ (Mn-Mn)} = -0.88 \text{ meV}$$

$$J \text{ (Mn-Fe)} < 0$$

$$\Delta = 73.02 \text{ meV}$$

$$\lambda = 9.92 \text{ meV}$$

$$S_{Mn}^z = 5/2$$

$$S_{Fe} = 2$$

$$L_{Fe} = 1 \quad L_{Mn} = 0$$

The Hund's rule ground state of Fe^{+2} is $S = 2$ and $L_H = 2$, but as we will see, it is convenient to use this $L = 1$ assignment due to the splitting of the $2L_H + 1$ states by the crystal field.

The remainder of the chapter is organized as follows. First our neutron scattering results will be presented and contrasted to the pure CsMnBr_3 case. Then a single ion analysis of Fe^{+2} according to the appropriate single ion Hamiltonian derived from equation (5.1) will be performed. The results of this analysis will then be confronted with experiment and qualitative conclusions will be drawn from this comparison.

5.2 The Neutron Scattering Experiment

We measured the inelastic magnetic response of $\text{CsMn}_{0.89}\text{Fe}_{0.11}\text{Br}_3$ at temperatures of 18K and 25K across the magnetic zone by neutron scattering techniques. Once again the measurements were made on the McMaster spectrometer (E-2) at the N.R.U. reactor, Chalk River.

The single crystal sample was cylindrical in shape with an estimated volume of 15 cm^3 and a mosaic spread of 0.5° (FWHM). It was mounted in a closed cycle refrigerator with its $hh\ell$ plane lying in the scattering plane. Measurements were made in the constant Q mode with the scattered neutron energy fixed at 14.90 meV and a pyrolytic graphite filter placed in the scattered beam to remove higher order contamination. Other experimental details are given in table A1.

As before the magnetic zone centre corresponds to $Q_z = 1.0$ in scans of the form (h, h, Q_z) and $Q_z = 1.5$ corresponds to the magnetic zone boundary. Scans along $(0, 0, Q_z)$ sample fluctuations within the easy (basal) plane and out of plane fluctuations are picked up by scattering geometries such

that Q is not parallel to the c axis, such as $Q = (-.75, -.75, Q_2)$. Constant Q scans for $Q_2 = 1.0$ and 1.05, 1.15, 1.2, 1.3, and 1.4 and 1.5 are shown in figures E2 to E6 respectively. Two excitations are clear in most of these scans with the clearest view of the two modes together being in the $Q = (0, 0, 1.3)$ scan at 18K in figure E5. The energy of these excitations is plotted as a function of wave vector across the magnetic zone for scans which sample in-plane fluctuations only, in figure E7. Also plotted on this graph is the measured spin wave dispersion in pure CsMnBr_3 as reported in Chapter 3.

The spectrum of $\text{CsMn}_{0.89}\text{Fe}_{0.11}\text{Br}_3$ is markedly different than that of CsMnBr_3 . Most notable of these differences is the appearance of a strong-intensity new mode which is flat at the mid-spin wave band energy of 4.5 ± 0.3 meV. The connectivity of the two branches of excitation is difficult to determine where they "cross" at $Q_2 = 1.15$, and thus this was left out of figure E7. If we refer to the portions of the excitation branches going to 10.0 ± 0.3 meV at the zone boundary and going to zero energy at the zone center as being host-like, then this host-like behaviour is clearly different than the spin wave response in pure CsMnBr_3 . The zone-centre response does not appear to be heading to the anisotropy gap value of 1.7 ± 0.2 meV as in CsMnBr_3 but rather seems to be going to zero energy. In addition the zone boundary host-like response is lifted up above that of 8.8 meV found in CsMnBr_3 to 10.0 meV.

Very interesting effects are found when out-of-easy plane fluctuations are sampled. The clearest effects are seen in figure E5 which shows scans at $Q_1 = (0, 0, 1.3)$ and $Q_2 = (-.75, -.75, 1.3)$. The two modes are of roughly equal intensity at $Q_1 = (0, 0, 1.3)$, however at $Q_2 = (-.75, -.75, 1.3)$

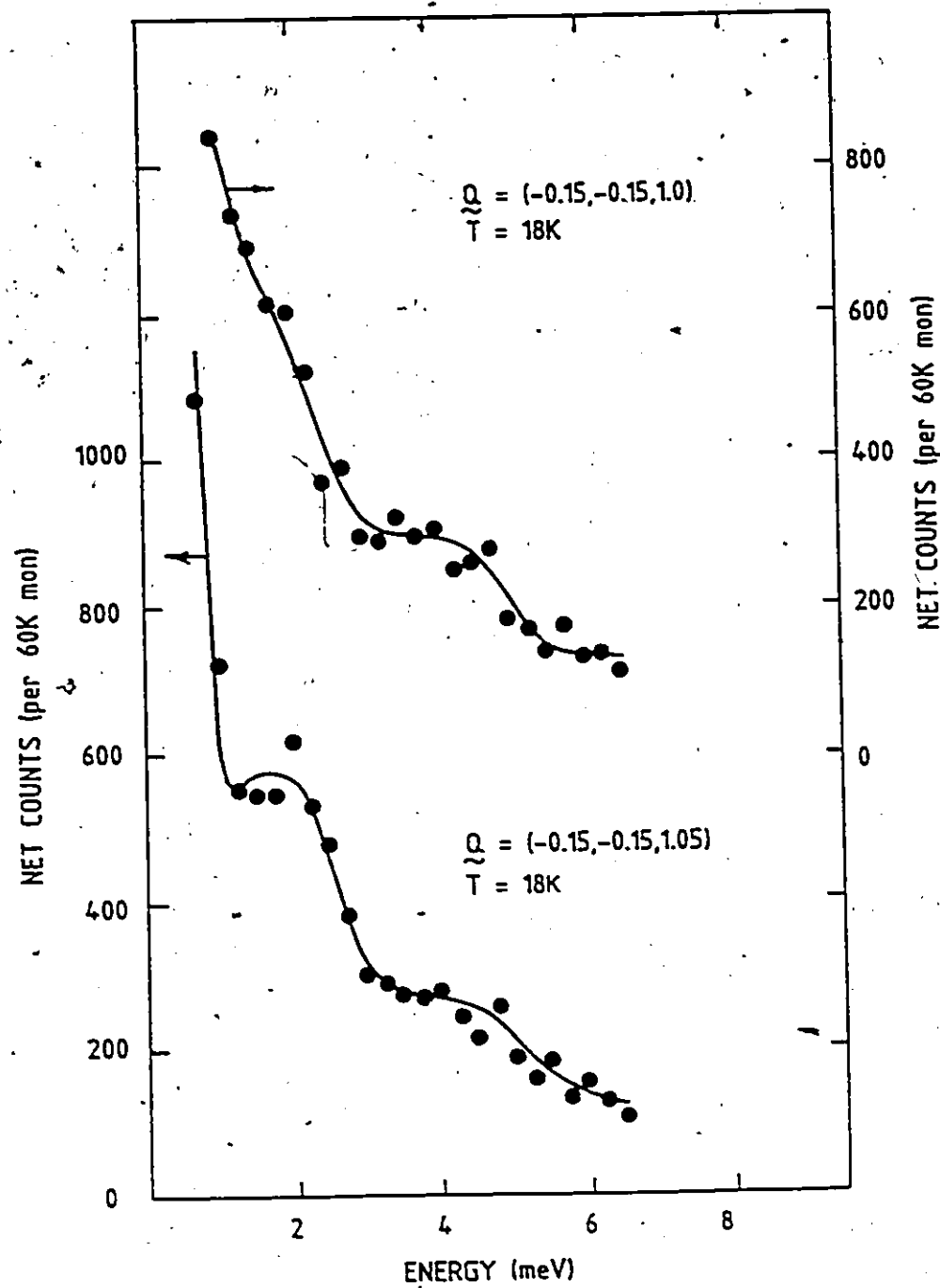


Figure E2: Inelastic scattering at $T = 18K$ at the magnetic zone centre, $Q = (-0.15, -0.15, 1.0)$ and 10% of the way to the zone boundary, $Q = (-0.15, -0.15, 1.05)$. The lower energy mode at $Q_z = 1.05$ has dispersed under the incoherent elastic peak at $Q_z = 1.0$.

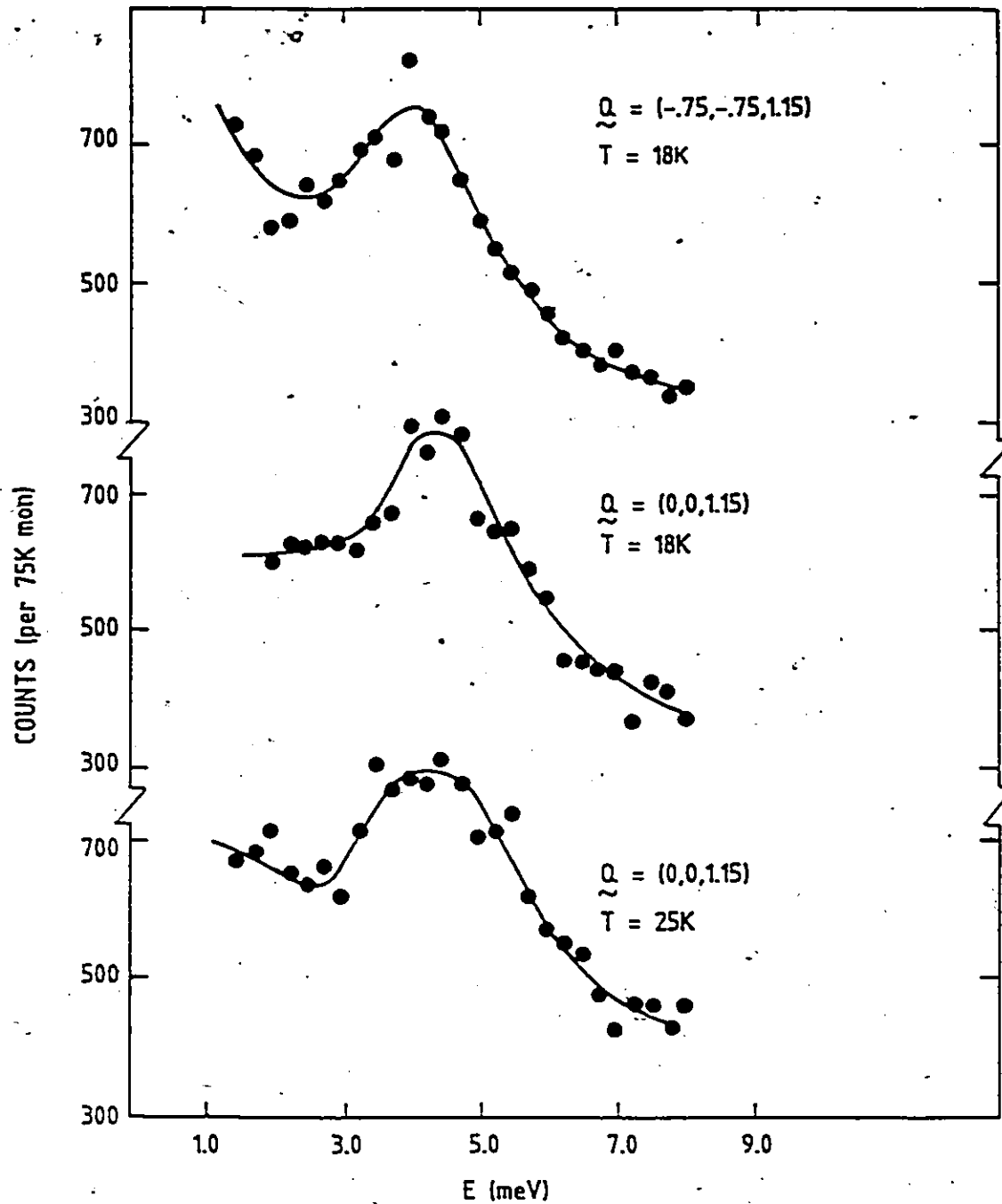


Figure E3: Inelastic scattering 30% of the way to the zone boundary at $Q_z = 1.15$. The scans at $\vec{Q} = (0, 0, 1.15)$ sample fluctuations within the basal plane while the $\vec{Q} = (-.75, -.75, 1.15)$ has substantial contribution to its intensity from out-of-plane fluctuations. This is the wavevector at which the two modes "cross".

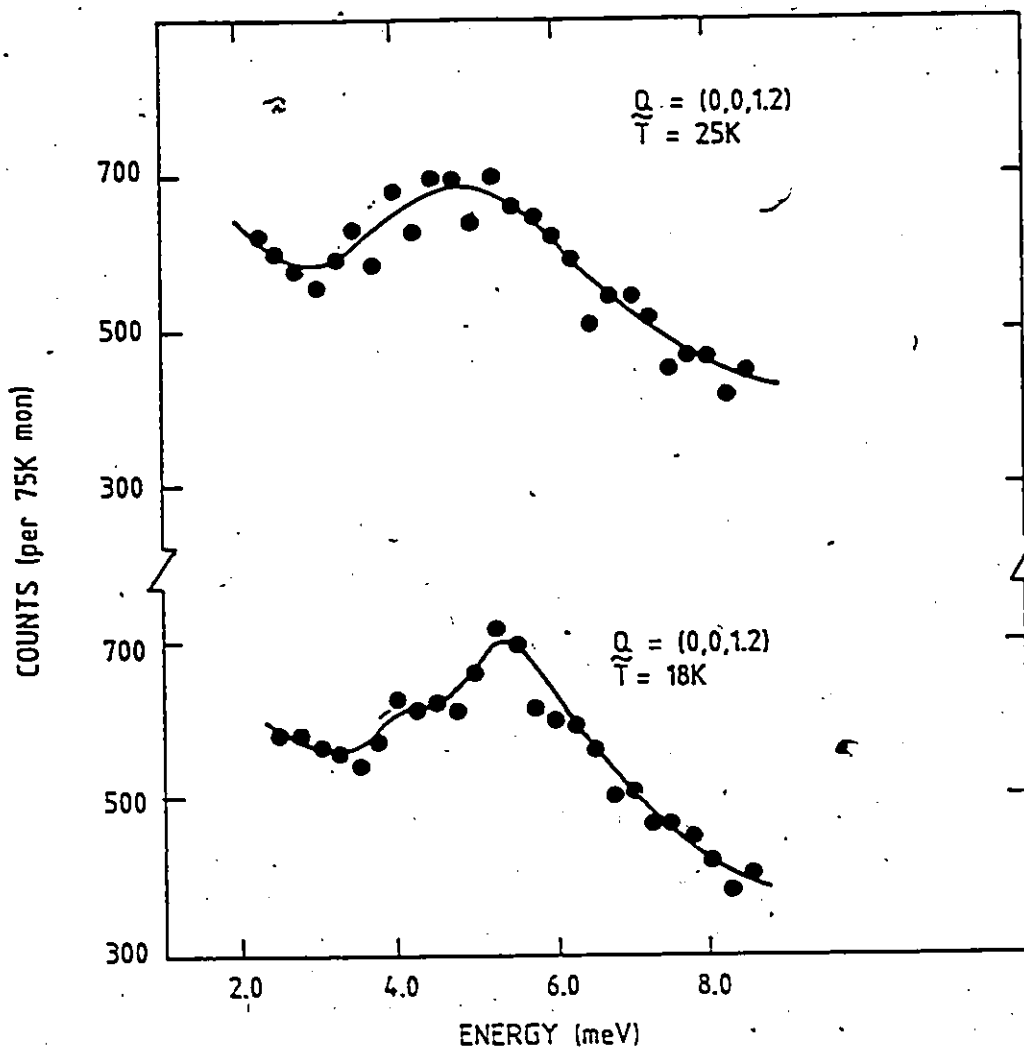


Figure E4: Inelastic scattering 40% of the way to the zone boundary at $Q_z = 1.2$ and at $T = 18K$ and $25K$. Two unresolved modes are present in the $T = 18K$ scan while thermal broadening at $T = 25K$ is sufficient to hide this structure of the scattering.

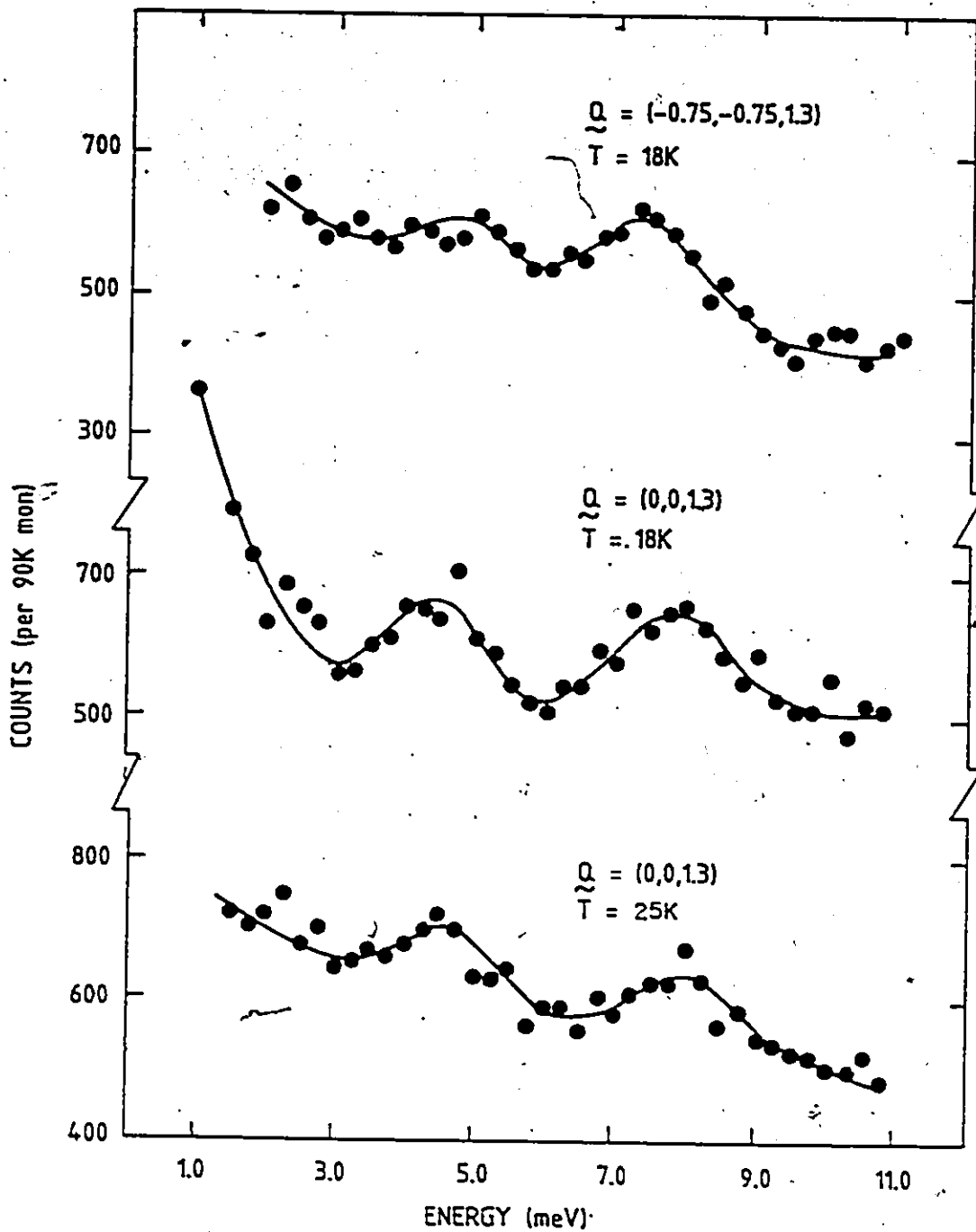


Figure E5: Inelastic scattering at 60% of the way to the zone boundary, $Q_z = 1.3$. Two modes are clearly resolved in the $Q = (0, 0, 1.3)$ scan at $T = 18K$. The scan at $Q = (-.75, -.75, 1.3)$ reveals an interesting polarization dependence to the scattering. Note that the intensity of the lower energy mode drops off strongly as out-of-basal-plane fluctuations are sampled, while the upper energy peak relaxes to slightly lower energies.

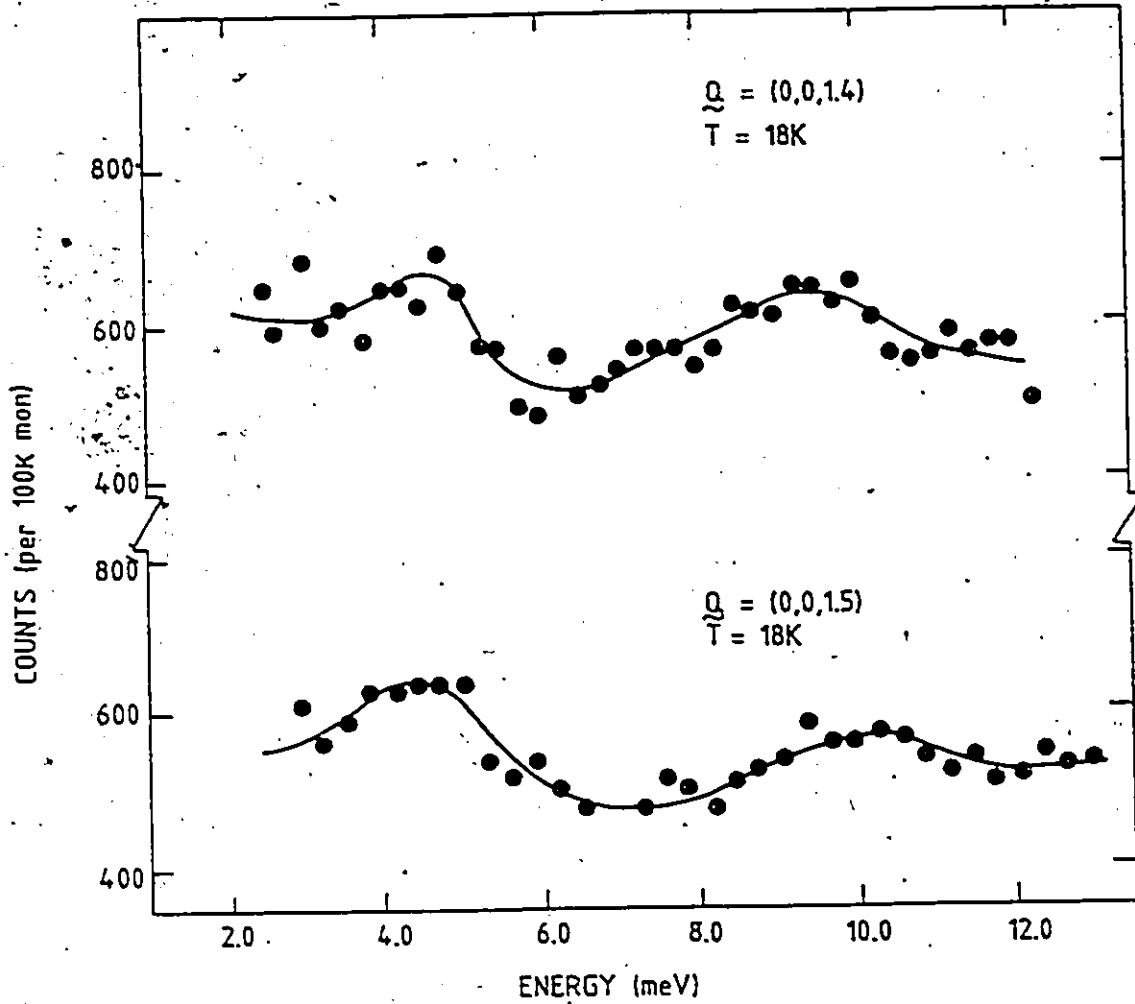


Figure E6: Inelastic scattering at 80% of the way to the zone boundary, $Q_z = 1.4$, as well as at the zone boundary, $Q_z = 1.5$, for $T = 18K$:

the lower energy mode at ~ 4.5 meV is drastically reduced in intensity compared with the higher energy host-like mode. One would expect a reduction in intensity on going from Q_1 to Q_2 due to the fall off of the magnetic form factor, however both modes fall off equally due to this cause. We therefore take this as evidence that the lower energy mode at 4.5 meV is strongly easy-plane-like. This suggests that it is the impurity mode due to Fe^{2+} which we know displays marked planar anisotropy in this environment.

An additional interesting effect which is clear from comparing the same two scans, Q_1 and Q_2 is that the higher energy mode softens in energy from 7.8 ± 0.3 meV to 7.3 ± 0.3 meV as out-of-plane fluctuations are sampled. This can also be seen in scans at $Q = (0,0,1.15)$ and $Q = (-.75,-.75,1.15)$ at $T = 18K$ shown in figure E3. We have not established the nature of the softening of these modes. However a plausible explanation is that what we have referred to as the host-like mode is actually the superposition of a host and a surface mode of similar, but not identical, energies. This surface mode is also strongly easy-plane-like as it arises from motion of the spin in the exchange field of the strongly easy-plane-like impurity moment. Thus as out-of-easy-plane-fluctuations are sampled, the surface mode's intensity falls off quickly, leaving predominantly the host mode present, which fluctuates at a slightly lower energy.

The impurity and host modes are most distinct in energy at the zone boundary. Unfortunately due to the flatness of both modes' dispersion, and the fact that $\chi(Q)$, the wave vector dependent susceptibility, is at a minimum at the zone boundary, these modes are difficult to observe. These are shown in figure E6. Thus it is difficult to see if the upper host mode is actually comprised of two modes or not.

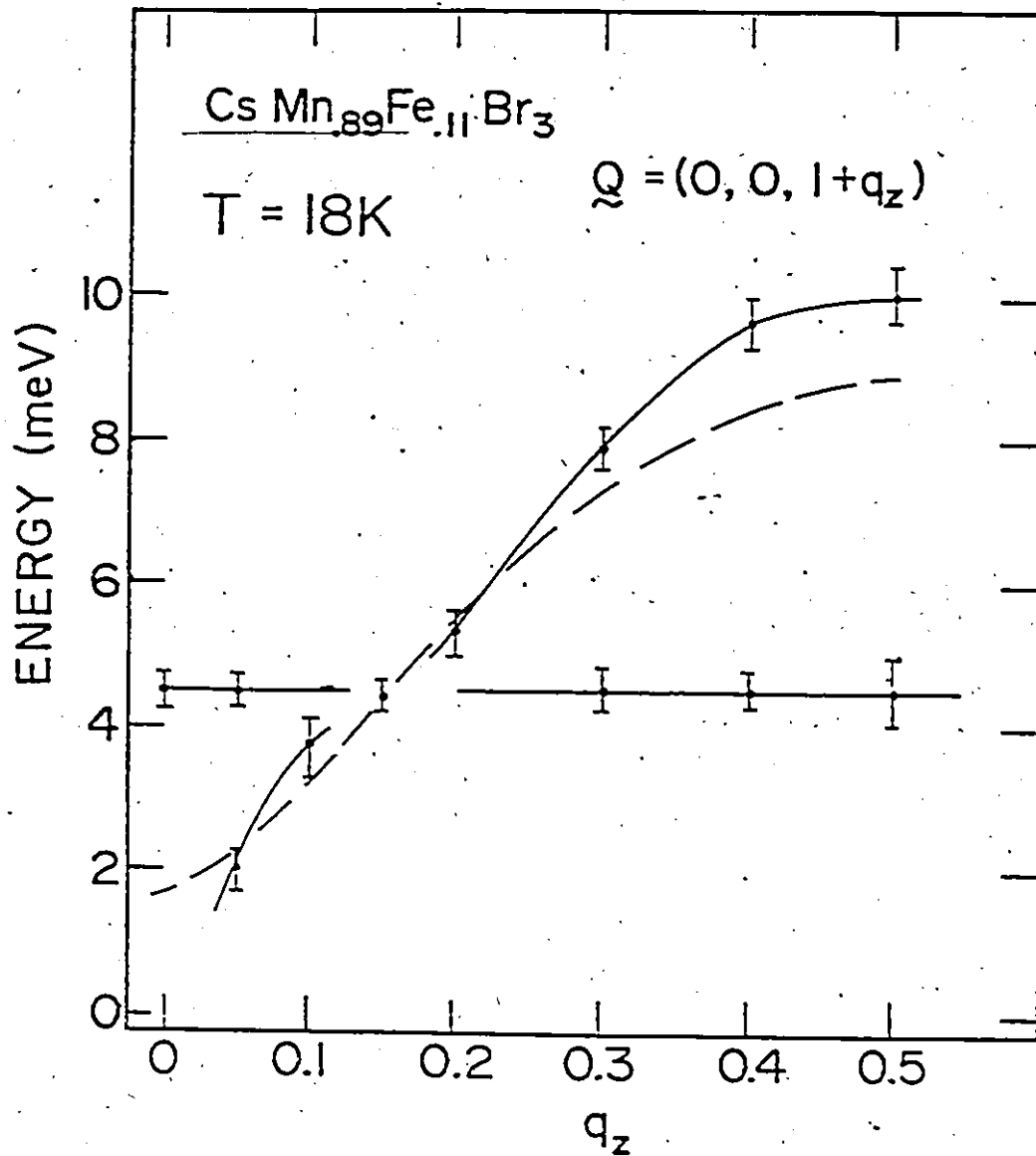


Figure E7: The dispersion of the magnetic excitations in $\text{CsMn}_{0.89}\text{Fe}_{0.11}\text{Br}_3$ at $T = 18\text{K}$ for wavevectors $\underline{Q} = (0, 0, 1+q_z)$ is shown. The solid lines are guides to the eye showing two modes. The dashed line is the spin wave dispersion of CsMnBr_3 taken from Chapter 3.

The magnetic zone centre response is shown in figure E2. Both modes are clearly visible at $Q_z = 1.05$, while the lower energy mode is not seen at $Q_z = 1.0$, the zone centre. This is consistent with two modes, one of which is going to zero energy at zero wave vector while the other is dispersionless at 4.5 meV. In the pure CsMnBr_3 system an out-of-easy plane spin wave was observed near 1.7 meV. A plausible explanation of the difference between the pure system's spectrum and that of $\text{CsMn}_{0.89}\text{Fe}_{0.11}\text{Br}_3$ is that the strong planar anisotropy of the Fe^{+2} moment lifts the out-of-plane, long wavelength (zone centre) spin wave up to 4.5 meV.

Relatively strong temperature effects can be seen on the modes as the temperature is raised from 18K to 25K. This can be seen for mid-zone spin waves in figures E3, E4 and E5. It appears both modes are affected by the temperature as seen in figure E5, the only scan where they can be observed separately. We expect the host spin wave branch to display thermal broadening at least as severe as the spin wave response in CsMnBr_3 as discussed in Chapter 3).

5.3 Single Ion Analysis

As we mentioned we are greatly aided in our analysis of Fe^{+2} in this environment by a previous study of Fe^{+2} in RbFeBr_3 by Lines and Eibshutz. Their work is relevant as the local environment of Fe^{+2} is virtually the same in both crystals.

We will discuss the level scheme of Fe^{+2} in a single ion picture in two ways. First a qualitative description of splittings will be given and then a detailed full Hamiltonian diagonalization will be employed to produce the eigenstates and their splittings according to equation (5.1).

The Fe^{+2} configuration with six "d" electrons results in a Hund's rule ground state of $S = 2$, $L_H = 2$. However the action of the cubic part of the crystal field on the orbital angular momentum is to split the $(2L_H+1) = 5$ levels into an upper orbital doublet and a lower-orbital triplet. The splitting of the doublet and triplet is sufficiently large to make the doublet not thermodynamically relevant for the temperatures which we are interested in. Thus we can define a new fictitious orbital angular momentum $L = 1$, as there are now $(2L+1) = 3$ thermodynamically relevant states. However within this triplet of states the matrix elements of real L_H are -1 times the value of equivalent matrix elements of L . In addition matrix elements of $(L_H^z)^2$ are 3 times those of $(L^z)^2$.

The coupling of spin and orbital angular momentum together via the spin-orbit coupling parameter, λ , leads to $(2S+1)(2L+1) = 15$ levels to be dealt with. As Fe^{+2} is a more than half filled shell, the interaction should act such that spin and real orbital angular momentum can lower their energy by aligning parallel. Of course this implies that spin and fictitious orbital momentum can lower their energy by aligning antiparallel. Thus the ground state will be a $J = S-L = 1$, triplet with an excited state quintet, $J = 2$, and septet, $J = 3$. This accounts for the 15 levels.

In this qualitative discussion let us just concern ourselves with the ground state triplet. This discussion can be followed most easily with reference to figure E8. The action of the non-cubic part of the crystal field can be considered by the application of a trigonal distortion parameter, Δ , relevant for this environment. As one can see by reference to the Hamiltonian, equation (5.1), the action of this term is to suppress

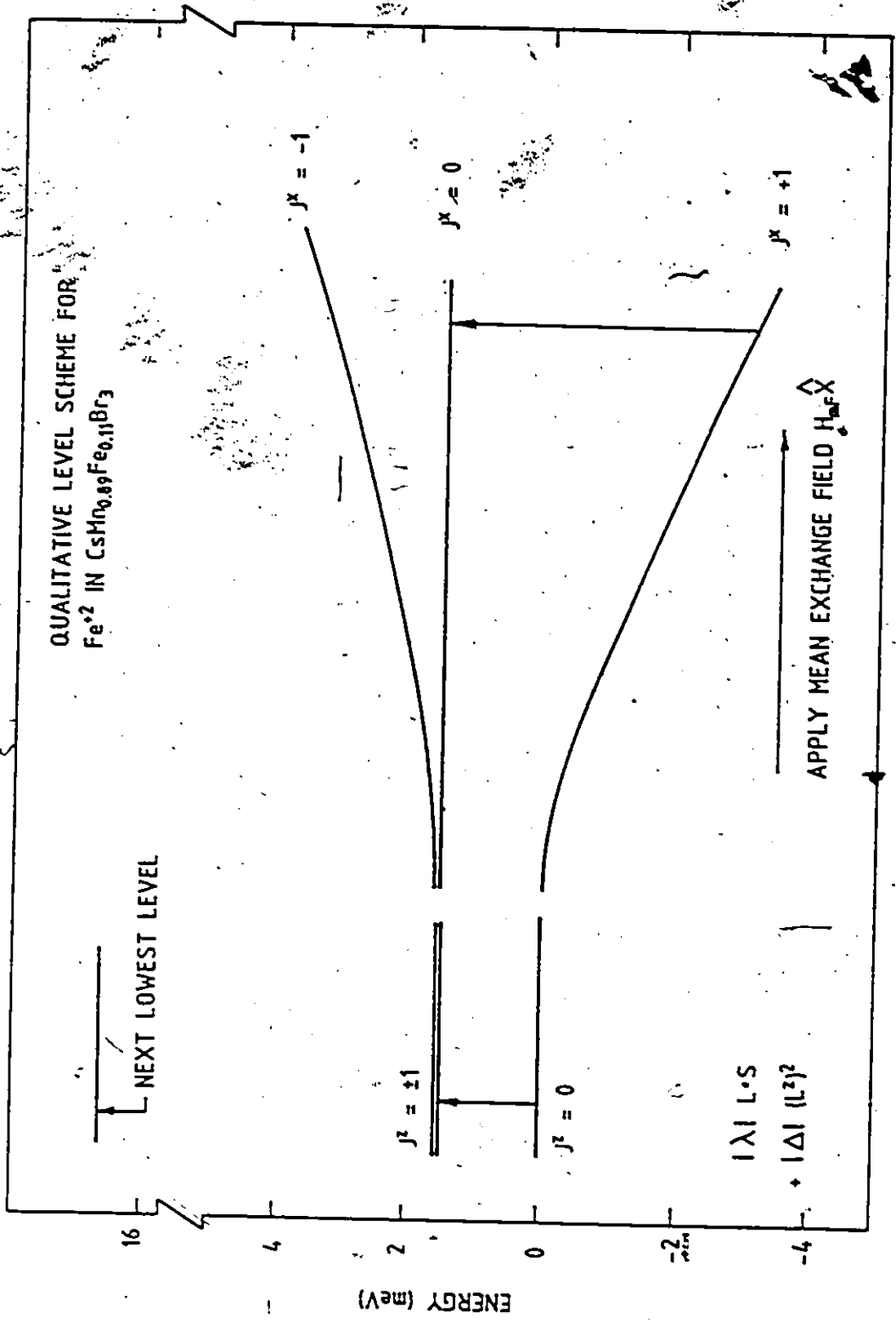


Figure E8: The qualitative level scheme for Fe⁺² in the CsMn_{0.89}Fe_{0.11}Br₃ environment. This shows only the lowest three of the levels for Fe⁺² and the J² and J^X assignments are, of course, approximate. Note that a 4.5 meV transition from the ground state is not possible in the absence of Mn-Fe exchange.

components of orbital angular momentum and by virtue of the spin-orbit coupling, spin angular momentum in the z direction. Thus it imposes strong easy plane anisotropy. Choosing the quantization axis as the z direction it is clear that the $J^z = 0$ level will be the ground state with an excited state, $J^z = \pm 1$, doublet. The splitting, given by Lines and Eibschutz on the basis of the terms in the Hamiltonian considered so far, of the ground state and excited state doublet is roughly 1.5 meV. It is clear that this is too little to produce an impurity mode at 4.5 meV.

Finally we must consider the effect of the exchange interactions with neighbouring Mn^{+2} moments. As opposed to the other terms in the Hamiltonian, the exchange term is not a single ion interaction. However it can be written as a single ion term which approximates the full exchange; but the analysis may then only be relevant at the zone boundary where a spin may fluctuate independently. This, of course, assumes non-interacting modes. Therefore we treat the $Mn^{+2}-Fe^{+2}$ exchange in this mean field approximation and include a term $H_{MF}^{\hat{x}} \cdot S_{Fe}$ in the Hamiltonian. The Mn^{2+} moment lives predominantly within the easy plane at low temperatures, and this will be reinforced by either an antiferromagnetic or ferromagnetic $Mn^{+2}-Fe^{+2}$ interaction, as the Fe^{+2} moment also displays easy-plane anisotropy.

The action of the mean exchange field on this lowest triplet of states is also shown in figure E8. The ground state singlet which has $J^z = 0$ will now rotate to align itself within the easy plane with the mean exchange field. If we now choose this \hat{x} axis as the quantization axis, then the ground state becomes $J^x = +1$. The other two degenerate states (in the absence of exchange) must take on $J^x = 0$ and -1 . The action of

the mean field on these states is to raise the energy of the $J^x = -1$ state while not affecting the $J^x = 0$ state, thus breaking their degeneracy.

It should be clear that the assignments of the $J^{x,z}$ values are approximate and qualitative only. Of course considerable mixing of the states will occur which will be treated in full presently. However this does give a physical picture of the behaviour of the low lying states of Fe^{+2} in this environment.

We have diagonalized the following single ion Hamiltonian

$$H = - H_{MF} S^z + |\Delta| (L^x)^2 + |\lambda| S \cdot L \quad (5.2)$$

$$|\Delta| = 13.02 \text{ meV}$$

$$|\lambda| = 9.92 \text{ meV}$$

within the $(2L+1)(2S+1) = 15$ level basis $|L^z, S^z\rangle$. Here L^z can take on values ± 1 and 0 while S^z can take on values $\pm 2, \pm 1$ and 0. The values used for $|\Delta|$ and $|\lambda|$ are the same as used in equation (5.1) while the mean exchange field, H_{MF} , was adjusted so that the lowest energy transition from the ground state was 4.5 meV.

The Hamiltonian matrix is given in table B1 with the matrix elements in symbolic form. The 15×15 matrix diagonalization is straightforward with standard computer library routines. The eigenvectors and eigenvalues of the Hamiltonian, such that the lowest transition from the ground state is at 4.5 meV, are given in table B2.

The ground state is given by (to leading order)

$$|0\rangle = .24|1,0\rangle - .44|0,1\rangle + .86|-1,2\rangle - .12|1,2\rangle$$

while the first excited state is (also to leading order)

$$|1\rangle = .56|0,0\rangle - .66|-1,1\rangle = .48|1,-1\rangle + .15|1,1\rangle$$

and the strength of the mean exchange term required to produce the correct splitting is $H_{MF} = 2.6$ meV.

A neutron can excite dipole transitions between states, thus it is of interest to see what the matrix elements of S^z , S^+ and S^- are between the lowest states.

$$\langle 1|S^z|0\rangle = 0.0$$

$$\langle 1|S^+|0\rangle = 0.33$$

$$\langle 1|S^-|0\rangle = -2.05$$

Hence, there is clearly a strong transition possible due to S^- . This is expected as the ground state corresponds strongly to a fully aligned ($S^z = 2$) moment with the mean exchange field. Thus the first excitation is expected to be an S^- transition.

The components of spin along the ordering direction for the lowest triplet of states are

$$\langle 0|S^z|0\rangle = 1.68$$

$$\langle 1|S^z|1\rangle = 0.22$$

$$\langle 2|S^z|2\rangle = 1.39$$

which again is as expected and consistent with our earlier qualitative discussion.

The mean exchange field strength of $H_m = 2.6$ meV yields an apparent value for the $Mn^{+2} - Fe^{+2}$ exchange constant according to

$$-H_m = 4J(Mn-Fe)S_{Mn}$$

This produces $J(Mn-Fe) = -0.26$ meV as compared with $J(Mn-Mn) = -0.88$ meV,

TABLE B1

Hamiltonian Matrix (symmetric) for Fe⁺² in CsMn_{0.89}Fe_{0.11}Br₃
 $|L^Z, S^Z\rangle$ basis

	$ 0,0\rangle, 1,-1\rangle$	$ -1,-2\rangle$
$\langle 0,0 $	D	
$\langle -1,1 $	$-A*L, D/2+L-HM$	
$\langle 1,-1 $	$-A*L, 0, L+D/2+HM$	
$\langle 1,0 $	0,0,0,D/2	
$\langle 0,1 $	0,0,0,-A*L,D-HM	
$\langle -1,2 $	0,0,0;0,-B*L,D/2+2*L-2*HM	
$\langle -1,0 $	0,0,0,D/2,0,0,D/2	
$\langle 0,-1 $	0,0,0,0,0,0,-A*L,D+HM	
$\langle 1,-2 $	0,0,0,0,0,0,0,-B*L,2*L+2*HM+D/2	
$\langle 1,1 $	0,D/2,0,0,0,0,0,0,0,-L-HM+D/2	
$\langle 0,2 $	0,0,0,0,0,0,0,0,0,-B*L,D-2*HM	
$\langle -1,-1 $	0,0,D/2,0,0,0,0,0,0,0,-L+HM+D/2	
$\langle 0,-2 $	0,0,0,0,0,0,0,0,0,0,-B*L,D+2*HM	
$\langle 1,2 $	0,0,0,0,0,D/2,0,0,0,0,0,0,-2*L-2*HM+D/2 ;	
$\langle -1,-2 $	0,0,0,0,0,0,0,D/2,0,0,0,0,-2*L+2*HM+D/2	

$A = \sqrt{3}$ $B = \sqrt{2}$ $C = \sqrt{6}$

- $L = \lambda = -9.92$ meV - spin orbit coupling
- $D = \Delta = 13.02$ meV - trigonal distortion
- $HM = H_{MF} = 2.6$ meV - mean exchange field

EXPLANATION OF TABLE B2

The eigenvectors and eigenvalues of Fe^{+2} given in table B2 are labelled according to the following scheme. The lowest energy eigenvector is given by $|0\rangle$ and the highest by $|15\rangle$. The listing is of the following form, eg.

	$ 0\rangle$
$ 0,0\rangle$	0
$ -1,1\rangle$	0
$ 1,-1\rangle$	0
$ 1,0\rangle$.239
$ 0,1\rangle$	-.4359
$ -1,2\rangle$.85583
$ -1,0\rangle$	-.06614
$ 0,-1\rangle$.03658
$ 1,-2\rangle$	-.02899
$ 1,1\rangle$	0
$ 0,2\rangle$	0
$ -1,-1\rangle$	0
$ 0,-2\rangle$	0
$ 1,2\rangle$	-.11677
$ -1,-2\rangle$.00325
eigenvalue	- 26.56 meV

The basis states are $|L^Z, S^Z\rangle$.

TABLE B2

Eigenvectors and Eigenvalues for Fe⁺²
in CsMn_{0.89}Fe_{0.11}Br₃

0>	1>	2>	3>	4>	5>	6>	
0.00000	.55542	0.00000	.13304	0.00000	-.06583	0.00000	
-.00000	-.65586	.00000	.46199	-.00000	.39678	-.00000	
0.00000	-.47651	0.00000	-.61599	0.00000	-.34112	0.00000	
.23947	-.00000	.10555	-.00000	-.64580	.00000	-.36724	
-.43590	0.00000	-.01002	0.00000	.34541	0.00000	.34829	
.85583	-.00000	-.10875	.00000	.36626	-.00000	.22273	
-.06614	0.00000	-.37600	0.00000	.40393	0.00000	-.62393	
.03658	-.00000	.50318	.00000	-.06771	.00000	.32924	
-.02899	.00000	-.75650	.00000	-.38660	-.00000	.42749	
.00000	.14601	-.00000	-.41204	-.00000	.44818	-.00000	
-.00000	-.06867	.00000	.39355	-.00000	-.67410	-.00000	
0.00000	.08582	0.00000	.22212	0.00000	.21028	0.00000	
0.00000	-.02993	0.00000	-.12421	0.00000	-.14954	0.00000	
-.11677	.00000	.01794	.00000	-.08537	-.00000	-.07296	
.00325	0.00000	.09877	0.00000	.06566	0.00000	-.09192	
-26.56	-22.01	-18.31	-6.86	-6.77	-1.50	1.27	
7>	8>	9>	10>	11>	12>	13>	14>
.13351	0.00000	-.31506	0.00000	-.62791	0.00000	-.39764	0.00000
.20135	-.00000	-.02488	.00000	-.35222	.00000	-.18372	.00000
-.25710	0.00000	-.19544	0.00000	-.27590	0.00000	.31100	0.00000
.00000	.19080	-.00000	.46564	.00000	.29973	.00000	.19112
0.00000	.17048	0.00000	.64674	0.00000	.30761	0.00000	.16316
-.00000	-.09541	-.00000	.22783	.00000	.09408	.00000	.04592
0.00000	-.00188	0.00000	-.18895	0.00000	.33656	0.00000	.39093
-.00000	-.07396	.00000	-.40982	.00000	.37502	-.00000	.56429
-.00000	-.03027	.00000	-.12242	-.00000	.01104	-.00000	.28041
.01429	-.00000	.71289	.00000	-.30225	.00000	-.09087	.00000
-.10157	-.00000	.58095	.00000	-.18940	.00000	-.04797	.00000
-.61523	0.00000	.05563	0.00000	.34272	0.00000	-.63247	0.00000
.69750	0.00000	.11450	0.00000	.40108	0.00000	-.54848	0.00000
-.00000	-.95845	-.00000	.22531	.00000	.05944	.00000	.02240
0.00000	.02021	0.00000	.20877	0.00000	-.74102	0.00000	.61997
5.84	21.79	25.03	27.73	30.20	31.45	34.39	34.49

which says that the $Mn^{+2}-Fe^{+2}$ coupling is substantially weaker than the $Mn^{+2}-Mn^{+2}$ coupling.

5.4 Discussion

Thus far we have treated only the single ion behaviour of the Fe^{+2} impurity ion. But this actually has serious ramifications for the behaviour of the Mn^{+2} surface ions as well. Our final point of the single ion analysis was that the $Fe^{+2}-Mn^{+2}$ exchange coupling was substantially weaker than the $Mn^{+2}-Mn^{+2}$ coupling. The natural prediction to make from this is that the Mn^{+2} surface mode behaviour, or alterations to the host mode due to surface effects, should be such that the energy of these fluctuations is lowered. Yet as we have seen, the zone boundary host-like mode is raised up in energy in $CsMn_{0.89}Fe_{0.11}Br_3$ to 10.0 meV from 8.8 meV in $CsMnBr_3$. These two effects then are not consistent with each other, according to this single ion analysis.

In addition to this is the lack of dispersion for the Fe^{2+} impurity mode. The proper energy splitting could only be achieved on application of the exchange field due to neighbouring Mn^{+2} ions. This would be expected to change the nature of the impurity mode to co-operative from single-ion-like and thus from dispersionless to a mode with dispersion. This can be precluded by weak matrix elements for the ground to excited state transitions, however we have seen that this is not the case.

A plausible physical picture of this system which addresses the inconsistency present in the single ion analysis is as follows. The frequency of the zone boundary impurity fluctuation is pushed to lower energies by the host mode-impurity mode interaction in this crystal. How-

ever, it is not suppressed so much that it goes to zero frequency as does the surface mode in $(\text{CD}_3)_4\text{Mn}_x\text{Cu}_{1-x}\text{Cl}_3$. This implies that the apparent $\text{Mn}^{+2}\text{-Fe}^{+2}$ exchange constant derived from single-ion analysis will be considerably lower than the actual $\text{Mn}^{+2}\text{-Fe}^{+2}$ exchange constant, with the actual $\text{Mn}^{+2}\text{-Fe}^{+2}$ exchange being considerably stronger than the $\text{Mn}^{+2}\text{-Mn}^{+2}$ exchange. The zone boundary surface mode then will also be at a higher frequency than the Mn^{+2} host mode even after host mode-surface mode interaction has been taken into account. This argument is shown qualitatively in figure E9. The strong suppression of the Fe^{+2} impurity mode frequency then makes it appear dispersionless. Hybridization of the two modes may also occur so that they do not cross, with the nature of the modes changing from Mn-like to Fe-like as the mode progresses across the zone.

This qualitative model would then account for all the features we have observed in $\text{CsMn}_{0.89}\text{Fe}_{0.11}\text{Br}_3$. It is important to note that our information on the surface mode behaviour is not very complete, coming only from the polarization shift of the higher energy branch of excitation at $Q_z = 1.3$. The physics of this model is then considerably different than for either of the two one dimensional magnetic vacancy systems described earlier. Here the two new modes would lie outside the host spin wave band in a non-interacting mode picture. They would both be suppressed by the interaction with the host mode, however the impurity mode suppression must be considerably stronger than that of the surface mode.

The model notwithstanding, we take the inconsistency present in the single-ion analysis as evidence that substantial mode-mode interactions are present in this system. The opening remarks of this thesis mentioned

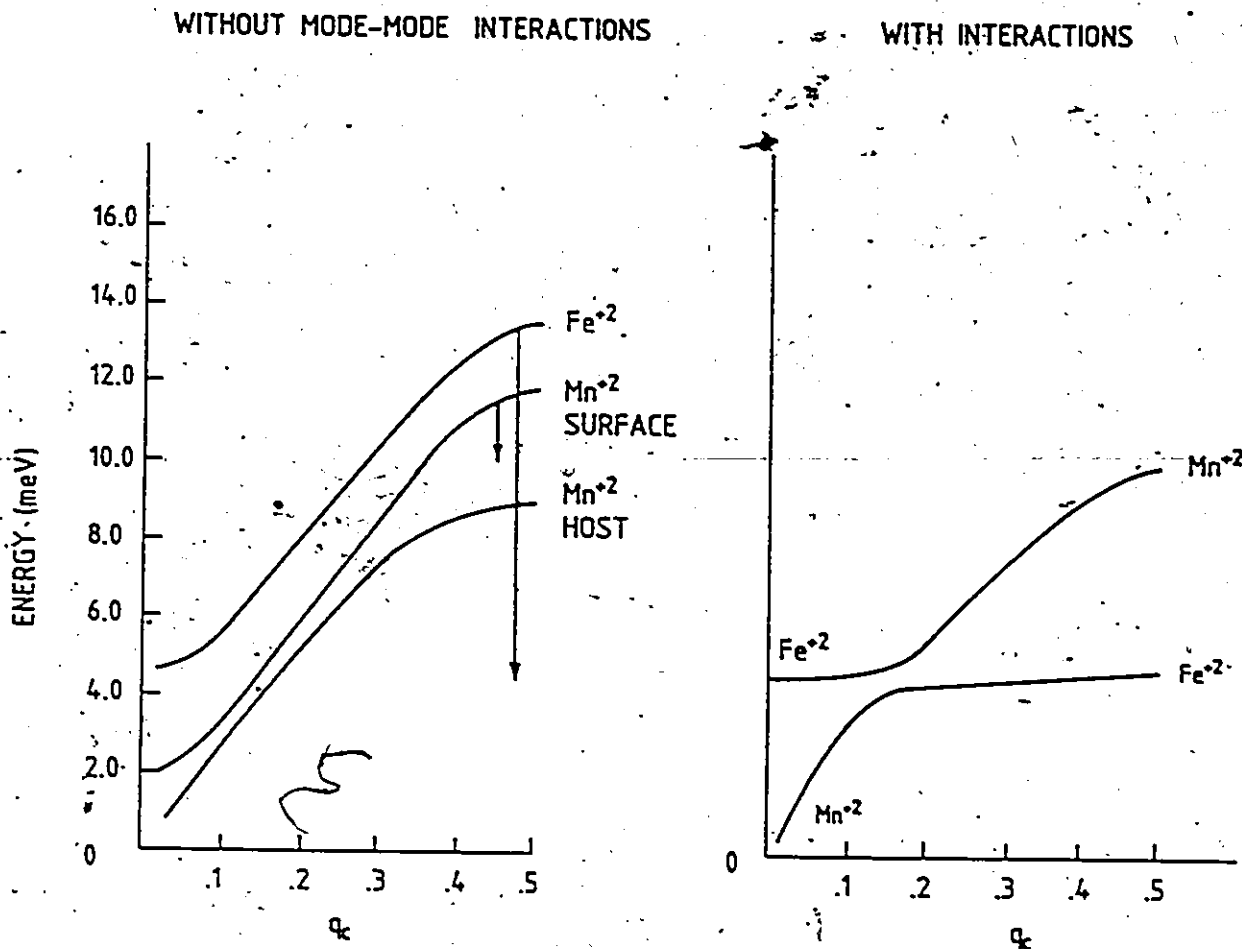


Figure E9: The interacting mode model is shown. In the absence of mode interactions three modes would be present with the Fe^{+2} impurity mode of highest energy at the zone boundary. The effect of the interactions is to strongly suppress the energy of the Fe^{+2} impurity mode, although not to zero energy. The Mn^{+2} surface mode is also suppressed to an energy close to the Mn^{+2} host mode at the zone boundary. Our single-ion calculations, which do not consider mode interactions, as well as our measurements are consistent with such a picture.

the failure of conventional mean field analysis for one dimensional systems, and thus we should not be too surprised by this result. It is also consistent with results on $(\text{CD}_3)_4\text{Mn}_x\text{Cu}_{1-x}\text{Cl}_3$ in which the host mode also has predominantly Heisenberg spin symmetry.

CHAPTER 6

THE MONTE CARLO METHOD

The thermodynamic properties of co-operative systems are only rarely understood in terms of exact solutions. Examples from magnetic systems include the one-dimensional classical Heisenberg and XY systems with nearest neighbour interactions only. These are particularly simple examples of co-operative phenomena because all the constituents in the co-operative system are identical and are localized at lattice sites in space. In addition only one interaction is relevant (that between a spin and its nearest neighbours) and the lattice is only connected to the interactions in so far as it determines the number and relative orientation of nearest neighbours. Of course there are other relevant contributions to the relative simplicity of any particular model, however relaxing any of these already mentioned conditions greatly complicates the understanding of a co-operative system, eliminating the possibility of exact solutions.

Most models of co-operative systems of current interest violate at least one of these conditions. For this reason it is very important to develop numerical and perturbative techniques to generate approximate solutions. With the growing availability of relatively high speed computers, the computer simulation has become the approximate technique of

choice in many areas of condensed matter physics. As opposed to perturbation techniques the computer simulation treats all interactions exactly, although it does not calculate all observables exactly.

The Monte Carlo method utilizes pseudo-random (hereafter referred to as random) number generators to examine the phase space, or thermodynamically relevant phase space, of some system and thereby calculate thermodynamic quantities. The applicability of the Monte Carlo method is not limited to this aim, as has been well documented (Binder, 1984).

The thermal average of any particular quantity, A , can be calculated by examining many different random configurations, v , of the system and numerically evaluating the energy, E_v , of these configurations according to the model Hamiltonian. The average is then given by

$$\langle A \rangle = \frac{\sum_v A_v \exp\{-E_v/kT\}}{\sum_v \exp\{-E_v/kT\}}$$

This is referred to as "simple sampling" as the distribution of points sampled in the system's phase space is uniform. Because the distribution of any such quantity in equilibrium is strongly peaked about its thermodynamic average value (Goodstein, 1975), this is not a very effective way of going about the calculation, as most of phase space does not contribute appreciably to the average. In practice it is only employed if the number of degrees of freedom of the system is small.

A much more effective way of going about the calculation is via "importance sampling" or the Metropolis (Metropolis et al., 1953) algorithm. According to this algorithm, the configurations themselves are generated with a probability weighted according to the Boltzmann factor. This means

that the thermodynamically relevant regions of phase space are preferentially sampled. The thermal average of some observable is then calculated from a straight average of the values extracted from these configurations, v' . That is as

$$\langle A \rangle = \sum_{v'} \frac{A_{v'}}{n}$$

where n is the number of configurations used in the average.

The Monte Carlo work contained in this thesis proceeds by the Metropolis algorithm for a classical spin chain. The difficulty involved in these problems, is the consideration of the effects of interactions which couple the spins to the crystallographic lattice. Specifically these are dipolar and single ion anisotropy terms in the Hamiltonian which induce the formation of an easy plane. Thus the angle a spin makes relative to the lattice is also important to its energy, in addition to the angle determined by the relative orientation of a pair of spins. This extra angle does not enter problems involving either bilinear or higher order exchange and in fact precludes the possibility of exact treatments for systems containing both exchange and interactions that couple the spin and the lattice.

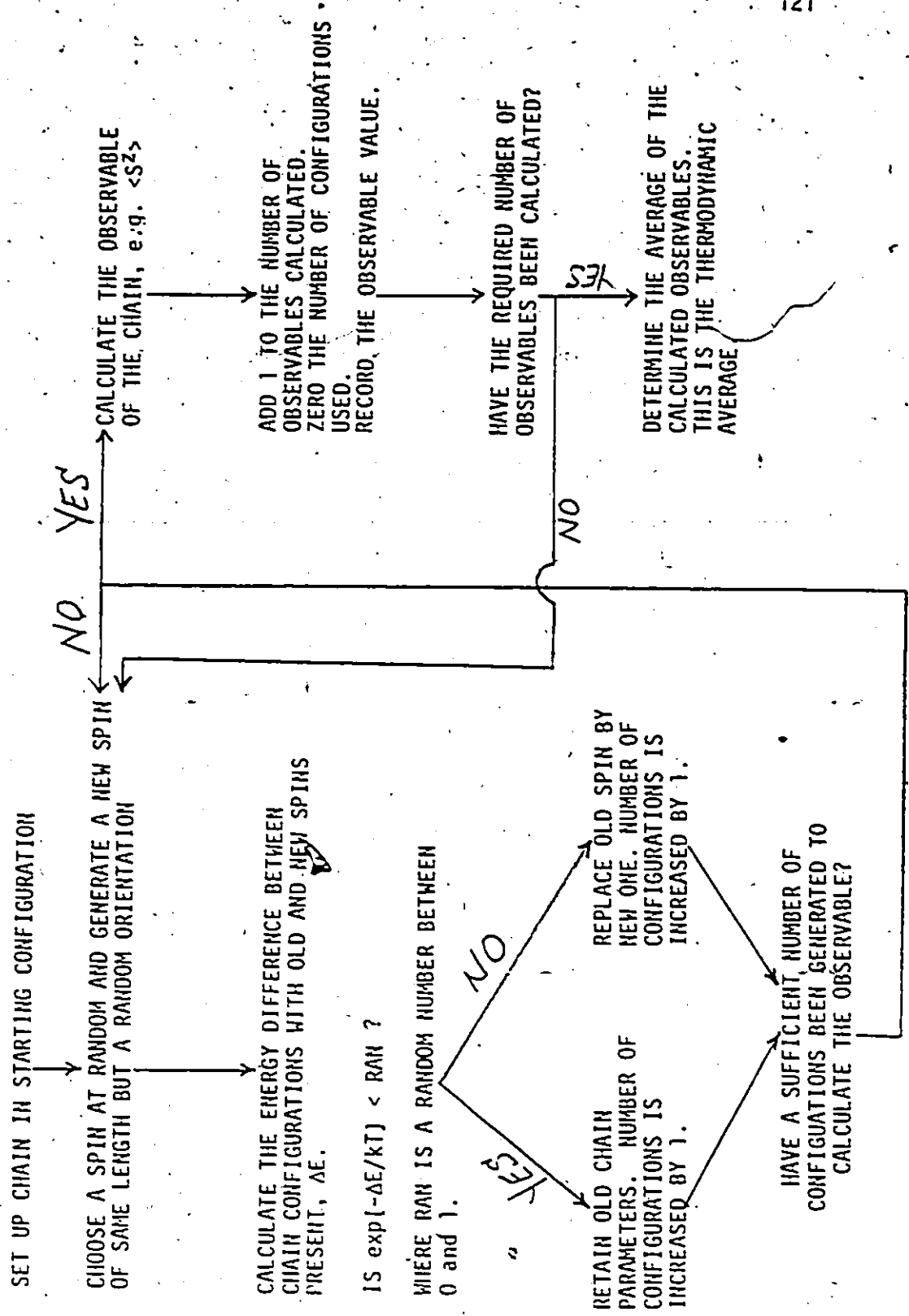
Although these anisotropic interactions are weak (compared with the bilinear exchange interactions), the effects on both the static and dynamic properties of the magnetic chain are expected to be quite profound at low temperatures. The next two chapters investigate three of these effects. In the next chapter, a Monte Carlo simulation of the magnetic chain involving dipolar interactions in addition to both bilinear and biquadratic exchange interactions is compared to the experimentally-determined susceptibility

of CsMnBr_3 . The relative importance of the higher order, biquadratic exchange mechanism for CsMnBr_3 is currently of interest (Falk et al., 1985) and the simulation provides a fresh perspective on this subject.

In Chapter 8, the spin correlations and configurations within the XY to Heisenberg cross-over temperature regime are examined for the anisotropic Heisenberg chain. In this regime the characteristic correlation lengths in the two symmetry directions behave very differently and these can be determined from the simulation. The cross-over behaviour can also be observed directly by plotting the configurations as a function of temperature. These configurations are examined for the presence of out-of-easy plane solitons (Chapter 4, this thesis).

The specific algorithm followed in all the simulations considered in this thesis is displayed in flow diagram form in table C1. A ring of N spin vectors, all of length S , are started off in some configuration. This configuration for the ensemble of spin vectors can be either random or have varying degrees of order associated with it. A single spin vector is chosen at random from the ring and replaced by a new spin vector of the same length but a random orientation. The difference in energy, Δ_1 , between the ensemble of spin vectors with the new spin vector present and that with the old spin vector present is calculated on the basis of some model Hamiltonian. The new spin is then either kept or discarded according to whether yet another random number between zero and one is larger or smaller than $\exp(-\Delta_1/kT)$, the Boltzmann factor, where T is the temperature. If the new spin lowers the energy of the ensemble of spins, $\Delta_1 < 0$, then it will be kept. However if it raises the energy of the ensemble it may still be kept, but the probability of this happening is weighted by the

TABLE C1



Boltzmann factor. This whole process is referred to as one Monte Carlo step per spin (MCS/spin).

Many such MCS/spin are executed and the process is stopped at various points to calculate some observables of the ensemble (for example the net moment in some direction). Observables are then sampled from many different ensembles and their average value can be calculated to produce a thermal average of the observables. In addition the configurations of an ensemble can be examined directly, yielding "snapshots" of the system at different temperatures.

However the simulation cannot treat an arbitrarily large system or execute arbitrarily many MCS/spin. Thus the observables are not calculated exactly even though the interactions are considered exactly. Two very important concerns must then be checked before the results of a simulation can be trusted. These are finite size effects and equilibration times.

One-dimensional systems with short-range interactions are particularly well suited to study by the Monte Carlo method. This is due to the absence of long-range order which implies that relatively few constituents are necessary to effectively represent an infinite co-operative system. If we consider the classical Heisenberg chain with a nearest-neighbour bilinear exchange of $J = -0.88 \text{ meV}$ (which is appropriate for CsMnBr_3), then Fisher's solution (Fisher, 1964) gives the correlation length as 70 Mn-Mn spacings at 2.5K. Thus a system of 600 Mn sites comprises roughly 9 correlation lengths and finite size effects would not be expected to be much of a problem at this temperature.

Both of these concerns are of course most important at low temperatures as the correlation lengths are longest while the probability of replacing a spin vector is least. Equilibration time problems can be checked by a variety of techniques. For example, the average value of some observable should not depend on the system's starting configuration. Usually the first number of MCS/spin are executed without using these ensembles in the calculations of some observable. This allows the system to come into equilibrium before observables are employed in the average. Thus there should be no difference between the average value of an observable taken from a system started off in a random configuration and one started off in a fully ordered configuration. Also some experimentation can be carried out on the dependence of an average value of an observable on the number of MCS/spin executed before the calculated observables were used in the average.

A similar technique can be used to investigate finite size effects. Any intensive variable must be independent of the size of the system. Thus experimentation can be carried out on whether a change in size causes a difference in the calculation of intensive variables.

A more difficult problem is assigning some uncertainty to a calculated observable. If there is no correlation at all between a set of configurations from which N observables, A , were calculated, then the uncertainty in the average value is

$$\Delta A = \left\{ \left[N \sum_i A_i^2 - \left(\sum_i A_i \right)^2 \right] / N^2 (N-1) \right\}^{0.5}$$

(Binder, 1984). The problem is that it is not efficient to use only those

configurations which are separated by a sufficient number of MCS/spin such that the configurations are entirely uncorrelated. This expression is then used, despite the possibility of correlation between the configurations, with the understanding that it is approximate only.

Of course, what also can be done is to estimate uncertainty from systematic discrepancies between the Monte Carlo results as a function of some variable, and any reasonable fit to the functional form of the same results. In addition many model Hamiltonians have limiting exact results associated with them. For example, the zero and infinite temperature behaviour of some facets of the model may be known exactly. If this is the case it gives a very important consistency check, as well as some indication of uncertainties associated with the simulation.

CHAPTER 7

BIQUADRATIC EXCHANGE FROM SUSCEPTIBILITY DATA IN CLASSICAL ONE-DIMENSIONAL HEISENBERG SYSTEMS

7.1 Introduction

The interaction between S-state magnetic moments in solids is most often represented by the Heisenberg Hamiltonian (equation (1.1)) which is bilinear in spin operators. This provides a good description of many magnetic systems; However it has long been realized that the Hamiltonian should contain terms of higher order in the spin operators. The physical origin of these higher order terms is twofold. They have been shown to be present as a direct consequence of the superexchange mechanism (Huang and Orbach, 1964). In addition, and what is believed to be more important, is the fact that any magnetostrictive system with a bilinear Heisenberg interaction between spins and Hooke's law type interaction between atoms can be represented by a Hamiltonian with an effective interaction biquadratic in spin operators (Néel, 1954 and Kittel, 1960).

To see this consider the Hamiltonian

$$H = k(a-a_0)^2 - 2(J_0 + \frac{\partial J}{\partial a} (a-a_0)) \underline{S}_i \cdot \underline{S}_j \quad (7.1)$$

for two spins \underline{S}_i and \underline{S}_j separated by a distance a . Minimizing the Hamiltonian with respect to the separation distance, a , between the spins we get

$$\frac{\partial H}{\partial a} = 0 = k(a-a_0) - \left(\frac{\partial J}{\partial a}\right) \underline{S}_i \cdot \underline{S}_j$$

which gives

$$(a-a_0) = k^{-1} \left(\frac{\partial J}{\partial a} \right) \underline{S}_i \cdot \underline{S}_j$$

and replacing this in the Hamiltonian (7.1) gives

$$H = -2J_0 \underline{S}_i \cdot \underline{S}_j - k^{-1} \left(\frac{\partial J}{\partial a} \right)^2 (\underline{S}_i \cdot \underline{S}_j)^2 \quad (7.2)$$

where we have assumed $\left(\frac{\partial J}{\partial a} \right)$ is a constant. It is important to note that as k must be positive, the biquadratic term must give a negative contribution to the total energy.

Interest in biquadratic exchange interactions has been present throughout the last three decades. However it resurfaced after somewhat of an experimental dormancy recently, due to direct spectroscopic neutron measurements of the transitions between Mn^{+2} pair and triad levels in the magnetic system $CsMn_{0.28}Mg_{0.72}Br_3$ (Falk et al. 1984 and 1985). This system has the same crystal structure as $CsMnBr_3$ and is a very good representation of a one-dimensional magnetic system. Inclusion of diamagnetic Mg^{+2} ions in the crystal matrix at the Mn^{+2} site means it is very easy to isolate magnetically pairs and triads of Mn^{+2} ions.

Since these measurements show that biquadratic exchange effects are appreciable in $CsMnBr_3$, we seek here to investigate whether biquadratic exchange effects can be discerned in the magnetic properties of pure one-dimensional magnetic systems consisting of unbroken chains of Mn^{+2} ions. It was pointed out by Falk et al. (1984), and is somewhat ironic, that the most powerful probe for investigating the details of magnetic systems, neutron scattering, is inappropriate for observing effects from biquadratic exchange in these pure systems. This is because the biquadratic exchange term has the same spin symmetry as the bilinear term and hence, to a good

approximation, the inelastic spectrum can be represented by an effective exchange term alone.

7.2 The Classical Heisenberg Chain

As mentioned in Chapter 1 of this thesis, Fisher solved exactly for the static behaviour of the one-dimensional classical Heisenberg system with nearest neighbour exchange, in 1964. The susceptibility is given by

$$\chi = g^2 \mu_B^2 N(S(S+1)/3kT)(1+u)/(1-u) \quad (7.3)$$

where

$$u = \coth \frac{1}{x} - x \quad (7.4)$$

and

$$x = kT/(2JS(S+1)).$$

with $g = 2$ for a spin only system, μ_B the Bohr magneton, k Boltzmann's constant and T the temperature.

$kT \frac{\chi}{N}$ depends only on the ratio kT/J for given S and we have plotted this in figure G1 for an antiferromagnet ($J < 0$) with $S = 5/2$. This is compared with the experimentally-determined susceptibilities of the quasi-one-dimensional materials CsMnBr_3 (Eibshitz et al., 1977 and Fitzgerald et al., 1982), $(\text{CH}_3)_4\text{NMnCl}_3$ (TMMC) (Dingle et al., 1969 and Walker et al., 1972) and $\text{CH}_3\text{NH}_3\text{MnCl} \cdot 2\text{H}_2\text{O}$ (MMC) (Simizu et al., 1984). It is immediately apparent that the values for MMC lie consistently below those for CsMnBr_3 and TMMC, which are relatively well described by Fisher's expression.

The authors of the MMC analysis claim that the discrepancies can be accounted for by an approximate correction (Weng and Griffiths, unpublished) which recognizes the finite (hence quantum mechanical) nature of S . We have also shown this approximate result in figure G1 by using the

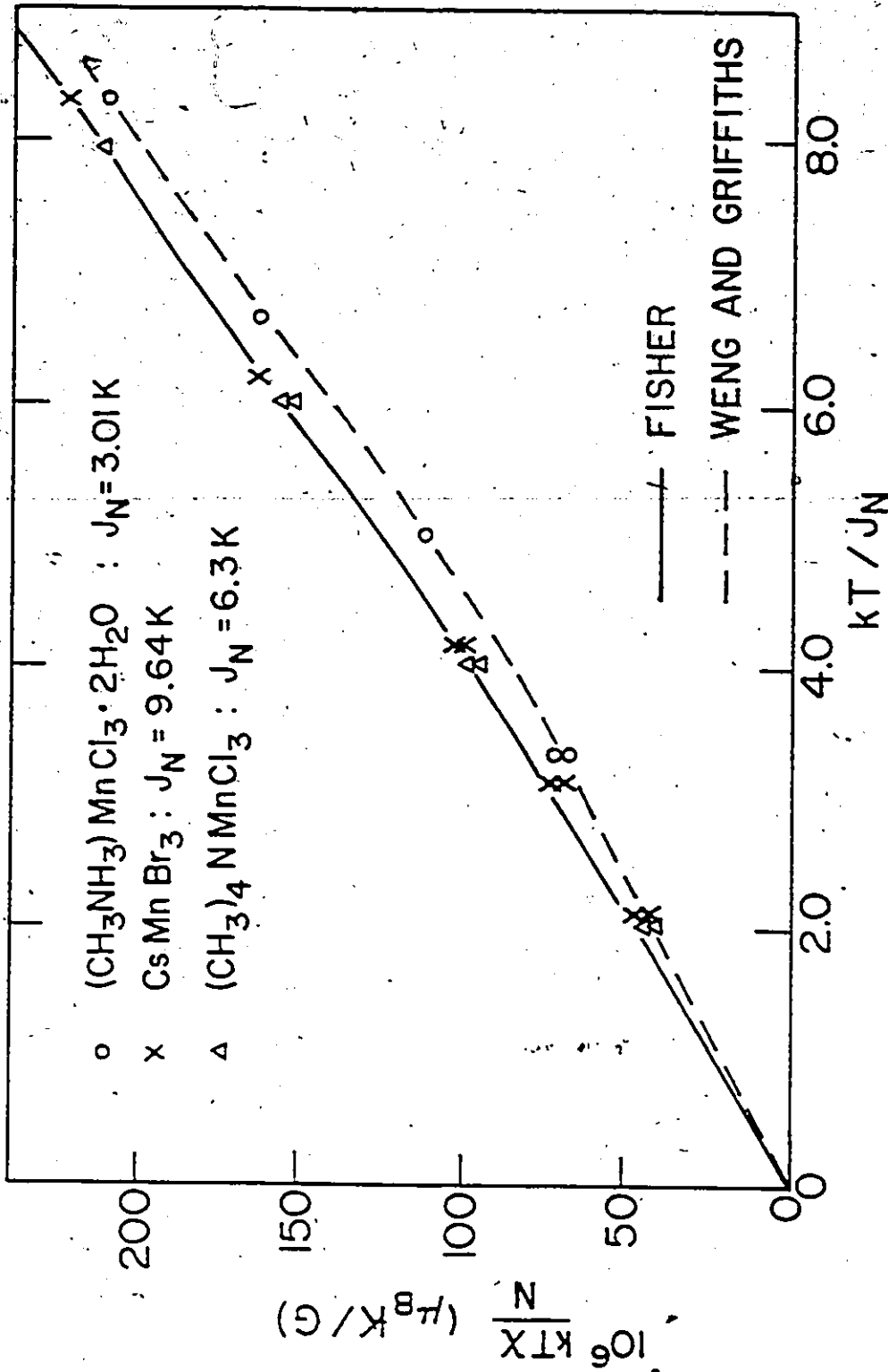


Figure G1: The experimental susceptibility of the three $S = 5/2$ Heisenberg chain compounds. Fisher's exact solution for limiting large S is also plotted, as is the solution with approximate corrections for finite S due to Weng and Griffiths. These corrections describe only one compound adequately, leading us to believe that deficiencies in the Hamiltonian are principally responsible for discrepancies between theory and experiment.

plot of this unpublished work used by Simuzi et al. (1984). This plot is consistent with the approximate theory's use by Fitzgerald et al. (1982) in their analysis of CsMnBr_3 . As all three of the systems considered have $S = 5/2$, this correction should apply equally in all cases. We are led to the conclusion then that the systematic discrepancies are not principally due to quantum effects but rather to small deficiencies in the Hamiltonian itself.

7.3 The Classical Heisenberg Chain with Both Bilinear and Biquadratic Exchange

Biquadratic exchange as well as bilinear Heisenberg exchange can be included in the analysis by considering a Hamiltonian

$$H = -2JS(S+1) \sum_j \{ \hat{S}_j \cdot \hat{S}_{j-1} + \alpha (\hat{S}_j \cdot \hat{S}_{j-1})^2 \} \quad (7.5)$$

where the sum is over nearest neighbours along the chain and the vectors \hat{S}_j are classical unit vectors which can take on any orientation in space.

This model Hamiltonian has been considered by several authors (Liu and Joseph, 1971; Liu and Joseph, 1972 and Nagata and Yamamoto, 1977); in addition an equivalent form

$$H = -2J \sum_i (\hat{S}_i \cdot \hat{S}_{i-1}) - 4K \sum_i (\hat{S}_i \cdot \hat{S}_{i-1})^2 \quad (7.6)$$

also occurs frequently in the literature. The relation between the biquadratic exchange strengths, K and α , used in these Hamiltonians is

$$K = J\alpha / [2S(S+1)]$$

We should point out that inclusion of a biquadratic exchange term, which reinforces the antiferromagnetic bilinear term, is a physically

appealing way of producing agreement between the calculated and measured susceptibilities. In all three cases the theoretical expression with bilinear exchange alone describes the measured susceptibilities at high temperatures where spin correlations are small but overestimates the susceptibility at low temperatures where the spin correlations are high. Because it goes as $(S_i \cdot S_{i-1})^2$ rather than $(S_i \cdot S_{i-1})$ the biquadratic term is most important at low temperatures and reinforces the antiferromagnetic interactions thus reducing the susceptibility and bringing theory and experiment into agreement.

Liu and Joseph (1972) have solved exactly the static behaviour of the Hamiltonian with biquadratic exchange included as well as the more general model Hamiltonian (Liu and Joseph, 1971)

$$H = \sum_i f(S_i \cdot S_{i+1})$$

where $f(S_i \cdot S_{i+1})$ is a well behaved function of the isotropic product $S_i \cdot S_{i+1}$, thus including interactions of higher order in the spins as well.

The solution for the susceptibility of the Hamiltonian with biquadratic exchange included (equation (7.5)) is of the same form as equation (7.3) with

$$u = \frac{\sqrt{x} \sinh\left(\frac{1}{x}\right) \exp\left(\frac{1}{4\alpha x} + \frac{\alpha}{x}\right)}{\sqrt{\alpha} \int_b^a \exp(z^2) dz} - \frac{1}{2\alpha} \quad (7.7)$$

where $a = (\alpha x)^{-0.5} (1 - 2\alpha) / 2$

$b = (\alpha x)^{-0.5} (1 + 2\alpha) / 2$

The results of fitting this expression to the experimentally-determined single-crystal susceptibilities of CsMnBr_3 , TMMC and MMC are shown in figure G2 and the top panel of figure G3. Also shown for comparison in all three cases is the best fit to the experiment of Fisher's expression (equations (7.3) and (7.4)).

In all three cases the fit is clearly superior when the expression with biquadratic exchange is used. This is especially pronounced for MMC and CsMnBr_3 as the exact expression for the classical system with bilinear exchange alone does not describe the susceptibilities well for temperatures such that $J_S(S+1) > kT$; that is below where the susceptibility "turns over". The best fit with bilinear exchange alone is better for TMMC, however a better fit still can be achieved using the expression with biquadratic exchange.

The bilinear and biquadratic exchange values taken from the best fits are:

$$\begin{array}{lll} \text{CsMnBr}_3 & : J = -0.785 \text{ meV} & K = 0.0040 \text{ meV} \quad (\alpha = -0.089) \\ \text{MMC} & : J = -0.2535 \text{ meV} & K = 0.0019 \text{ meV} \quad (\alpha = -0.13) \\ \text{TMMC} & : J = -0.55 \text{ meV} & K = 0.0016 \text{ meV} \quad (\alpha = -0.05) \end{array}$$

Biquadratic exchange makes the largest relative contribution in MMC and the smallest in TMMC, however the magnitude of the biquadratic exchange is largest, by a factor of two, in CsMnBr_3 .

The inclusion of higher order exchange effects, particularly bicubic, as calculated by Liu and Joseph (1971) could alleviate the slight discrepancy between experiment and theory which treats biquadratic exchange in MMC. A bicubic term in the Hamiltonian of the form $+K'(S_i - S_{i+1})^3$ with $K' > 0$ would be necessary to again reinforce the antiferromagnetic interact-

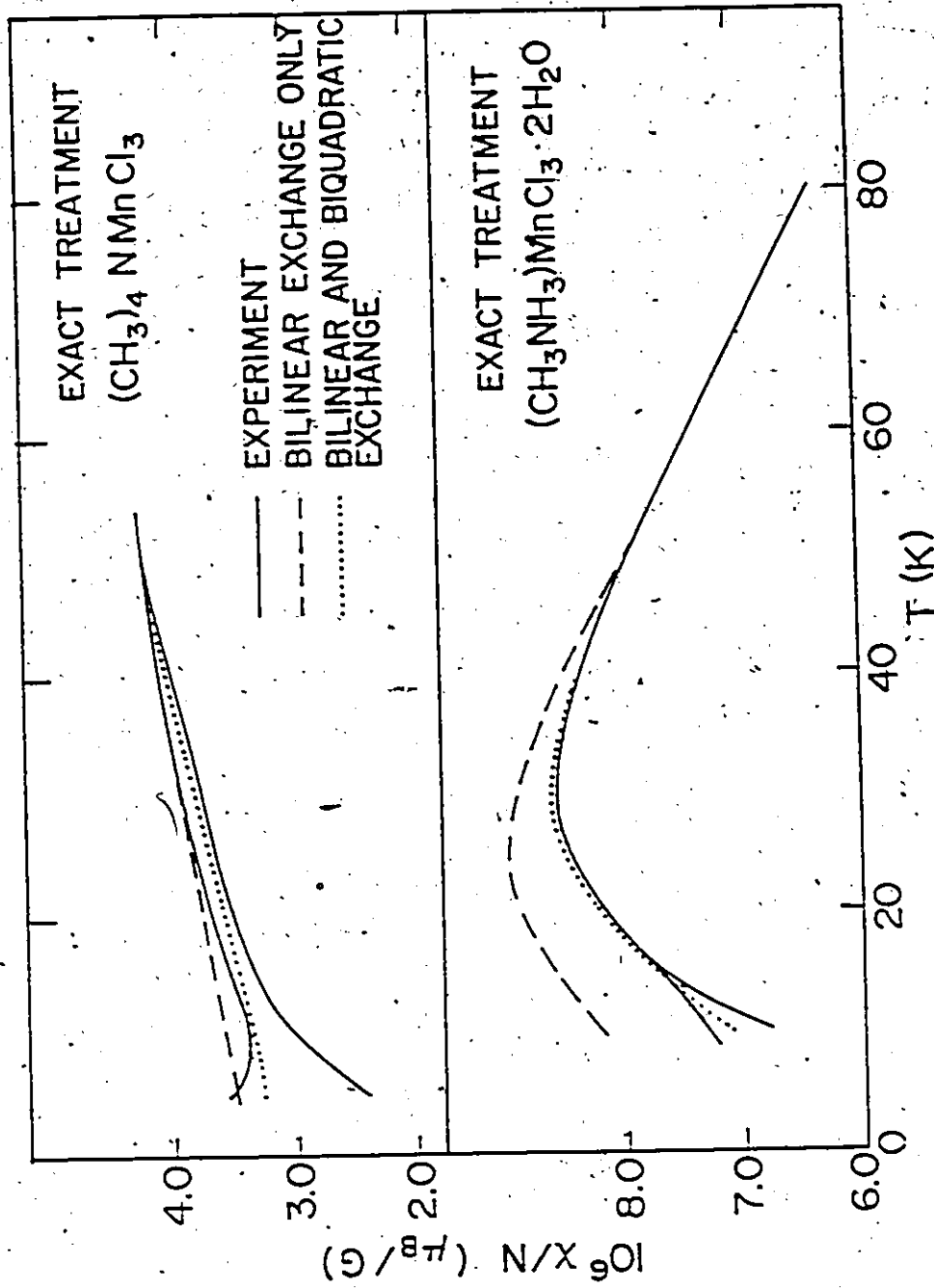


Figure 62: The best fit of the calculated susceptibility per site for a system with both biquadratic and bilinear exchange is compared with experimental data. Also plotted for comparison is the best fit to the data of Fisher's calculation. At low temperatures the experimental susceptibilities split with $\chi(H||c) > \chi(H \perp c)$ due to weak dipolar interactions.

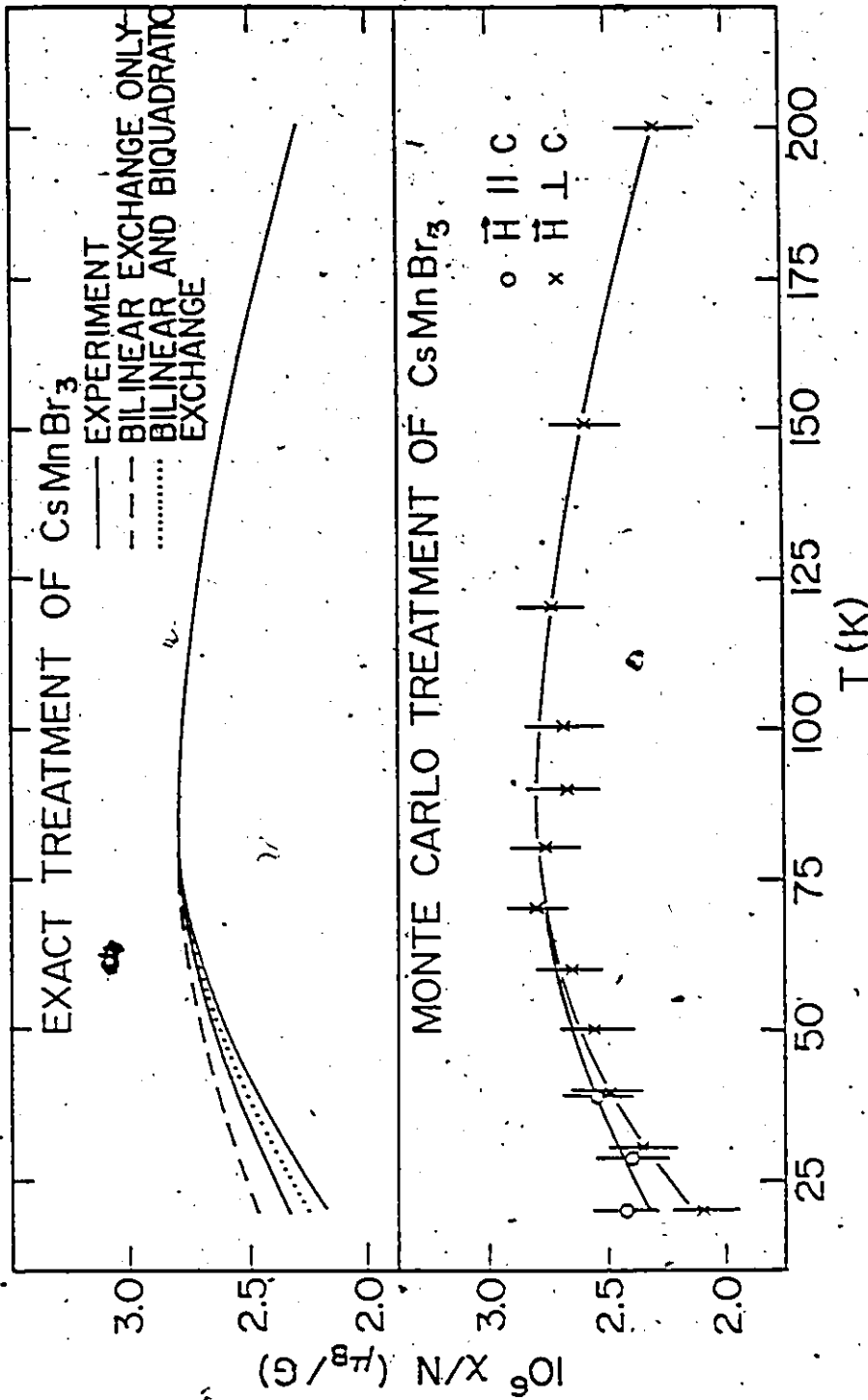


Figure G3: The best fit for the calculated susceptibility per site for a system with biquadratic and bilinear exchange, as well as for Fisher's calculation with bilinear exchange alone, are compared to experiment for $CsMnBr_3$. At low temperatures the experimental susceptibilities split with $\chi(H \parallel c) > \chi(H \perp c)$ due to weak dipolar interactions. The bottom panel shows the results of our Monte Carlo simulation of $CsMnBr_3$ which includes weak dipolar-induced anisotropy.

ions and further lower the theoretical susceptibility values. However these interactions would be expected to be most important at low temperatures where weak anisotropic dipolar and single ion interactions become dominant.

At low temperatures the measured susceptibilities display anisotropy with $\chi(H||c) > \chi(H\perp c)$, where c is the chain axis. This is due to the weak dipolar and single ion anisotropic interactions which tend to make the plane perpendicular to c an easy plane. The Hamiltonian we have considered thus far contains no such terms and hence we expect our results to lie somewhere between the two χ values at these temperatures, which they do. Approximate theories which deal with this anisotropy have been developed both for the bilinear Hamiltonian (Walker et al., 1972) and the Hamiltonian with both bilinear and biquadratic interactions (Yamamoto and Nagata, 1977). However it was found that for the cases we considered, a more favourable comparison to experiment was afforded by a Monte Carlo calculation of χ for CsMnBr_3 . The Monte Carlo calculation treats all the interactions exactly, as explained in the preceding chapter. These results will be discussed in the next section.

Of course, each of these materials undergoes a magnetic phase transition to a three-dimensionally ordered state at sufficiently low temperature. This is due to the weak inter-chain interactions as a truly one-dimensional system with short-range interactions displays no long-range order for $T > 0$. Hence all our analysis is restricted to temperatures at which the inter-chain correlations are believed to be negligible and these weak three-dimensional interactions average out, this is above $2T_N$.

7.4 Monte Carlo Treatment of CsMnBr₃

In order to describe a real system, the Hamiltonian should contain dipolar interactions and single ion anisotropy terms. In this case there is no exact solution for the susceptibility, and we have used the Monte Carlo method.

CsMnBr₃ alone was treated in this way, because the anisotropy is stronger than in TMMC (Chapter 3, this thesis) and more importantly because detailed spectroscopic information regarding the strength of the biquadratic exchange term is available for CsMn_xMg_{1-x}Br₃ only (Falk et al., 1984 and 1985).

The Hamiltonian

$$H = -2J \sum_i S_i \cdot S_{i+1} - 4K \sum_i (S_i \cdot S_{i+1})^2 - \delta \sum_i S_i^z S_{i+1}^z + 2\mu_B H^\alpha \sum_i S_i^\alpha$$

was used in the simulation, with parameter values of $J = 0.785$ meV, $K = 0.0040$ meV and $\delta = 0.03$ meV. H^α represents a magnetic field applied along the α direction. As we will see these parameters are appropriate for CsMnBr₃. Experimentation with other parameters was also carried out.

The Monte Carlo calculation proceeded by the Metropolis algorithm for a chain of classical spin vectors, as described in the preceding chapter. Our results, which are shown in figures G3 and G5 are for a system of 1000 spins where we have executed 4000 MCS/spin. The first 1000 MCS/spin were performed without using the configurations in determining the average value of the observable. In this case the observable is the induced moment along the field direction.

Finite size effects are not expected to be important for this length of chain at the temperatures we are considering. Fisher's solution of the statics of the classical one-dimensional Heisenberg system gives a correlation length of about 10 Mn-Mn spacings at 20K (our lowest temperature considered) for an exchange interaction strength appropriate for CsMnBr_3 . Thus our system represents 100 correlation lengths at 20K and of course more at higher temperature. Just the same we experimented with doubling and tripling the size of the system for selected values of temperature and field and no change in the determination of the observables was found.

As already stated, equilibration can be checked at low temperatures by looking for dependencies in the observables on drastically different starting conditions. Towards this end, we examined systems started off completely at random as well as those started off in a completely ordered state. The ordered state corresponds to all spins lying within the easy plane (perpendicular to the chain axis) and exactly antiparallel to both of their nearest neighbours. No difference was found in the determination of the susceptibility as a function of temperature between either starting configuration. In addition some experimentation was carried out on the number of MCS/spin performed as well as the number executed before configurations were included in the thermodynamic averaging.

The susceptibility is derived by calculating the average induced moment along the field direction for three different strengths of field; 10 kgauss, 17.5 kgauss and 25 kgauss. Each of these calculations is done independently with different random starting configurations for each value of field. The approximate uncertainty of each induced moment is calculated according to equation (6.1). These values for the induced moment,

along with their approximate uncertainty, are plotted versus applied field and the best fit straight line was fitted to the data, subject to the constraint that the line passes through the origin. A typical plot is shown in figure G4. In all cases the straight line fit was very good indicating that the fields chosen were not so high as to induce non-linear field dependencies on the susceptibilities. Of course, the susceptibility is given by the slope of the induced moment versus field plot.

With all our information taken into account we estimate that our determination of χ is accurate to within $\sim 1.5 \times 10^{-7} \mu_B / (\text{G-spin})$, almost independent of temperature over the range considered.

The results of the Monte Carlo calculation for CsMnBr_3 are plotted along with the experimentally measured $\chi(T)$ in the lower panel of figure G3. Clearly the description of the experiment by the calculation is very good. The splitting between the susceptibilities measured with H along the chain axis and perpendicular to it are in agreement with the calculation to within the quoted accuracy.

Figure G5 shows the two measured susceptibilities (in the two symmetry directions) at 20K only. We have plotted the results of the Monte Carlo simulation with bilinear exchange of 0.775 meV (very close to the value of 0.785 meV used in figure G3) and dipolar interactions of 0.03 meV (as in figure G3) but we gradually "turn on" the biquadratic exchange interactions. Agreement with experiment can only occur for $0.003 < K < 0.006$ meV for H perpendicular to c and $0.0035 < K < 0.0085$ meV for H along c. These values are consistent with the value $K = 0.004$ meV obtained from the best fit to the full temperature dependence of χ obtained in the preceding section, which ignored anisotropic interactions.

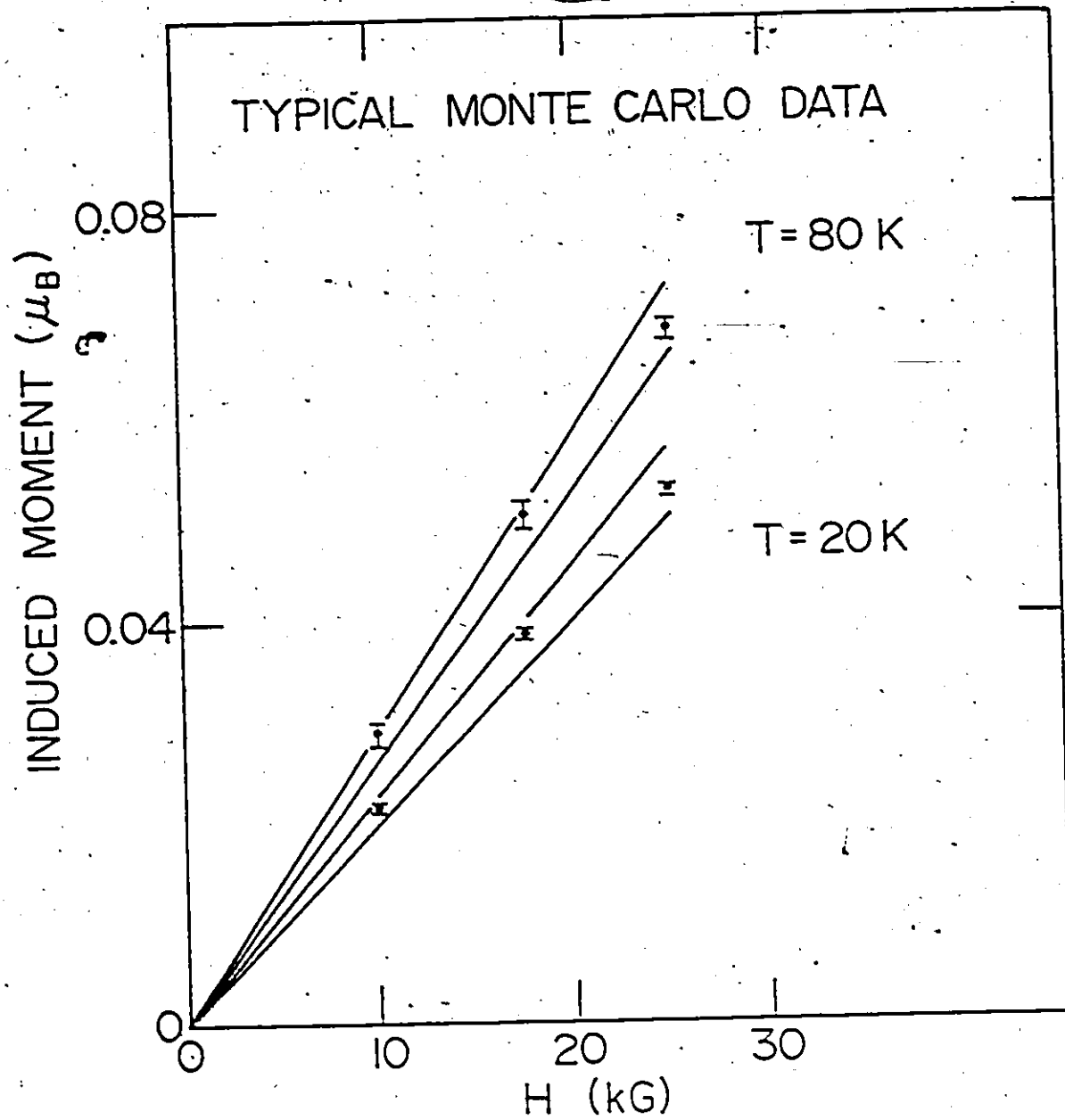


Figure G4: Typical data from the Monte Carlo simulation is shown for two different temperatures and trial parameters in simulating CsMnBr_3 . The error bars originate from the approximate expression given in the text and the divergence in the high and low slope line fits to the data give the quoted uncertainty of $\sim 1.5 \times 10^{-7} \mu_B/\text{G}$ for the susceptibility. It is seen that no non-linearities in the induced moment with applied field could be detected over the field range considered.

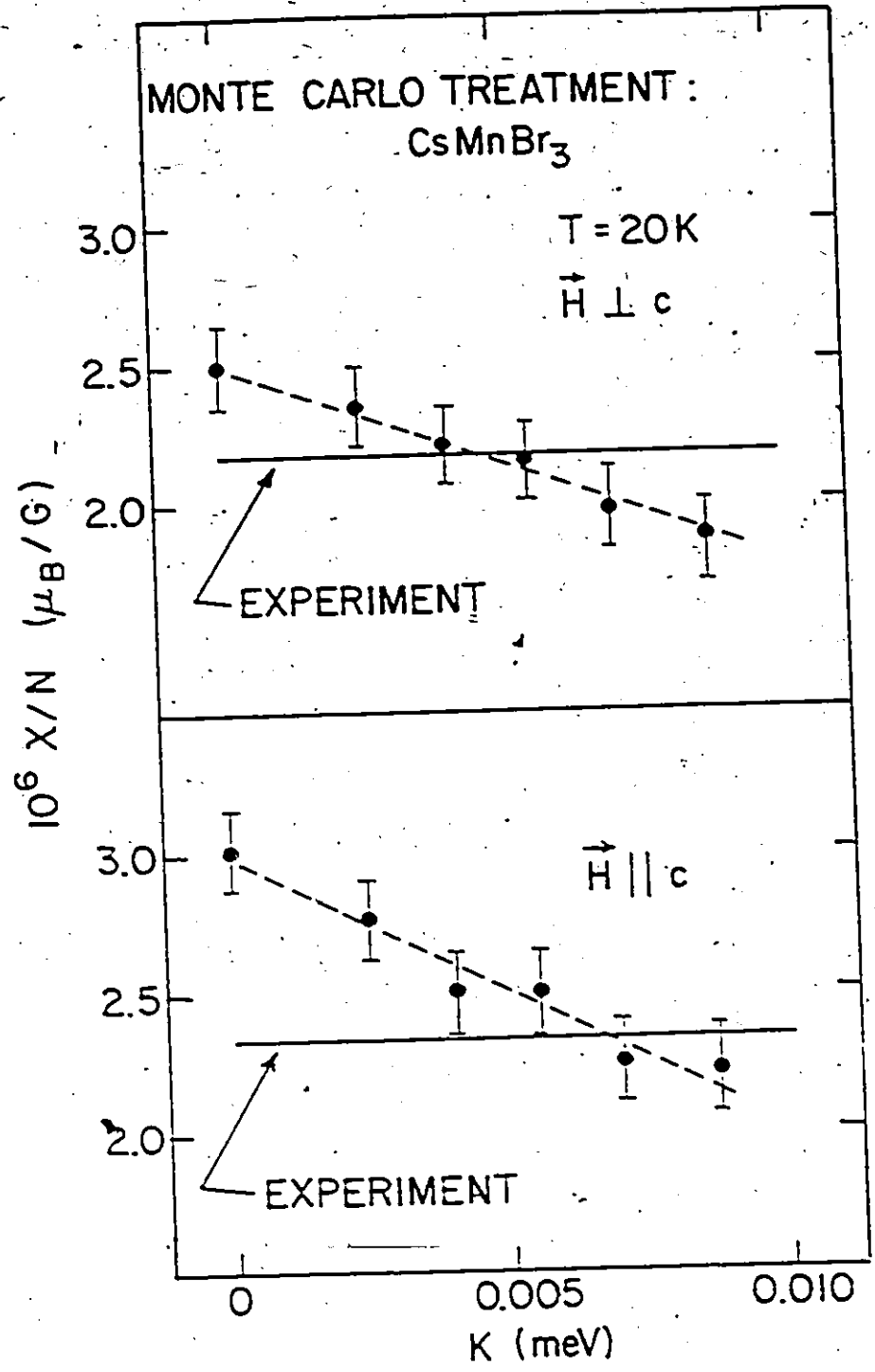


Figure G5: The susceptibility per site in the two symmetry directions, as determined from the Monte Carlo simulation, are compared to experiment for CsMnBr₃ at T = 20K for different values of the biquadratic exchange. For J = 0.775 meV and a dipolar interaction strength of $\delta = 0.03$ meV, the biquadratic exchange interaction lies in the range $0.0035 \text{ meV} < K < 0.006 \text{ meV}$.

7.5 Discussion

Our discussion focusses on two points. Firstly, how can we reconcile the Hamiltonian parameters known from neutron scattering measurements of the spin waves in these compounds, to those determined by analysing the susceptibilities? To the best of our knowledge, no detailed spin wave measurements have been made on MMC, hence our discussion will concern only CsMnBr_3 and TMMC. Secondly, how does our determination of the biquadratic exchange energy in CsMnBr_3 compare with direct spectroscopic neutron measurements made on $\text{CsMn}_x\text{Mg}_{1-x}\text{Br}_3$ by Falk et al.?

The determination of the nearest neighbour exchange constant is complicated by one factor. This is that the Néel state is not the quantum mechanical ground state so that zero point motion exists even at $T=0$. This has been investigated by several authors (Anderson, 1952 and Oguchi, 1960) and it results in the spin wave dispersion relation being written (for nearest neighbour bilinear exchange alone) as

$$\hbar\omega = -4JRS \sin(q_c \pi) \quad (7.9)$$

with $R = 1.07$ for $S = 5/2$.

Classically the Néel state is the ground state (all spins anti-parallel to nearest neighbours) and $R=1$. These results for the correction factor, R , assume an ordered state which actually does not exist for our case.

There is only rough agreement between the bilinear exchange constant found in either TMMC or CsMnBr_3 taken from the best fit to Fisher's classical expression for the susceptibility using bilinear exchange alone and the value taken from the neutron measurement of the spin wave dispersion.

These values are -0.569 ± 0.005 meV and -0.82 ± 0.01 for TMMC and CsMnBr_3 respectively. However the main point we have made in this chapter is that this expression for the susceptibility does not fit the experiment for $kT < JS(S+1)$ for the two compounds, with the effect more pronounced for CsMnBr_3 than for TMMC.

The spin wave dispersion relation for a system with both nearest neighbour bilinear and biquadratic exchange has been calculated by Falk et al. (1984). They get the same expression as given by equation (7.9) except that $-J$ is replaced by $|J-4KS^2|$. We find that for both CsMnBr_3 and TMMC the exchange parameters are consistent between the two methods of determining them; susceptibility and spin wave dispersion. However now we have the considerable advantage of having the calculated susceptibility describing the measured susceptibility at all temperatures considered.

The second point is how does our analysis of biquadratic exchange in CsMnBr_3 compare with the neutron spectroscopic measurements of Falk et al.? Their initial measurements were made by examining the exchange splittings of Mn^{+2} pairs in $\text{CsMn}_{0.28}\text{Mg}_{0.72}\text{Br}_3$. As CsMnBr_3 and CsMgBr_3 are isostructural with essentially the same unit cell dimensions, the comparison of our work on CsMnBr_3 to their work on $\text{CsMn}_{0.28}\text{Mg}_{0.72}\text{Br}_3$ is relevant.

On the basis of four observed transitions they obtained a very good fit for the bilinear and biquadratic exchange constants. They obtained

$$J = -0.838 \pm 0.005 \text{ meV}$$

$$K = 0.0022 \pm 0.0002 \text{ meV.}$$

This gives biquadratic exchange which is roughly half that determined by us.

Subsequent work by this same group examined transitions between Mn^{+2} in linear triads in the same crystal. They obtained three measured transitions which they then fit to three exchange parameters, now including the next nearest neighbour bilinear exchange constant. Although a unique determination of the exchange parameters could have been achieved, Falk et al. chose to retain the biquadratic exchange constant identical to that determined in their Mn^{+2} pair work. They obtained a reasonable description although small discrepancies are present, with

$$J = -0.816 \pm 0.002 \text{ meV}$$

$$J' = -0.010 \pm 0.003 \text{ meV}$$

$$K = 0.0022 \pm 0.0002 \text{ meV} \text{ as before}$$

where J' is the next nearest neighbour bilinear exchange constant. As before this biquadratic exchange value is a factor of two smaller than the one we determined.

However if the unique determination of the three exchange parameters is made from the three Mn^{+2} triad transitions observed, then we obtain

$$J = -0.771 \pm 0.002 \text{ meV}$$

$$K = 0.0042 \pm 0.0002 \text{ meV}$$

$$J' = -0.013 \pm 0.003 \text{ meV}$$

which is in agreement with our analysis of $CsMnBr_3$.

Although we do not understand why the strength of the biquadratic exchange interactions should be greater in Mn^{+2} triads and pure $CsMnBr_3$ than in Mn^{+2} pairs, it is not unreasonable that both the bilinear exchange gradient near the equilibrium atom separation, $\partial J / \partial a$, and the stiffness

constant of a Hooke's law type interaction between nearest neighbour atoms, change as Mg^{+2} ions are replaced by Mn^{+2} ions. The picture resulting from our analysis provides consistency among our calculations, the susceptibility work and neutron scattering work on the spin waves in the "pure" $CsMnBr_3$ as well as in the neutron spectroscopic study of linear triads of Mn^{+2} in $CsMn_{0.28}Mg_{0.72}Br_3$.

CHAPTER 8

CROSSOVER BEHAVIOUR AND SOLITONS IN AN ANISOTROPIC HEISENBERG CHAIN

8.1 Introduction

The presence of dipolar interactions between magnetic moments in solids implies that we can anticipate the overall interaction to be anisotropic even for S state magnetic moments. We have already pointed out that for the magnetic chain systems CsMnBr_3 and TMMC the dipolar interactions result in the formation of an easy plane at sufficiently low temperatures.

Although these anisotropic interactions are weak (compared with the leading exchange interactions), their effects are believed to be quite profound on both the static and dynamic properties of these materials at low temperatures. As the temperature is reduced, the system must cross-over from being Heisenberg-like to being XY-like. Spin correlations will be different for spin components in the easy plane and perpendicular to the easy plane; neither correlation will be in accord with what is expected for a classical Heisenberg chain. In addition, there is the prediction by Mikeska of the existence of large, non-linear fluctuations in the spectrum of out-of-easy plane fluctuations for such systems (see Chapter 4, this thesis). These Sine-Gordon solitons would not be found in the isotropic Heisenberg system (although so-called "pulse" solitons may be (Tjon and Wright, 1977)).

No exact solutions exist for mixed Heisenberg and XY systems (as discussed in Chapter 7, this thesis); hence it is useful to apply numerical techniques to these problems. We have applied the Monte Carlo method to examine the features of the spin correlations within the crossover temperature region. The simulation produces two types of results. In section 8.2 numerical calculations of the spin correlations in the symmetry directions are shown. In section 8.3 the crossover behaviour is directly examined by looking at "snapshots" of the configurations of the ensembles of spins along the chain as a function of temperature. These configurations are examined for the existence of out-of-easy plane soliton-like fluctuations.

Throughout we have used the Hamiltonian

$$H = -2J \sum_i S_i \cdot S_{i+1} + \delta \sum_i S_i^Z S_{i+1}^Z \quad (8.1)$$

with numerical values of $J = -0.88$ meV and $\delta = 0.03$ MeV which are appropriate for CsMnBr₃ (Chapter 3, this thesis). Note that this Hamiltonian is consistent with equation (4.1). It is believed however that the results will have a more general applicability to other one dimensional systems.

8.2 Static Spin Correlations

A spin correlation length, ξ_α , can be defined according to the equation

$$\langle S_i^\alpha S_{i+n}^\alpha \rangle \sim \exp(-n\xi_\alpha^{-1})$$

where α is one of the orthogonal axes, x, y or z. For easy plane symmetry there are two correlation lengths of interest, ξ_x and ξ_z . Exact expressions are known for the correlation lengths of both the classical XY chain (Wegner,

1964) and the classical Heisenberg chain (Fisher, 1964); at low temperatures they differ by a factor of two for the same exchange parameters.

The effect of anisotropy on the spin correlations of a Heisenberg chain has been studied via transfer matrix techniques by two sets of authors. Loveluck et al. (1975) examined the case where the anisotropy is single ion like, $\pm A \sum_i (S_i^z)^2$, and could produce either easy plane (+A) or easy direction (-A) anisotropy. Hone and Pires (1977) examined the case of the system where the anisotropy takes the form $\sum_i (S_i^z S_{i+1}^z)$ and a strength specific to TMMC. Both sets of authors solve for the correlation lengths in terms of eigenvalues of the resulting eigenvalue equation of the transfer matrix formalism.

The zero temperature properties of a classical system described by equation (8.1) are known exactly. The spins will be antiparallel to nearest neighbours and lie within the easy (x-y) plane. In a truly one-dimensional system, long-range order exists only at zero temperature. Thus it is not surprising that only the in-plane ($\alpha = x$) correlation length diverges at zero temperature, while the out-of-plane correlation length is expected to go to some finite value, as at zero temperature the spins have condensed into the easy plane. These expectations are borne out by both studies but they also find a maximum for the out-of-plane correlation length at non-zero temperature.

We have numerically calculated the static spin-pair correlation functions for both symmetry directions $\langle S_i^\alpha S_{i+n}^\alpha \rangle$, $\alpha = x, z$ for n less than twenty-five. This has been carried out for temperatures between 5K and 50K by a classical Monte Carlo simulation. The system consisted of a ring of 1200 sites started from a completely random configuration of spin orienta-

tions. After the first 16,000 MCS/spin had been performed, 80 configurations, separated by 50 MCS/spin, were used to calculate the averages. Possible effects of finite system size and equilibration times were dealt with by the methods described in Chapter 6. No quantitative analysis of the uncertainty associated with the simulation results in this chapter will be attempted. Rather some estimate of the uncertainty can be obtained by examining systematic discrepancies of the simulation data from any reasonable fit to the same data. The resulting correlation functions were fit to the expression

$$\langle S_i^\alpha S_{i+n}^\alpha \rangle = (-1)^n [S_0(T)]^2 \exp(-n/\xi_\alpha(T))$$

and $\xi_\alpha(T)$ as well as $S_0(T)$ were extracted from the data.

Representative data and the corresponding fits are shown in figure H1. In all cases values of $\langle S_i^\alpha S_{i+n}^\alpha \rangle$ below $[S_0^\alpha]^2/3$ were not used in the fits. It is clear that the fits are very good even for correlations beyond the characteristic length associated with this value.

We are fortunate in dealing with this system that there are exact results for $S_0^\alpha(T)$ in the limit of zero and infinite temperature, and it is a very useful check on the whole simulation to see how well our data behaves in these limiting conditions. At zero temperature the spins have condensed into the easy plane; hence $S_i^z = 0$ for all i and $\langle (S_i^x)^2 \rangle = S(S+1)/2$. At infinite temperature the anisotropy is not thermodynamically relevant and $\langle (S_i^z)^2 \rangle = \langle (S_i^x)^2 \rangle = S(S+1)/3$.

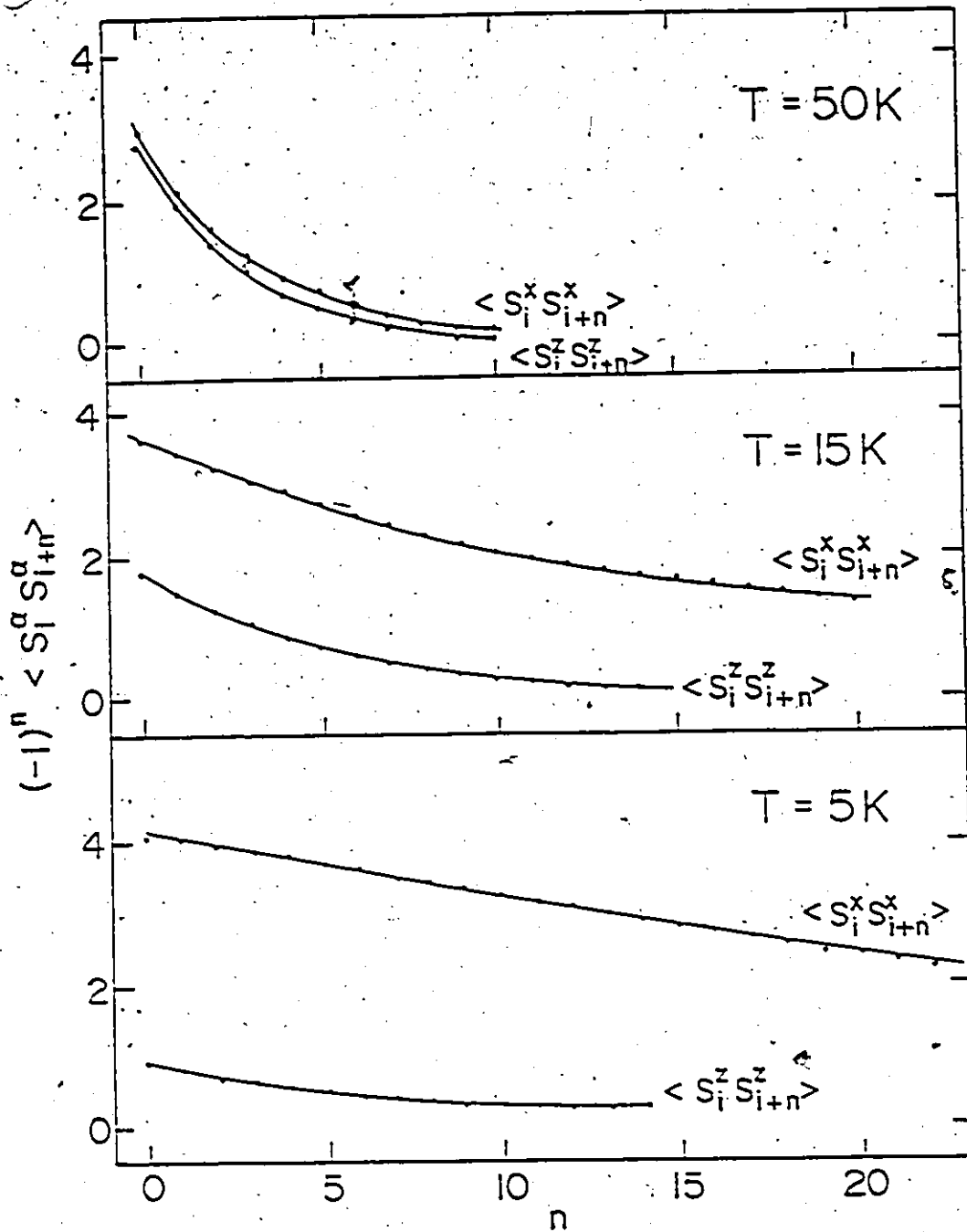


Figure H1: Representative data from the numerical calculation of $(-1)^n \langle S_i^\alpha S_{i+n}^\alpha \rangle$ for both in-easy-plane, $\alpha = x$, and out-of-easy-plane, $\alpha = z$, correlations are shown. The solid lines are the fits of the data to $[S_0^\alpha(t)]^2 \exp(-n\xi_\alpha^{-1}(T))$. The resulting $S_0^\alpha(T)$ values are shown in Figure H2 while the correlation lengths, $\xi_\alpha(T)$, are shown in figure H3.

This quantity $S_0^\alpha(T) = \sqrt{\langle S_i^\alpha \rangle^2}$ is plotted versus temperature in figure H2. It is clear that a very reasonable infinite-temperature extrapolation of $S_0^\alpha(T)$ is $\sqrt{S(S+1)/3}$ while it is also very reasonable to extrapolate $S_0^x(T)$ at zero temperature to $\sqrt{S(S+1)/2}$. Our data show a monotonic decrease of $S_0^z(T)$ with temperature, but the most dramatic drop in this quantity with temperature must occur below 5K. We conclude that our data are consistent with these exact results and this important check on our simulation is satisfied.

The resulting correlation lengths as a function of temperature are shown in figure H3. It is clear that there are large differences between in-plane and out-of-plane correlation lengths below 20K. As expected the in-plane correlation length appears to be proceeding towards a divergence at zero temperature while the out-of-plane correlation length seems to be tending to a finite value at zero temperature. No maximum in the out-of-plane correlation length is found above 5K in the simulation. This is in apparent disagreement with the work of Hone and Pires, which showed a weak maximum in the out-of-plane correlation length for TMMC at about 9K. The strength of the easy plane anisotropy is greater in CsMnBr_3 than in TMMC (Chapter 3, this thesis). The work by Loveluck et al. suggests that this should push the maximum in the correlation length to higher temperatures, and thus such an effect should have been observable.

It was pointed out by Loveluck et al. that the correlation length defined in terms of eigenvalues of equations resulting from the transfer matrix formalism do not produce exactly the same result as that obtained using our definition. This discrepancy could then lie in the differing

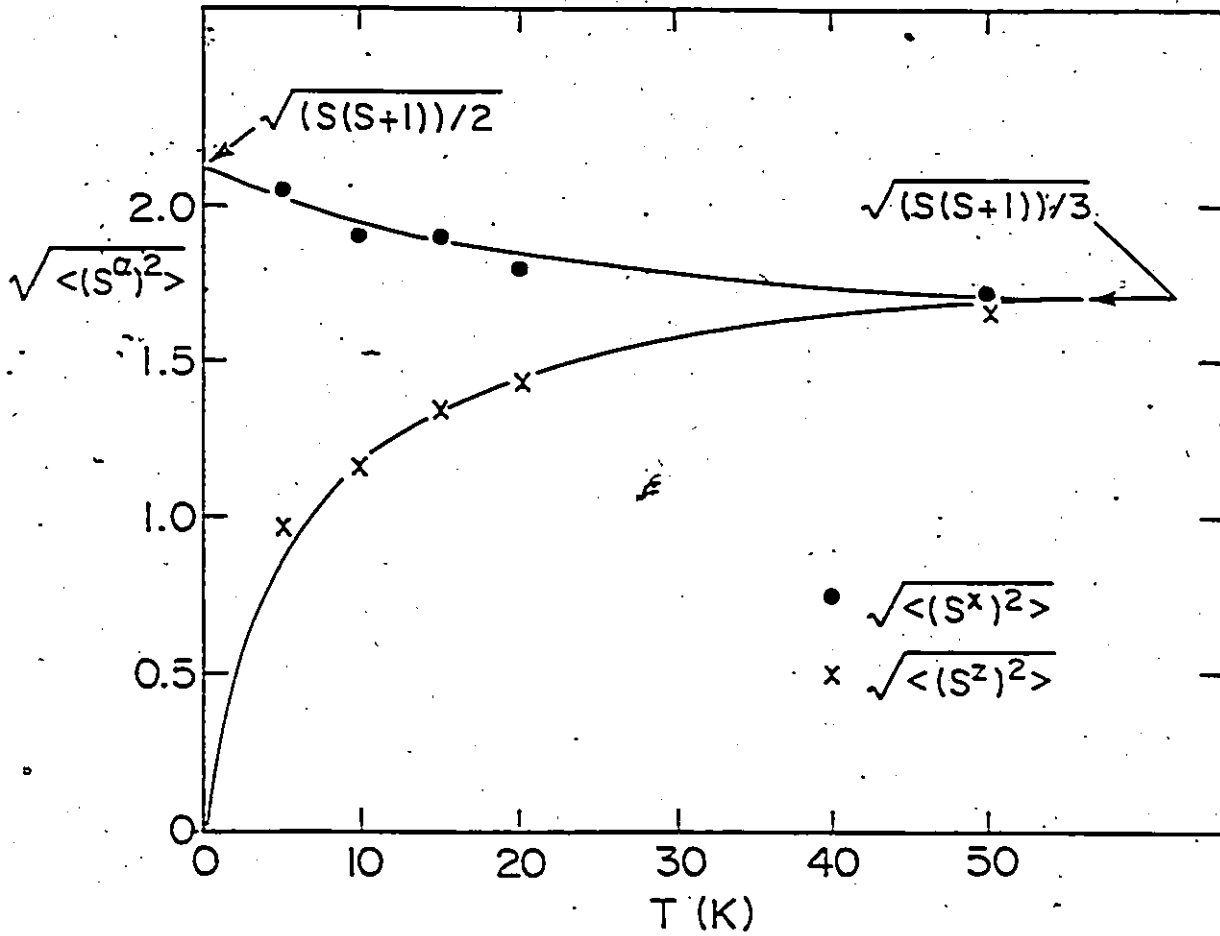


Figure H2: Values of $\sqrt{\langle S^\alpha \rangle^2} = S_0^\alpha(T)$ extracted from the simulation data are shown as a function of temperature. The lines drawn are guides to the eye consistent with zero and infinite temperature properties of the classical Heisenberg chain with easy-plane anisotropy as described in the text.

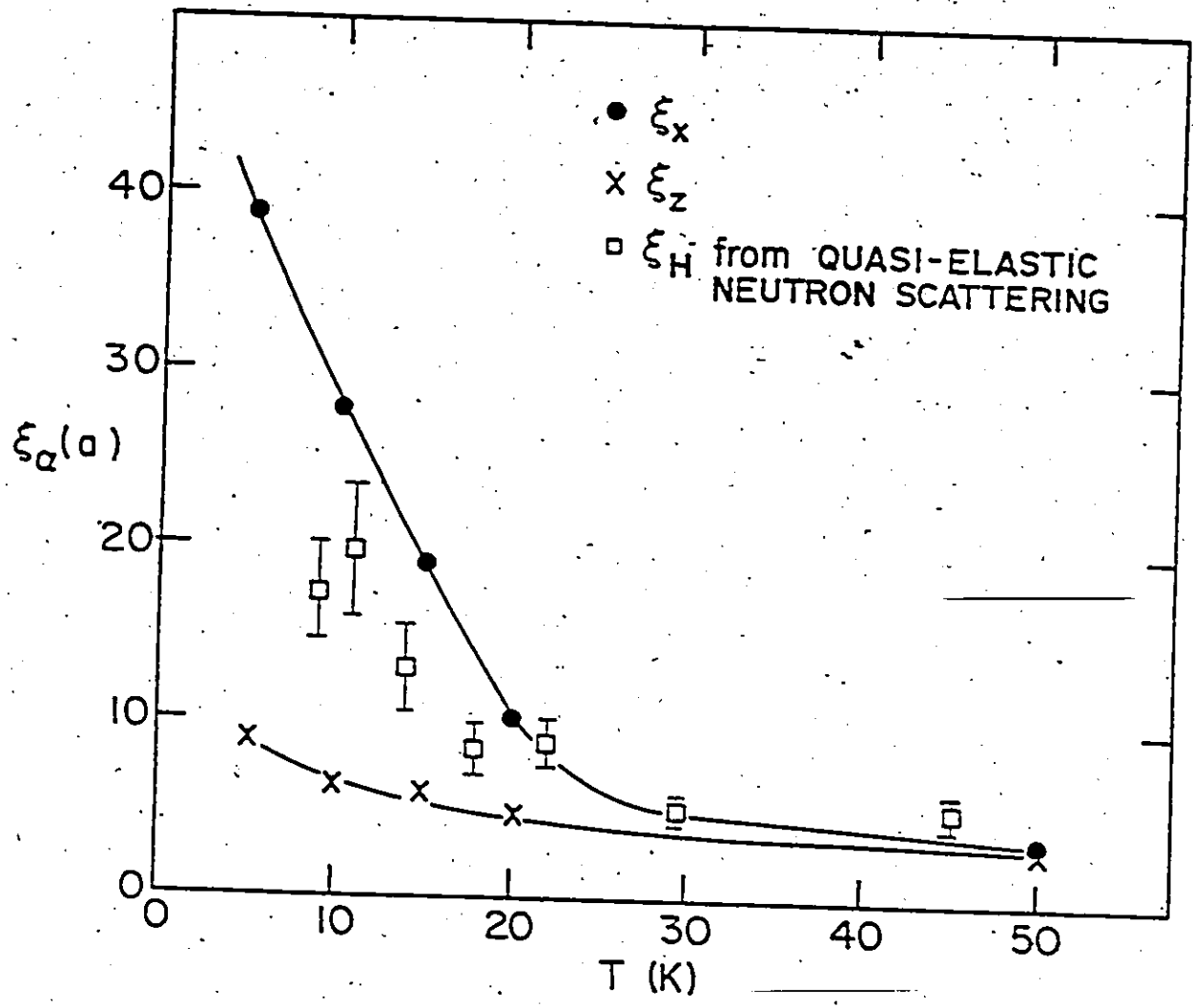


Figure H3: Values for both in-easy-plane, $\alpha=x$, and out-of-plane, $\alpha=z$, correlation lengths, $\xi_\alpha(T)$, extracted from a fit to the simulation data are shown. Also shown are the values of correlation length, $\xi_H(T)$, taken from analysis, in terms of an isotropic Heisenberg Hamiltonian, of neutron scattering measurements by Fitzgerald et al. on CsMnBr₃. All correlation lengths are in units of nearest neighbour spin separation, a , and the lines are guides to the eye.

definitions of the correlation length. However we do not see physically why a characteristic correlation length should fall off with decreasing temperature as the transfer matrix formalism suggests at low temperatures.

The experimental determination of the correlation lengths is very difficult for the anisotropic chain. For the isotropic Heisenberg chain the correlation length can be extracted from quasi-elastic neutron scattering measurements across the magnetic zone centre (actually, across the ridge of the maximum of the wavevector dependent susceptibility). This type of analysis has been applied to measurements on CsMnBr_3 (Fitzgerald et al., 1982) and TMMC (Birgeneau et al., 1971) in their paramagnetic regimes. The problem resides in the fact that what is measured in a neutron scattering experiment are the spin-pair correlation functions at a particular wavevector transfer, Q , and energy transfer, $\hbar\omega$, for components of spin, α , which are perpendicular to the Q of the scattering event. Thus, if anisotropy is present in a system, a superposition of correlation functions is usually measured and some average correlation length then extracted if analysis in terms of an isotropic Heisenberg chain is used.

The correlation length extracted from quasi-elastic neutron scattering data by Fitzgerald et al. is plotted on the same graph, figure H3, as our results for the numerical extraction of the correlation lengths for a Hamiltonian relevant for CsMnBr_3 . It is clear that their results lie between the two correlation lengths at lower temperatures.

Unfortunately there does not appear to be any easy way of determining the two correlation lengths independently via quasi-elastic scattering. To our knowledge the best treatment has been by Boucher et al. (1979) who examined both the Heisenberg-XY transition of TMMC and also the XY-to-Ising

transition in the same compound on application of a magnetic field in the easy plane. Here the theoretical correlation functions were averaged together to compare with the one experimentally-determined characteristic correlation length.

The presence of the easy plane produces interesting temperature dependencies for some of the static spin correlation functions. Out-of-easy-plane spin components will only appear at finite temperatures. Thus, as opposed to the in-plane correlation functions which all fall off with increasing temperature, some of the out-of-plane correlation functions will peak at finite temperature as these correlations must be thermally excited before they can fall off. This is shown in figure H4 for $\langle S_i^z S_{i+n}^z \rangle$ with $n=4,5,6$ as a function of temperature. A mild peak is present in these plots at roughly 17K.

8.3 Spin Configurations and Out-of-Easy-Plane Solitons

The qualitative features of the crossover from XY to Heisenberg behaviour can be observed directly by the Monte Carlo method. The simulation can be run and stopped at will to allow "snapshots" of the system to be made up as a function of temperature.

This is what is shown in figure H5. The spin configuration in the anisotropic Heisenberg chain is best specified by the angle the spin makes within the easy plane and some indication of the component of spin coming out of the easy plane. Thus what we have plotted is the angle within the easy plane made by one sublattice relative to an arbitrary zero angle, as well as the square of the reduced out-of-easy plane spin components, S_i^z averaged over two neighbouring spins on each sublattice along the chain.

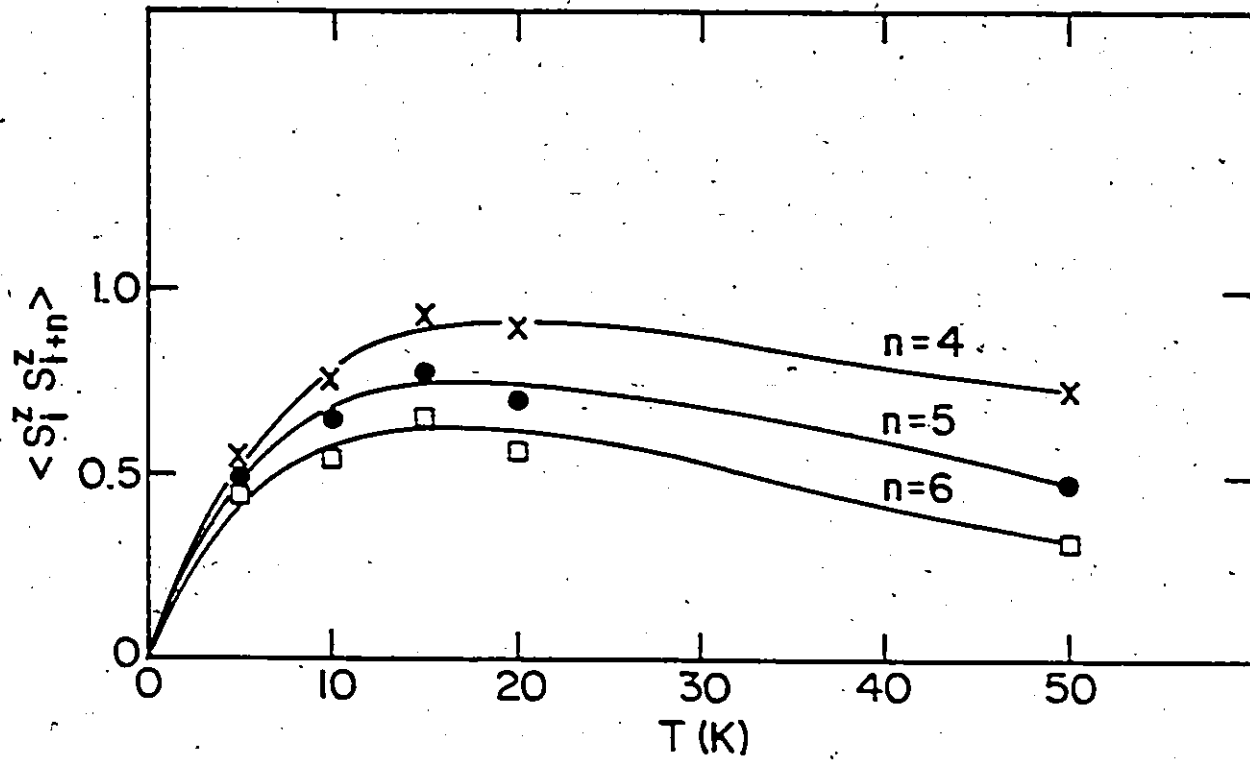
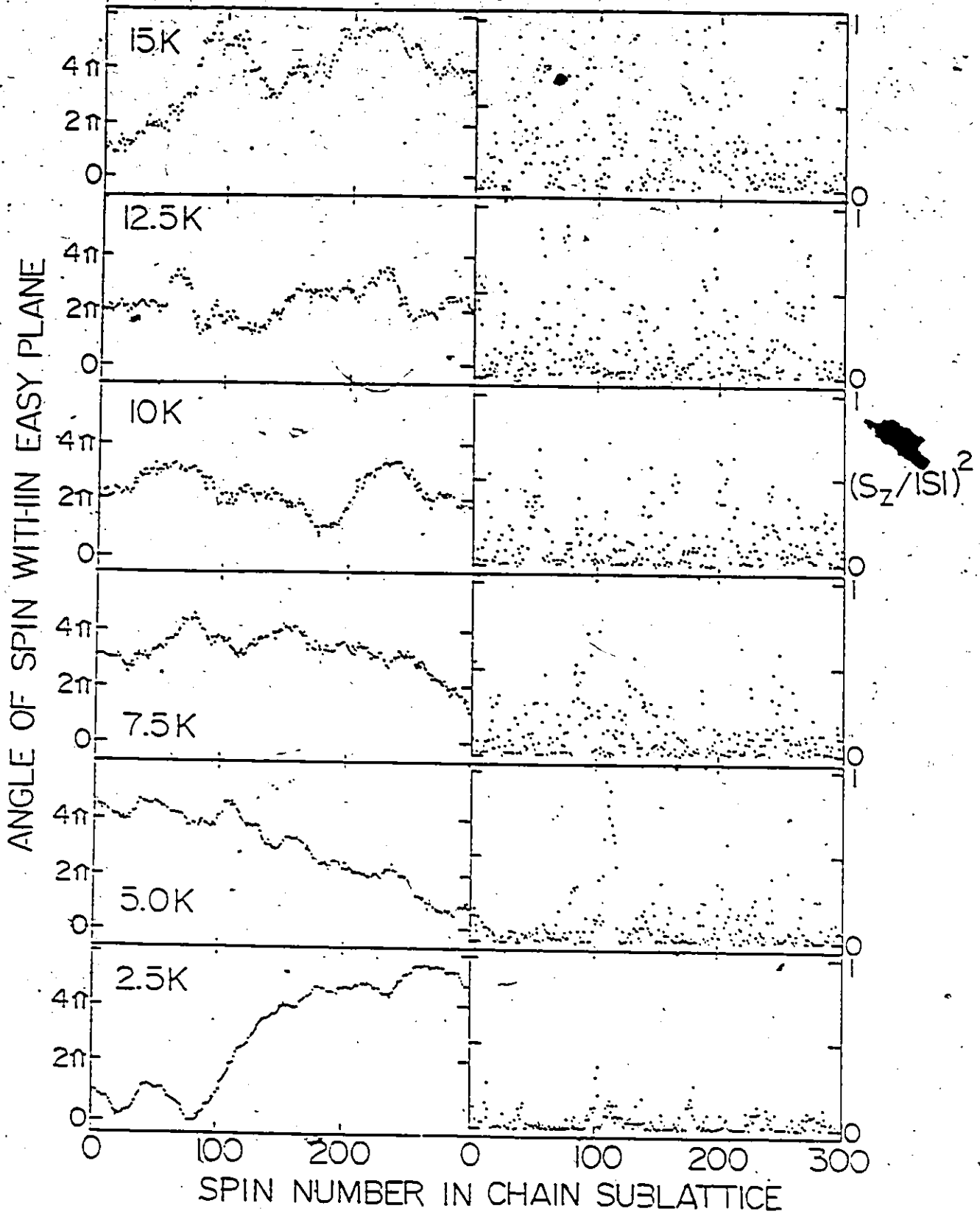


Figure H4: The out-of-easy-plane static correlation functions $\langle S_i^z S_{i+n}^z \rangle$ for $n = 4, 5$ and 6 are shown as a function of temperature. The lines are a guide to the eye consistent with the absence of out-of-easy-plane spin components at $T = 0$.

Figure H5: Spin configurations are shown as a function of temperature in the XY to Heisenberg cross over regime. The angles which one sublattice of spins make within the easy plane are shown on the left. The square of the reduced out of easy plane spin components, $(S_z^i/|S_i|)^2$, averaged over neighbouring spins on each sublattice, are shown on the right. Two jumps by π within the easy plane in the 12.5K configuration are identified as out-of-easy-plane solitons.



The system used in the simulation consisted of a ring of 600 spins with the same Hamiltonian, equation (8.1), as before. The "snapshots" were taken after 20,000 MCS/spin. Each ensemble of spins was started in a different random configuration. In all cases it was assumed that nearest neighbour spins on the same sublattice differed in angle within the easy plane by an angle less than or equal to π . At low temperatures the consequences of this assumption are not important, however it leads to some degree of arbitrariness in the direction of easy-plane angle change for temperatures above 15K. Hence these temperatures are not included in this analysis.

Some of the qualitative features of figure H5 are quite clear. From the reduced out-of-easy-plane spin component along the chain, it is clear that very little S^z components are present at 2.5K and 5.0K, but they become much more prevalent as the temperature is further raised. At 15K it is quite common to have spins at full deflection out of the easy plane.

The configurations of the angle made within the easy plane are quite interesting. At zero temperature the configuration is known exactly for such a classical system. The ground state is the Néel state with all spin vectors lying within the easy plane. At non-zero temperature it seems that there are three types of configurations present. At low temperatures, $T < 5K$, there is strong short-range order but long-range drift is present. This is to say nearest-neighbour spins on the same sublattice make almost exactly the same angle within the easy plane, but over a long distance this angle can drift by several revolutions. At intermediate temperatures, $T \sim 12.5K$,

the configurations display short-range drift but no long-range drift. Finally at high temperatures, $T \geq 15K$, the configurations display both long and short-range drift.

What is interesting here is that the intermediate temperature regime bears a strong resemblance to configurations described by out-of-easy plane solitons in the anisotropic Heisenberg chain as proposed by Mikeska (1980) and discussed in Chapter 4 of this thesis. The solitons in this model correspond physically to propagating domain walls which connect ground-state configurations that differ from each other by the interchange of the two sublattices within the easy plane. The motion of the spins as a soliton passes by is to come out of the easy plane, acquire large deflection out of the plane and finally return to the easy plane π out of phase with their previous ground state. Mikeska showed that the motion of a parameter related simply to S_i^z could be mapped onto a Sine-Gordon equation of motion in the classical continuum limit. These solutions were discussed in Chapter 4 of this thesis and are given by equation (4.4). If we suppress the time dependence by setting it to zero, the configuration of the angles the spins make within the easy plane, ϕ in equation (4.4), in the presence of a single soliton is

$$\phi(z) = \phi_0 + \pi \text{sign}(z-z_0)/2$$

Here z is the position along the chain and z_0 is the position of the soliton. Thus the long-range behaviour of the spin configurations should be quite regular if this model is relevant.

Examination of the configuration at $T = 12.5\text{K}$ shows something quite close to this description. Large stretches of spins, corresponding to about 100 spins, are present which make the same angle within the easy plane (if fluctuations within the easy plane about this value are averaged out). We clearly see two jumps of roughly π occurring within the easy plane in the first one hundred sublattice sites. These regions are examined in greater detail in figure H6. Both sublattices are plotted by adding π to the angle within the easy plane of one sublattice relative to the other. In addition the $(S^z/|S|)^2$ values are plotted for both sublattices.

It is clear that two major excursions out of the easy plane are present in the configuration for the region plotted. The centre of the large excursions corresponds to the points where the π jumps within the easy plane occur. Elsewhere there are of course fluctuations present but some sense of a ground state of spins lying within the easy plane can be perceived. We conclude that this configuration displays the presence of out-of-easy plane solitons.

Chapter 4 of this thesis describes neutron scattering measurements of the soliton response in CsMnBr_3 . This work examined dynamic spin correlations near zero-energy transfer and the magnetic zone centre and showed a qualitative difference between the in-plane and out-of-easy plane spectrum of spin fluctuations. At 15K, the out-of-plane fluctuations could be qualitatively described by the presence of solitons as described by Mikeska (1980). The measurements at higher temperatures did not follow the predictions of the noninteracting soliton theory. This is seen to be consistent with the present Monte Carlo results as the soliton picture

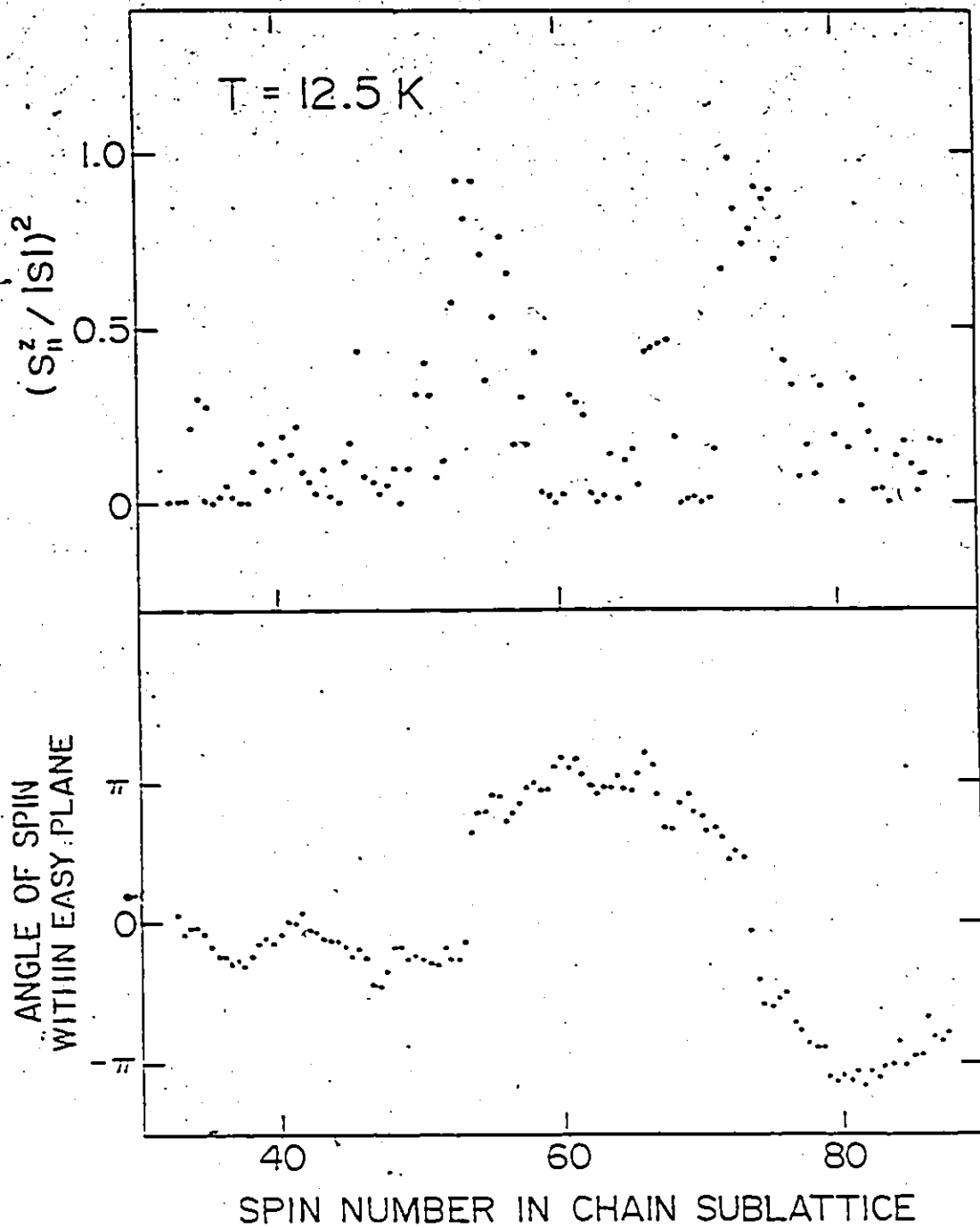


Figure H6: The section of the 12.5K configuration which displays the two out-of-easy-plane solitons is shown in greater detail. Each sublattice is plotted for $(S_n^z / |S|)^2$, while the angles one sublattice of spins make within the easy-plane is plotted along with those made by the other sublattice by adding π to the angles of one sublattice.

appears to be viable only within a rather narrow temperature range in the XY-to-Heisenberg crossover region. At low temperatures there are too few out-of-plane fluctuations present to give rise to soliton-like behaviour, while at high temperatures the easy plane is not thermodynamically relevant. The creation energy of a soliton in this system (at zero velocity) is $E_0 = 4JS^2\sqrt{(\delta/J)} \approx 40K$ while the characteristic energy of the easy plane is $\approx 20K$.

Earlier work examining soliton configurations in Monte Carlo simulations has been done for the classical XY chain (Gerling and Landau, 1984; Staudinger et al., 1985). By utilizing a numerical calculation of the spin dynamics of these configurations, these authors were able to examine, in one case anyway, the important consideration of stability. These considerations have been taken up theoretically for other systems (Fluggen and Mikeska, 1983; Wysin et al., 1986; and Etrich et al., 1985). The most relevant treatments for our work consider the classical antiferromagnet with easy plane anisotropy and a magnetic field applied within the easy plane. Both Fluggen and Mikeska (1983) as well as Wysin et al. (1986) examine the out-of-easy plane soliton mode in this system and reach opposing conclusions as to its stability at small fields. Fluggen and Mikeska predict the out-of-plane soliton is stable for all values of applied field. Wysin et al. predict the existence of a critical field only above which can a static or zero velocity soliton be stable. The stability criteria due to Wysin et al. change according to the soliton's velocity, and moving out-of-easy plane solitons can be stable at lower fields. The case with zero magnetic field has not specifically been taken up.

In addition there is some concern as to whether stable solitons in continuum systems become unstable when this unphysical continuum condition is relaxed and a discrete lattice system considered. Etrich et al (1985) considered the discrete ferromagnetic chain with easy plane anisotropy and a magnetic field applied within the easy plane. They found considerable modification to the continuum modes with two in-plane static soliton modes possible. These modes differ from each other according to whether the soliton configuration is symmetric with respect to a spin, or the bond between two spins. The "bond symmetric" soliton was found to have the same stability as the in-plane solution in the continuum model, however the "spin symmetric" soliton was found to be unstable for all values of field.

We were not able to examine the stability of these soliton configurations in the same manner as Gerling and Landau. However we did allow these same configurations to evolve for an additional 200 MCS/spin. Considerable differences are of course present. However one out-of-easy plane soliton configuration was still present in almost exactly the same position along the chain while the other was slightly modified but a strong fluctuation out of the easy plane was clear at the "correct" position.

Also present in the various configurations are excursions of the spins out of the easy plane, without an accompanying jump of the angle made within the easy plane by the spins. It is not clear whether these are the superposition of a soliton with other excitations or some unstable configuration. One of these which is particularly close to satisfying

the criteria for what we expect a soliton configuration to look like is shown in figure H7. The difference between the two configurations, figures H6 and H7, is clear; the excitation shown in figure H7 is clearly not an out-of-easy-plane soliton, though its correct description may be in terms of a soliton of some other type.

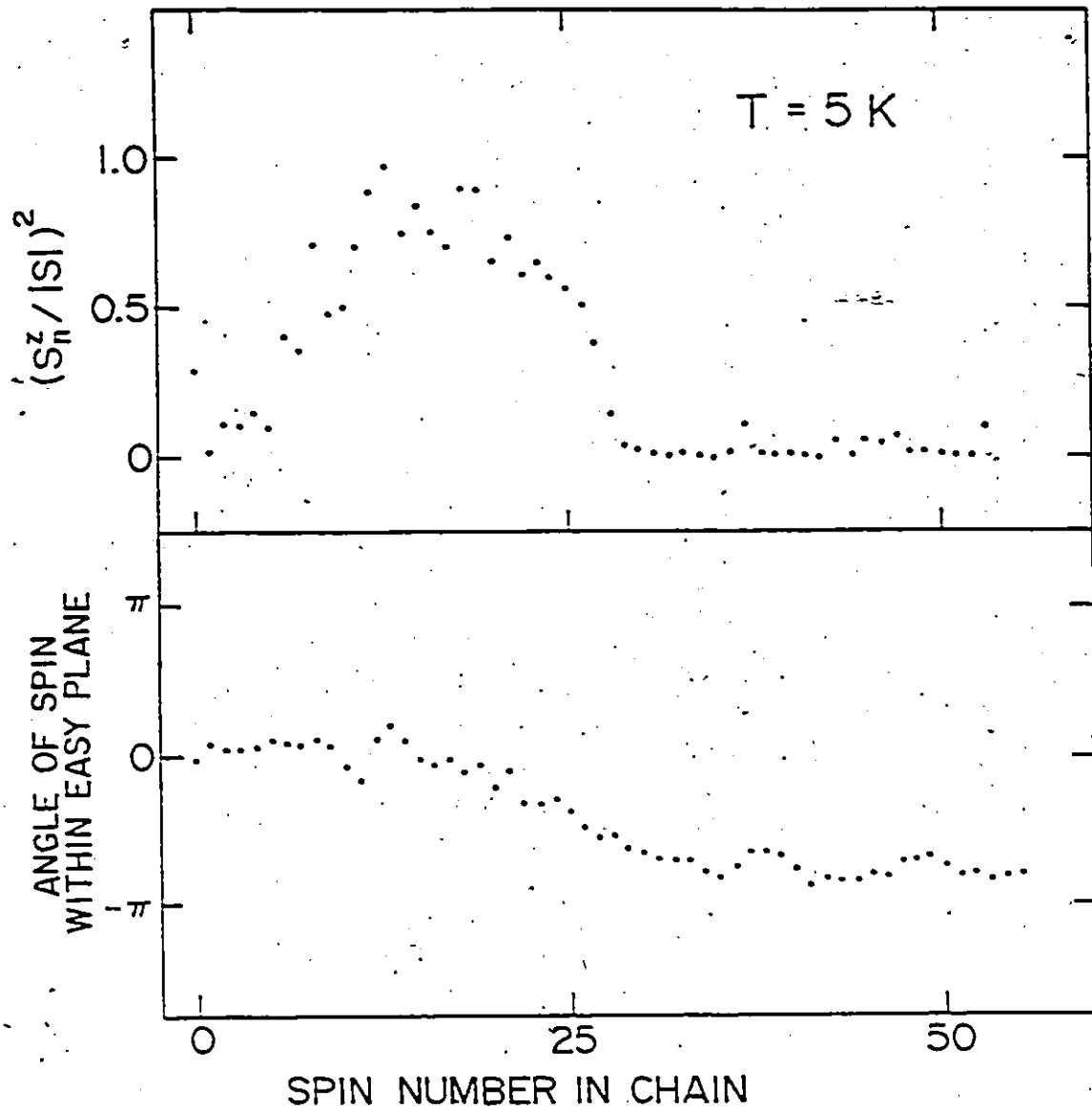


Figure H7. A large fluctuation of spins out of the easy plane at 5K is plotted in detail. The change of the angles made by the spins within the easy-plane is not sharp and thus this type of configuration is not identified as being soliton-like. The nature of this type of configuration is not clear.

CHAPTER 9
CONCLUDING REMARKS

This thesis has investigated several interesting aspects of the one-dimensional magnetic systems CsMnBr_3 and $\text{CsMn}_{0.89}\text{Fe}_{0.11}\text{Br}_3$. The nature of fluctuations and impurities in one-dimensional systems was previously known to be pathological to long-range order. The object of this thesis was not to demonstrate this fact once again, but rather to use these systems, where the fluctuation spectrum of the system is so important in understanding the phenomena, and thereby hopefully contribute to the overall understanding of the dynamics and hence the statistical mechanics of magnetic systems.

Specifically we examined both the delocalized (spin waves) and localized (solitons) excitations of the one-dimensional, weakly anisotropic, Heisenberg antiferromagnet CsMnBr_3 at low temperatures with neutron scattering techniques. Spin waves could be observed over most of the magnetic zone, and the response compared favourably with theory which considers cooperative excitations in the absence of long-range order. A strong qualitative difference was observed between the spectrums of in-plane and out-of-easy-plane spin fluctuations at small energy transfer and near the magnetic zone centre at 15K. The out-of-easy plane fluctuations could be qualitatively described by Sine-Gordon solitons as proposed by Mikeska. Soliton-like spin configurations could also be observed directly in "snapshots" of a magnetic chain system representative of CsMnBr_3 , produced by a Monte Carlo simulation.

This same Monte Carlo simulation also demonstrated the strong difference between in-plane and out-of-easy-plane correlation lengths within the Heisenberg to XY crossover temperature regime for a system such as CsMnBr_3 .

We measured the inelastic fluctuation spectrum of the magnetic-impurity chain system $\text{CsMn}_{0.89}\text{Fe}_{0.11}\text{Br}_3$ at low temperatures by neutron scattering techniques. The response was markedly different from either CsMnBr_3 or previously studied magnetic-vacancy chain systems. Our results indicate strong host model-impurity mode interactions are present, which arise as a consequence of the system's one dimensional nature.

Finally we utilized the calculational ease afforded by one dimension to investigate the strengths of biquadratic exchange interactions in several pure Mn^{+2} chain systems, including CsMnBr_3 . Our results showed that biquadratic exchange has an appreciable influence on the susceptibility of some pure Mn^{+2} chain systems, and checked nicely with neutron spectroscopic measurements by Falk et al. on $\text{CsMn}_{0.28}\text{Mg}_{0.72}\text{Br}_3$.

In conclusion, the rich behaviour observed in these "simple" one-dimensional co-operative systems made for an interesting set of topics of study.

BIBLIOGRAPHY

- Aharony, A., to appear in J. Magn. Magn. Mat. (1986).
- Allroth, E. and Mikeska, H.J., J. Phys. C 10, 313 (1977).
- Anderson, P.W., Phys. Rev. 86, 694 (1952).
- Bacon, G.E., Neutron Diffraction, Clarendon Press, Oxford (1975).
- Bernasconi, J. and Schneider, T., Physics in One Dimension, Springer-Verlag, Berlin (1981).
- Binder, K., Applications of the Monte Carlo Method in Statistical Physics, Springer-Verlag, Berlin (1984).
- Birgeneau, R.J., Dingle, R., Hutchings, M.T., Shirane, G. and Holt, S.L., Phys. Rev. Lett. 26, 718 (1971).
- Birgeneau, R.J. and Shirane, G., Phys. Today, 31, 32 (1978).
- Birgeneau, R.J., Cowley, R.A., Shirane, G. and Yoshizawa, H., J. Stat. Phys. 34, 817 (1984).
- Bishop, A.R., Krumhansl, J.A. and Trullinger, S.E., Physical D 1, 1 (1980).
- Boucher, J.P., Regnault, L.P., Rossat-Mignod, J., Villain, J. and Renard, J.P., Sol. St. Comm. 31, 311 (1979).
- Boucher, J.P., Mezei, F., Regnault, L.P. and Renard, J.P., Phys. Rev. Lett. 55, 1778 (1985).
- Breitling, W., Lehman, W., Weber, R., Lehner, N. and Wagner, W., J. Magn. Magn. Mat. 6, 113 (1977).
- Cooper, M.J. and Nathans, R., Acta Crystallogr. 23, 357 (1967).
- Cowley, R.A. and Buyers, W.J.L., Rev. Mod. Phys., 44, 406 (1972).
- Cowley, R.A., Shirane, G., Birgeneau, R.J., Svensson, E.C. and Guggenheim, H.J., Phys. Rev. B 22, 4412 (1980).

- Deitz, R.E., Walker, L.R., Hsu, F.S.L., Haemmerle, B., Vis, B., Chau, C.K. and Weinstock, H., Sol. St. Comm. 15, 1185 (1974).
- De Raedt, H. and De Raedt, B., Phys. Rev. B 15, 5379 (1977).
- De Raedt, H., Phys. Rev. B 19, 2585 (1979).
- Dingle, R., Lines, M.E. and Holt, S.L., Phys. Rev. 187, 643 (1969).
- Edgar, A., Siegel, E. and Urban, W., J. Phys. C 13, 6649 (1980).
- Eibshutz, M., Sherwood, R.C., Hsu, F.S.L. and Cox, D.E., AIP Conf. Proc. 10, 684 (1972).
- Endoh, Y., Heilmann, I.U., Birgeneau, R.J., Shirane, G., McGurn, A.R. and Thorpe, M.F., Phys. Rev. B 23, 4582 (1981).
- Etrich, C., Mikeska, H.J., Magyari, E., Thomas, H. and Weber, R., Z. Phys. B 62, 97 (1985).
- Falk, U., Furrer, A., Kjems, J.K. and Gudel, H.U., Phys. Rev. Lett. 52, 1336 (1984).
- Falk, U., Furrer, A., Kjems, J.K. and Gudel, H.U., J. Appl. Phys. 57, 3332 (1985).
- Fisher, M.E., Am. J. Phys. 32, 343 (1964).
- Fishman, S. and Aharony, A., Phys. Rev. B 18, 3507 (1978).
- Fitzgerald, W.J., Visser, D. and Ziebeck, K.R.A., J. Phys. C 15, 795 (1982).
- Fluggen, N. and Mikeska, H.J., Sol. St. Comm. 48, 293 (1983).
- Gerling, R.W. and Landau, D.P., J. Magn. Magn. Mat. 45, 267 (1984).
- Goodstein, D.L., States of Matter, Prentice-Hall Inc., Englewood Cliffs, New Jersey (1975).
- Heilmann, I.U., Birgeneau, R.J., Endoh, Y., Reiter, G., Shirane, G. and Holt, S.L., Sol. St. Comm. 31, 607 (1979).

- Heilmann, I.U., Kjems, J.K., Endoh, Y., Reiter, G., Shirane, G. and Birgeneau, R.J., Phys. Rev. B 24, 3939 (1981).
- Hone, D. and Pires, A., Phys. Rev. B 15, 323 (1977).
- Huang, N.L. and Orbach, R., Phys. Rev. Lett. 12, 275 (1964).
- Hutchings, M.T., Shirane, G., Birgeneau, R.J. and Holt, S. L., Phys. Rev. B 5, 1999 (1972).
- Hutchings, M.T. and Windsor, C.G., J. Phys. C 10, 313 (1978).
- Jackman, J.A., Ph.D. Thesis, University of Guelph (1983).
- Kakurai, K., Pynn, R., Dorner, B. and Steiner, M., J. Phys. C 17, L123 (1984).
- Kalt, H., Siegel, E., Pauli, N., Morsebach, H., Weise, J. and Edgar, A., J. Phys. C 16, 6427 (1983).
- Kittel, C., Phys. Rev. 120, 335 (1960).
- Kjems, J.K. and Steiner, M., Phys. Rev. Lett. 41, 1137, (1978).
- Krumhansl, J.A. and Schrieffer, J.R., Phys. Rev. B 11, 3535 (1975).
- Kumar, P., Phys. Rev. B 25, 483 (1982).
- Lines, M.E. and Eibschutz, M., Phys. Rev. B 11, 4583 (1975).
- Liu, L.L. and Joseph, R.I., Phys. Rev. Lett. 26, 1378 (1971).
- Liu, L.L. and Joseph, R. I., J. Phys. Chem. Sol. 33, 451 (1972).
- Locke, K.E., Ph.D. Thesis, McMaster University (1981).
- Loveluck, J., Lovesey, S.W. and Aubry, S., J. Phys. C 8, 3841 (1975).
- Lovesey, S.W., J. Phys. C 6, 1856 (1973).
- Lovesey, S.W., J. Phys. C 7, 2008 (1974).
- Lovesey, S.W., Theory of Neutron Scattering from Condensed Matter, Volumes 1 and 2, Clarendon Press, Oxford. (1984).

- Lovesey, S.W. and Merserve, R.A., J. Phys. C 6, 79 (1973).
- Lovesey, S.W., Bolucani, U., Borsa, F. and Tognetti, V., Magnetic Excitations and Fluctuations, Springer-Verlag, Berlin (1984).
- Marshall, W. and Lowde, R.D., Rep. Prog. Phys. 31, 705 (1968).
- Metropolis, N., Rosenbluth, A.W., Rosenbluth, M.N., Teller, A.H. and Teller, E., J. Chem. Phys. 21, 1087 (1953).
- Mikeska, H.J., J. Phys. C. 11, L29 (1978).
- Mikeska, H.J., J. Phys. C 13, 2913 (1980).
- Mori, H., Prog. Theor. Phys. 33, 423 (1965a).
- Mori, H., Prog. Theor. Phys. 34, 399 (1965b).
- Nagata, K. and Yamamoto, Phys. Lett. 60A, 237 (1977).
- Nagler, S.E., Buyers, W.J.L., Armstrong, R.L. and Briat, B., Phys. Rev. Lett. 49, 598 (1982).
- Nagler, S.E., Buyers, W.J.L., Armstrong, R.L. and Ritchie, R.A., J. Phys. C 17, 4819 (1984).
- Néel, L., Bull. Soc. Franc. Minéral. Crist. 77, 257 (1954).
- Oguchi, T., Phys. Rev. 117, 117 (1960).
- Oyedele, J.A. and Collins, M.F., Can. J. Phys. 56, 1482 (1978).
- Rebbi, C., Scient. Am., February, 92 (1979).
- Regonault, L.P., Boucher, J.P., Rossat-Mignod, J., Renard, J.P., Bouillot, J. and Stirling, W.G., J. Phys. C 15, 1261 (1982).
- Reiter, G., Phys. Rev. Lett. 46, 202 (1981).
- Rubinstein, J., J. Math. Phys. 11, 258 (1970).
- Sasaki, K., Prog. Theor. Phys. 71, 1169 (1984).
- Shirane, G. and Birgeneau, R.J., Physica B 86-88, 639 (1977).

- Simuzi, S., Chen, J.Y. and Friedberg, S.A., J. Appl. Phys. 55, 2398 (1984).
- Squires, G.L., Introduction to the Theory of Thermal Neutron Scattering, Cambridge University Press, Cambridge (1978).
- Staudinger, M., Gerling, R.W., Murty, C.S.S. and Landau, D.P., J. Appl. Phys. 51(1), 3335 (1985).
- Steiner, M. and Dorner, B., Sol. St. Comm. 12, 537 (1973).
- Steiner, M., Villain, J. and Windsor, C.G., Adv. in Phys. 25, 87 (1975).
- Thorpe, M.F., J. de Phys. 36, 1178 (1975).
- Tjon, J. and Wright, J., Phys. Rev. B 15, 3470 (1977).
- Tomita, H. and Mashiyama, H., Prog. Theor. Phys. 48, 1132 (1972).
- Tomita, H. and Mashiyama, H., Prog. Theor. Phys. 51, 1312 (1974).
- Villain, J., J. de Phys. 35, 27 (1974).
- Villain, J., Physica B 79, 1 (1975).
- Walker, L.R., Dietz, R.E., Andres, K. and Darack, S., Sol. St. Comm. 11, 593 (1972).
- Wegner, F., Z. Phys. 206, 465 (1964).
- Wysin, G.M., Bishop, A.R. and Oitmaa, J., to appear in J. Phys. C (1986).
- Yamamoto, I. and Nagata, K., J. Phys. Soc. Jap. 43, 1581 (1977).
- Yoshizawa, H., Cowley, R.A., Shirane, G., Birgeneau, R.J., Guggenheim, H.J. and Ikeda, H., Phys. Rev. Lett. 48, 438 (1982).